Pontifícia Universidade Católica
do Rio de Janeiro

Alexandre Velloso Pereira Rodrigues

Essays on Two-stage Robust Models for Power Systems: Modeling Contributions and Applications of the Column-and-Constraint-Generation Algorithm

Tese de Doutorado

Thesis presented to the Programa de Pós-Graduação em Engenharia Elétrica of PUC-Rio in partial fulfillment of the requirements for the degree of Doutor em Engenharia Elétrica.

Advisor : Prof. Alexandre Street de Aguiar
Co-Advisor: Prof. David Pozo Camara

Rio de Janeiro
August 2020

Pontifícia Universidade Católica
do Rio de Janeiro

Alexandre Velloso Pereira Rodrigues

Essays on Two-stage Robust Models for Power Systems: Modeling Contributions and Applications of the Column-and-Constraint-Generation Algorithm

Thesis presented to the Programa de Pós-Graduação em Engenharia Elétrica of PUC-Rio in partial fulfillment of the requirements for the degree of Doutor em Engenharia Elétrica. Approved by the Examination Committee.

Prof. Alexandre Street de Aguiar
Advisor
Departamento de Engenharia Elétrica – PUC-Rio

Prof. David Pozo Camara
Co-Advisor
Skolkovo Institute of Science and Technology – Skoltech

Prof. Anthony Papavasiliou
Université Catholique de Louvain – UCLouvain

Prof. Pascal Van Hentenryck
Georgia Institute of Technology – GA TECH

Prof. Phillipe Vilaça Gomes
Departamento de Engenharia Elétrica – PUC-Rio

Prof. Pierluigi Mancarella
University of Melbourne – UM

Prof. Rodrigo Moreno
Universidad de Chile – UCh

Rio de Janeiro, August 25th, 2020

Alexandre Velloso Pereira Rodrigues

Alexandre Velloso Pereira Rodrigues received his M.Sc. degree in Mathematical Methods in Finance from the National Institute for Pure and Applied Mathematics (IMPA), Rio de Janeiro, Brazil in 2005. Since 2010, he has been working for the Brazilian Innovation Agency – Financiadora de Estudos e Projetos (Finep). Currently, he is a visiting scholar at the School of Industrial and Systems Engineering (ISyE) at the Georgia Institute of Technology, Atlanta, USA.

Bibliographic data

Velloso Pereira Rodrigues, Alexandre

Essays on Two-stage Robust Models for Power Systems: Modeling Contributions and Applications of the Column-and-Constraint-Generation Algorithm / Alexandre Velloso Pereira Rodrigues; advisor: Alexandre Street de Aguiar; co-advisor: David Pozo Camara. – 2020.

168 f. : il. color. ; 30 cm

1. Tese (doutorado) – Pontifícia Universidade Católica do Rio de Janeiro, Departamento de Engenharia Elétrica, Rio de Janeiro, 2020.

Inclui bibliografia.

1. Engenharia Elétrica – Teses. 2. Algorítmo de Geração de Linhas e Colunas. 3. Otimização Robusta Ajustável. 4. Fluxo de Potência Ótimo com Critério de Segurança. 5. Programação Diária. 6. Planejamento de Expansão da Transmissão. I. Aguiar, Alexandre Street de. II. Pozo Camara, David. III. Pontifícia Universidade Católica do Rio de Janeiro. Departamento de Engenharia Elétrica. IV. Título.

CDD: 621.3

Acknowledgments

Abstract

Velloso Pereira Rodrigues, Alexandre; Street de Aguiar, Alexandre (Advisor); Pozo Camara, David (Co-Advisor). **Essays on Two-stage Robust Models for Power Systems: Modeling Contributions and Applications of the Column-and-Constraint-Generation Algorithm**. Rio de Janeiro, 2020. 168p. PhD Thesis – Departamento de Engenharia Elétrica, Pontifícia Universidade Católica do Rio de Janeiro.

This dissertation is structured as a collection of five papers formatted as chapters. The first four papers provide modeling and methodological contributions in scheduling or investment problems in power systems using the adaptive robust optimization framework and modifications to the column-and-constraint-generation algorithm (CCGA). The first paper addresses the security-constrained short-term scheduling problem where automatic primary response is considered. A two-stage robust model is adopted, resulting in complex mixed-integer linear instances featuring binary variables associated with first- and second-stage decisions. A new tailored CCGA which explores the structure of the problem is devised. The second paper uses deep neural networks for learning the mapping of nodal demands onto generators' set point for the first paper's model. Robust-based modeling approaches and the CCGA are used to enforce feasibility for the solution. This method results in important computational gains as compared to results of the first paper. The third paper proposes an adaptive data-driven approach for a two-stage robust unit commitment model, where the polyhedral uncertainty set is characterized directly from data, through the convex hull of a set of previously observed non-dispatchable generation profiles. The resulting problem is suitable for the exact CCGA. The fourth paper proposes an adaptive two-stage distributionally robust transmission expansion model incorporating long- and short-term uncertainties. A novel extended CCGA is devised to tackle distributionally robust subproblems. Finally, under a different and higher-level perspective, the fifth paper investigates the adequacy of systematic inducement prizes for fostering innovations in theoretical and computational aspects for various modern power systems challenges.

Keywords

Column-and-Constraint Generation Algorithm; Adaptive Robust Optimization; Security-Constrained Optimal Power Flow; Unit Commitment; Transmission Expansion Planning; Deep Neural Network.

Resumo

Velloso Pereira Rodrigues, Alexandre; Street de Aguiar, Alexandre; Pozo Camara, David. **Ensaios em Modelos de Dois Estágios em Sistemas de Potências: Contribuições em Modelagem e Aplicações do Método de Geração de Linhas e Colunas**. Rio de Janeiro, 2020. 168p. Tese de Doutorado – Departamento de Engenharia Elétrica, Pontifícia Universidade Católica do Rio de Janeiro.

Esta dissertação está estruturada como uma coleção de cinco artigos formatados em capítulos. Os quatro primeiros artigos apresentam contribuições em modelagem e metodológicas para problemas de operação ou investimento em sistemas de potência usando arcabouço de otimização robusta adaptativa e modificações no algoritmo de geração de linhas e colunas (CCGA). O primeiro artigo aborda a programação de curto prazo com restrição de segurança, onde a resposta automática de geradores é considerada. Um modelo robusto de dois estágios é adotado, resultando em complexas instâncias de programação inteira mista, que apresentam variáveis binárias associadas às decisões de primeiro e segundo estágios. Um novo CCGA que explora a estrutura do problema é desenvolvido. O segundo artigo usa redes neurais profundas para aprender o mapeamento das demandas nodais aos pontos de ajuste dos geradores para o problema do primeiro artigo. O CCGA é usados para garantir a viabilidade da solução. Este método resulta em importantes ganhos computacionais em relação ao primeiro artigo. O terceiro artigo propõe uma abordagem adaptativa em dois estágios para um modelo robusto de programação diária no qual o conjunto de incerteza poliedral é caracterizado diretamente a partir dos dados de geração não despachável observados. O problema resultante é afeito ao CCGA. O quarto artigo propõe um modelo de dois estágios adaptativo, robusto em distribuição para expansão de transmissão, incorporando incertezas a longo e curto prazo. Um novo CCGA é desenvolvido para lidar com os subproblemas. Finalmente, sob uma perspectiva diferente e generalista, o quinto artigo investiga a adequação de prêmios de incentivo para promover inovações em aspectos teóricos e computacionais para os desafios de sistemas de potência modernos.

Palavras-chave

Algorítmo de Geração de Linhas e Colunas; Otimização Robusta Ajustável; Fluxo de Potência Ótimo com Critério de Segurança; Programação Diária; Planejamento de Expansão da Transmissão; Redes Neurais Profundas.

Table of contents

List of figures

List of tables

1
Introduction

This doctorate thesis, which is organized as a collection of independent essays, has two main objectives, both related to improving current industry practices in modern power systems:

1. Firstly, as the main objective, to provide specific mathematical frameworks, based on two-stage robust optimization models and on modified versions of the column-and-constraint-generation algorithm, to determine solutions for selected practical problems in power systems. These selected problems relate to short- and medium-term generators' scheduling, and to long-term transmission expansion planning. In these applications, robust approaches are applied to model uncertain net load or component failures, while modifications to the column-and-constraint-generation algorithm are tailored to tackle each resulting formulation.

2. Secondly, to analyze challenges and technological gaps of current approaches to power system models in Brazil, as well as how innovations for these models are financed and implemented. Moreover, to discuss, in the perspective of the Brazilian case, whether inducement prizes would constitute a suitable systematic mechanism to foster innovation in theoretical and computational aspects for the various existing challenges.

This first chapter provides an introduction to the work reported in this document. In Section 1.1, challenges associated with modern power systems are outlined. Sections 1.2 and 1.3 provide motivation, respectively, for the applications of the two-stage robust optimization approach and the column-and-constraint-generation solution algorithm. Finally, the document structure and the specific objectives of each chapter are presented in Section 1.4.

1.1
Modern Power System Challenges

Electric power systems are among the largest and most complex engineered systems ever designed and constructed. As an example, in the

United States, power systems ship hundreds of billion of dollars in electricity every year and are composed by hundreds of thousands of kilometers of high-voltage transmission lines, thousands of generators, millions of kilometers of distribution lines, and millions of geographically dispersed consumers. These large structures are expected to generate, transport, and distribute the electricity required by virtually every economic activity of modern society at very high standards of reliability, accessibility, and cost affordability. However, the once stable, vertically integrated, and regulated systems featuring predictable net demand underwent deep changes associated with market deregulation processes [1–3], technology disruptions on both demand and supply side, and new environmental constraints.

Initiated in the 1980s, market reforms were a long process of general liberalization of electricity sector and modification of the regulatory framework. These reforms facilitated the dissolution of large integrated companies with the aim to reduce costs, increase price transparency, enabling third party access, and fostering economically driven generation capacity expansion [1, 2]. In this new environment, the investments in capacity expansion became less centralized and coordinated, while the profit-maximizing agents were incentivized to pursue innovations in various technologies to reduce costs and increase efficiency.

On the generation side, due to technological advances and environmental incentives, non-dispatchable renewable energy generation from large solar and wind power units has undergone a sharp increase in the last two decades. These sources are already major components in some electricity markets and are expected to penetrate even further. For instance, main intergovernmental organizations such as the United Nations have indicated that increasing investments in clean energy technologies is an important mechanism in tackling climate change and its undesired effects [4, 5][1]. High integration of these clean, however, intermittent and variable energy sources brings additional challenges that have been widely discussed [6–17]. Notwithstanding the environmental benefits, non-dispatchable renewable sources are driven by complex time-varying spatial and temporal dynamics [18]. Thus, to benefit the most from such intermittent sources, conventional generation and/or fast operational actions might be required to provide (up and down) reserves in a reliable fashion.

[1] On 25 September, the United Nations General Assembly unanimously adopted the Resolution A/RES/70/1. “Transforming Our World, the 2030 Agenda for Sustainable Development". Among the sustainable goals of this resolution, goal number 7 refers to sustainable energy - “Sustainable Development Goal 7: Ensure access to affordable, reliable, sustainable, and modern energy for all"

On the demand and/or distribution side, the load has also become less predictable. The number of microgrids, distributed renewable energy sources at the consumer level, as well as plug-in electric vehicles and energy storage systems have risen in recent years, configuring a shift from a conventional to a smart-grid paradigm. In this context, distribution networks are expected to become active systems: New communication technologies will facilitate the interaction with the transmission system and fast controllable distributed energy resources, including batteries and flexible loads, will operate to efficiently balance supply and demand [19].

These features of modern power systems represent fundamental changes in many of the assumptions that traditional power systems were built on. As a consequence, systems are being demanded and operated in circumstances for which they were not built. In this configuration, it has been progressively more challenging to satisfy the aforementioned very high standards that society demands from power systems. The necessity for addressing these challenges has been driving intense research aimed at new models and algorithms both in industry and academia.

Power system's operations require constant equilibrium between nodal loads and generation, which is ensured on the scale of seconds by automatic primary response mechanisms that govern the synchronized generators. These generators respond automatically to frequency variations, caused for example by power imbalances, by adjusting their power outputs until frequency is normalized and the power balance is restored. For longer timescales, ranging from a few minutes to hours or even days ahead, the operation and planning are strongly based on the solution of mathematical optimization problems, as independent system operators and/or planners seek consistent and efficient schedules that comply with many complex physical constraints.

Power system's models are usually arranged in time-horizon layers for which there are different approximations of the physical reality and different representations of the relevant uncertainties. Some of the most studied decision-making problems in power systems are outlined next:

– **Short-term scheduling problems**: The goal of short-term scheduling problems such as the economic dispatch problem and the optimal power flow problem is to determine setpoints for the generators at minimal cost to meet forecasted load demand. The security-constrained version of the optimal power flow problem requires that the dispatch allows for steady-state points of operations for prescribed security criterion such as the failures of main lines and/or generators. The security-constrained optimal power flow is a nonlinear and nonconvex problem based on

the ac optimal power flow constraints ([20] and [21]). Short-term scheduling problems are fundamental building blocks for power systems and are solved many times a day by system operators under various circumstances, either in real-time or in large-scale studies. These needs have been intensified by increasing unpredictability of non-dispatchable renewable generation.

– **Unit commitment problem**: The main purpose of the unit commitment problem [8, 22, 23] is to manage generating resources by scheduling the on/off statuses of generators and determining their dispatch levels in order to meet demand at minimum cost. The programming horizon is usually of many hours or a few days ahead, divided into a few smaller time periods (for example hours). The unit commitment problem normally considers a series of combinatorial engineering constraints, such as minimum uptime and downtime for generators, ramping limitations for generators to increase or decrease the power output, and the network constraints. Computational complexities of this problem potentially arise from a large number of binary variables related to on/off generators' statuses, a large number of nodes or buses, and tight restrictions on the transmission network. Adding to the complexity, unit commitment models frequently co-optimize energy and reserves to limit risks associated with non-dispatchable renewable generation uncertainties and/or component failures.

– **Network topology optimization**: The aim of this problem is to reduce operational cost or guarantee feasibility by modifying the network topology. Under this category, transmission switching represents the deliberate switching of the on/off status of a transmission line by the operator [24]. Even though counterintuitive, significant operating cost reductions and system reliability enhancements may be achieved by not allowing flow through certain lines [25, 26]. This is explained by Braess' Paradox [27]. Broadly, due to Kirchhoff's voltage law, every network cycle adds constraints to the power flow problem. By removing lines and breaking loops, it is possible to reduce network congestion and approach the desired merit-order dispatch; that is, cheapest generators are dispatched first [27, 28].

At the distribution level, auxiliary systems perform periodic operations on tap changers and capacitors bank in order to guarantee that the point of operation remains at appropriate levels [29]. This problem is usually called a volt/var control. However, the high insertion of distributed photovoltaic generation (a form of clean and renewable energy) can

cause, due to its uncertain and intermittent nature, operational problems [19, 29]. Therefore, as per [19] and [29], new models and strategies for operating distribution systems with a high penetration of distributed photovoltaic generation might be needed.

– **Long-term hydrothermal scheduling problem**: Planning the operation for systems with high penetration of hydro generation, as is the case for Brazil, Norway, and Colombia, among others, is a complex task [30, 31]. The operator needs to coordinate power generation with operational restrictions that involve multiple uses of water such as irrigation, navigability, consumption, etc [32,33]. In addition, generating plants are sometimes arranged in cascades on the same river [34–36], with inflows subject to significant uncertainty [30, 31, 37, 38]. The long-term hydrothermal scheduling problem normally takes into account multi annual periods (for example in the Brazilian case) and is usually formulated as a multistage (several decision instances) stochastic problem [31,39,40]. In a simplified way, hydrothermal scheduling models program the generation from water sources, featuring low operational cost, along with other more expansive sources, aiming at minimal long-term cost, while ensuring the availability of natural resources for future energy consumption [31]. Because the complexity increases with the number of states (such as reservoir storage levels) and stages (decision instances), relevant simplifications are necessary to apply state-of-the-art techniques for solving this problem [39–42].

– **Transmission expansion problem**: Unlike generation investment, which is generally market-driven and hence decentralized, network infrastructure is generally centrally planned. The transmission expansion planning problem consists in determining which transmission lines will be built aiming at minimizing the combined costs for investment and future operational cost. However, it is relevant to highlight that this problem is generally related to strategic policies, as the outcome of a transmission plan extends far beyond providing a simple least-cost connection between the generation and loads. For example, it may directly or indirectly shape the economic development for covered regions [43], or even facilitate policies for fostering innovation in various generation technologies. As for electrical aspects, the system reliability, operational flexibility, reserves deliverability, and long-run adaptability [43] are key concepts that are significantly affected by the selected transmission capacity updates. On the uncertainty side, planners have been dealing with several deep

uncertainties arising from social and economic transformations, political and environmental issues, and technology disruptions, among others [43].

To tackle current challenges, many techniques invented in optimization are used in power systems, for example: linear programming [31, 44, 45], Lagrangian relaxation [46–48], mixed-integer programming [22, 41, 49], convex programming [50, 51], non-linear programming [49, 52], stochastic optimization [31, 53–55], robust optimization [56–58], etc. In this sense, modern power systems represent a huge success story for optimization.

The next section motivates the use of the two-stage robust optimization approach in power systems problems.

1.2 Two-stage Robust Optimization in Power System Applications

For many years, power systems' operations relied on deterministic approaches [59]. However, as summarized in the prior section, uncertainties in modern power systems have risen to much higher levels. In this context, traditional approaches might not be adequate either because short-term deterministic models (where the exact demand and non-dispatchable generation are assumed to be known) must be run within a much narrower time frame or because uncertainty and/or component failures require explicit modeling.

Besides the deterministic framework, propelled by available historical data, stochastic optimization approaches have been largely employed in academic papers to cope with uncertain non-dispatchable renewable generation [60]. In this approach, uncertain data are assumed to be random and to follow a known (or partially known) probability distribution. However, there are relevant situations where the availability of abundant data is not sufficient to ensure computational tractability of stochastic-optimization-based models with an accurate representation of the uncertainty factors (the interested reader is referred to [61] and [60] for a discussion on the subject). For example, an accurate representation of a parametric joint probability distribution of a high-dimensional uncertainty vector in stochastic unit commitment models generally requires a large number of scenarios. Many scenario-reduction techniques, clustering methods, and sampling techniques have been proposed to mitigate the tractability issue associated with large stochastic models. However, it is important to mention that the sample size needed to ensure primal and dual solution stability imposes additional tractability challenges to stochastic models. In this sense, stochastic-programming-based approaches are technically random methods. For instance, the sampling-variability level

of optimal schedules and marginal costs (generally used as ex-ante day-ahead commitment and prices, respectively) may be prohibitive for industry practice even when a large number of scenarios are used and the objective function variability is controlled within a given probability confidence level. Moreover, there are potential regulatory flaws stemming from relying on a method that may give rise to different solutions on different computers. Thus, the aforementioned tractability and solution stability issues associated with stochastic-based models constitute relevant challenges that, to some extent, prevent the wide adoption of stochastic models in industry practice.

In contrast, robust models enabling the use of exact solution methods are deterministic approaches that, regardless of very specific technicalities associated with commercial solvers (affecting all methods relying on them), should always yield the same solutions no matter the hardware platform.

Another relevant aspect to be taken into consideration in stochastic-programming-based approaches is to ensure a proper time-series representation capable of capturing the dynamics of uncertain renewable generation. As per references [18] and [62], the true underlying stochastic process driving renewable generation is a high-dimensional, non-Gaussian, and time-varying random process exhibiting complex spatial and time dependences that are difficult to capture with current state-of-the-art time-series models. In this context, the problem of characterizing the scenarios of wind power generation for multiple units is still an open field of research (see recent work [62] addressing this topic). In addition, parametric models in high-dimensional applications generally suffer from statistical issues such as the presence of a huge number of parameters that significantly jeopardize their accuracy in out-of-sample tests.

Such issues associated with model tractability and/or difficult representation of complex structures in the time-series models justify the need for alternative approaches to characterize uncertainty, even in the presence of abundant historical data.

These facts have motivated the use of the two-stage robust optimization models, which are commonly referred to as adaptive robust optimization framework, to address component failures and/or uncertain non-dispatchable renewable generation in power system's problems. Uncertainties are, in general, represented by polyhedral uncertainty sets relying on assumptions about the uncertainty factors (see [63] and [64]). Under this framework, the solution is that which performs the best in the worst-case scenario. General two–stage robust models comprise three optimization levels and may be formulated in

different ways. For example:

$$z^* = \min_{\mathbf{x}\in\mathcal{X}}\{\mathbf{c}(\mathbf{x}) + \max_{\mathbf{u}\in\mathcal{U}} \min_{\mathbf{y}\in\mathcal{Y}(\mathbf{x},\mathbf{u})} \mathbf{h}(\mathbf{y})\} \tag{1-1}$$

or

$$z^* = \min_{\mathbf{x}\in\mathcal{X}}\{\mathbf{c}(\mathbf{x}) \,|\, \phi(\mathbf{x}) = \max_{\mathbf{u}\in\mathcal{U}} \min_{\mathbf{y}\in\mathcal{Y}(\mathbf{x},\mathbf{u})} \mathbf{h}(\mathbf{y});\ \phi(\mathbf{x}) < \epsilon\} \tag{1-2}$$

These very flexible general structures can accommodate different problems and models. For instance, first-stage decision $\mathbf{x}$ may represent generators' commitment decision (for unit commitment problems), investments in lines (for transmission expansion planning problems) or short-term generators' setpoints (for optimal power flow problems). The second level usually models the worst-case realization $\mathbf{u}$ of uncertain parameters within an admissible set of events $\mathcal{U}$ for a given fist-stage decision $\mathbf{x}$. The set $\mathcal{U}$ is the so-called *uncertainty set*. The third-level model (or second-stage decision) determines $\mathbf{y}$, which represents the best system response in terms of cost or reliability for given first-stage decision $\mathbf{x}$ and second-level realization $\mathbf{u}$.

A key aspect in robust models is the uncertainty set description $\mathcal{U}$. Traditionally, $\mathcal{U}$ has been modeled as a polyhedral set. The budget-constrained approach [8] has been largely employed due to its simplicity and capability of controlling conservativeness with a single parameter. The reader is referred to Chapter 4 for a thorough discussion. While the recent literature on two-stage robust optimization has considered probability agnostic models (see [65], [63], and [64]), relevant efforts have been made to account for the information extracted from data to devise more realistic descriptions of the uncertainties. The interested reader is referred to [66], and [12] for applications in short-term operational models and to [67] for a hybrid-robust-and-stochastic approach applied to the transmission expansion problem.

1.3 Column-and-Constraint-Generation Algorithm for Robust Models

Assuming a linear fixed cost function, the third-level problem, parameterized by first-stage decision and second-level uncertainty realization, can usually be cast by the following linear program:

$$g(\mathbf{x},\mathbf{u}) = \min_{\mathbf{y}} \mathbf{h}^\top \mathbf{y} \tag{1-3}$$

subject to

$$\mathbf{W}\mathbf{y} \geq \mathbf{b} + \mathbf{B}\mathbf{u} - \mathbf{T}\mathbf{x} \qquad : \boldsymbol{\lambda}, \tag{1-4}$$

where matrices $\mathbf{W}$, $\mathbf{B}$, and $\mathbf{T}$, and vector $\mathbf{b}$ are fixed parameters. This structure is particularly convenient since $g(\cdot,\cdot)$ is a convex function on both $\mathbf{x}$ and $\mathbf{u}$. By strong duality, it is possible to recast the two lowermost levels as a single nonlinear problem,

$$\phi(\mathbf{x}) = \max_{\mathbf{u},\boldsymbol{\lambda}} (\mathbf{b} + \mathbf{B}\mathbf{u} - \mathbf{T}\mathbf{x})^\top \boldsymbol{\lambda} \tag{1-5}$$

subject to

$$\mathbf{W}^\top \boldsymbol{\lambda} = \mathbf{h} \tag{1-6}$$

$$\boldsymbol{\lambda} \geq \mathbf{0} \tag{1-7}$$

$$\mathbf{u} \in \mathcal{U} \tag{1-8}$$

This problem is frequently referred to as *oracle* or *oracle subproblem* and is generally NP-hard. Nonlinearity arises due to the product $\mathbf{u}^\top \mathbf{B}^\top \boldsymbol{\lambda}$ and typical mixed-integer linear program techniques are frequently applied to linearize this term. Even though (1-5)–(1-8) is potentially complex, the fact that, for fixed optimal second-stage solutions $\mathbf{u}^*, \boldsymbol{\lambda}^*$, the objective value in (1-5) is convex with respect to the first-stage decision vector $\mathbf{x}$, presents a perfect situation to use the Benders decomposition method [8]. Benders decomposition is an iterative procedure between a *master problem* that determines $\mathbf{x}$ only and the oracle subproblem (1-5)–(1-8). Each iteration the method provides dual information (dual cuts) about the subproblems in the form of valid hyperplanes (cuts) that restrict the master problem [44]. There are cases, however, where this approach requires many iterations of the potentially NP-hard subproblem to converge. Another drawback of this method is that it requires convexity for the third-level problem (1-3)–(1-4).

These situations motivate the use of the column-and-constraint-generation algorithm [68], which is also an iterative procedure relying on a master problem and oracle subproblems. A key difference is that the column-and-constraint-generation algorithm provides much stronger primal cuts than the Benders decomposition. This method leverages the fact that the two lowermost levels correspond to a maximization, within a polyhedral uncertainty set $\mathcal{U}$, of a convex function given by the output of the inner minimization (1-3)–(1-4). Therefore, from standard results of convex analysis, one of the vertices belongs to the optimal solution set [44]. Unlike Benders decomposition, the column-and-constraint-generation algorithm adds to the master problem, at each iteration, the primal constraint (1-4) parameterized by the newly determined vertex $\mathbf{u}^*$. Another advantage over Benders decomposition is that the constraints generated by

column-and-constraint-generation algorithm do not rely on dual information from (1-3)–(1-4). This is particular useful for applying the method to cases where (1-3)–(1-4) is not convex, as in Chapter 2.

1.4 Document Structure and Contributions

This doctoral dissertation is structured as a compendium of five papers which are presented as chapters that can be read separately. Therefore, each Chapter 2–6 is an independent essay encompassing motivation, notation, introduction, and conclusion. All papers have been reformatted to fit this document requirements. Minimal rewording to the original work or inclusion of new graphs or tables has been performed to provide a better fit. The papers related to Chapters 2, 4, and 5 have been accepted/published, the paper for Chapter 3 has been submitted, and paper for Chapter 6 is under preparation for submission.

Chapter 2 addresses the $N-1$ security-constrained short-term scheduling problem, where the automatic primary response is explicitly considered. Specifically, under each contingent state, the nodal demands must be satisfied and the synchronized units generating below their limits are constrained to follow a linear model for primary response. The resulting formulation is a mixed-integer linear program since the primary response model introduces disjunctions to the scheduling problem. In the presence of these disjuntions, exact methods relying on traditional Benders' decomposition do not scale well. As an alternative, a tailored decomposition scheme that deals with a resulting nonconvex third-level problem is proposed. This scheme is based on modifications to the column-and-constraint-generation algorithm. The method involves procedures for preprocessing dedicated cuts and for numerically determining the post-contingency responses. Heuristics to generate high-quality primal solutions and upper bounds for the method are also discussed. Finally, the proposed method is tested on large-scale systems. The contents of this chapter are based on a paper accepted for the *Electric Power Systems Research* [69].

Chapter 3 also addresses the $N-1$ security-constrained short-term scheduling problem with automatic primary response of synchronized generators, although using a different approach from that of Chapter 2. As in [28, 48, 70–72] it is assumed that data from previous solves are available. The proposed approach involves deep neural networks that produces a function/policy which maps the vector of nodal net loads onto the nominal dispatch, disregarding power flow constraints and the automatic primary

response. The feasibility with respect to problem constraints is enforced by robust-based methods. First, inspired by [48], a Lagrangian dual scheme is adopted to penalize physical constraints included in the learning model. During the training phase, a first dedicated column-and-constraint-generation algorithm is applied directly to the leaning model to add new constraints, for a few critical contingent states, to be penalized in the Lagrangian dual scheme. In these constraints, a tailored approximation for the post-contingency generation is adopted to limit the number of predictors of the deep neural network model. After the training phase, a modified version of the column-and-constraint-generation algorithm from Chapter 2 is applied to find the nearest feasible solution to the prediction. The proposed approach is tested on large-scale systems.

Chapter 4 presents a two-stage robust unit commitment model for the day-ahead energy and reserve scheduling under high renewable integration. An alternative scenario-based framework whereby uncertain renewable generation is characterized by a polyhedral uncertainty set relying on the direct specification of its vertices is proposed. A simple, yet efficient, adaptive data-driven procedure is adopted to dynamically update the uncertainty set with observed daily renewable-output profiles. Within this setting, the proposed data-driven two-stage robust unit commitmeent model ensures protection against the convex hull of realistic scenarios empirically capturing the complex and time-varying intra-day spatial and temporal interdependences among renewable units. The resulting formulation is solved by the column-and-constraint-generation algorithm until ϵ-global optimality. Out-of-sample experiments reveal that the proposed approach is capable of attaining efficient solutions in terms of cost and robustness while keeping the model tractable and scalable. The contents of this chapter are based on the paper published in the *IEEE Transactions on Sustainable Energy* [73].

Chapter 5 describes a distributionally robust optimization approach for the transmission expansion planning problem, considering both long- and short-term uncertainties on the system demand and non-dispatchable renewable generation. On the long-term level, as is customary in industry applications, deep uncertainties arising from social and economic transformations, political and environmental issues, and technology disruptions are addressed by long-term scenarios devised by experts. In this setting, many exogenous long-term scenarios containing partial information about the random parameters, namely, the average and the support set, can be considered. For each long-term scenario, a conditional ambiguity set models the incomplete knowledge about the probability distribution of

the uncertain parameters in the short-term operation. Consequently, the mathematical problem is formulated as a distributionally robust model with multiple conditional ambiguity sets. The resulting infinite-dimensional problem is recast as an exact, although very large, finite mixed-integer linear programming problem. To circumvent scalability issues, a new enhanced-column-and-constraint-generation decomposition algorithm with an additional Dantzig–Wolfe procedure is proposed. In comparison to existing methods, the proposed decomposition scheme leads to a better representation of the recourse function and, consequently, tighter bounds. Numerical experiments based on the benchmark IEEE 118-bus system are reported to corroborate the effectiveness of the method. The contents of this chapter are based on the paper accepted for the *IEEE Transactions on Power Systems* [74].

On a different note, **Chapter 6** investigates the use of inducement prizes as a general mechanism to foster innovation in theoretical and computational aspects of power systems' models. It is argued that many structural changes mostly associated with market deregulation processes, technology disruptions on both demand and supply side, and new environmental constraints deeply modified the once stable and predictable power systems. It is also discussed that, as a consequence, important modeling and computational challenges arose for various operative horizons and that the main operations in power systems are increasingly based on the solution of complex and large optimization problems and/or forecasting methods. In view of these challenges, the use of prizes in power systems is contextualized in light of regulation measures that facilitated the implementation of open innovation initiatives in US public agencies and is motivated by prior experiences with inducement prizes on the industry and government levels to foster innovation in various fields. Particularly, we discuss the contest platform called *Grid Optimization* [75] proposed by the Advanced Research Projects Agency-Energy (ARPA-E) seeking to increase flexibility, safety, and the integration of non-dispatchable renewable generation. Finally, it is argued that the main operative decision-making challenges in power systems possess, at a very high degree, the main key features of the problems that are likely to have their solutions improved by a series of competitions and prizes. This qualitative analysis is mostly based on methodologies from the National Endowment for Science, Technology and the Arts (Nesta) [76].

2
An Exact and Scalable Problem Decomposition for Security-Constrained Optimal Power Flow

In this chapter, we present decomposition techniques for solving large-scale instances of the security-constrained optimal power flow (SCOPF) problem with primary response. Specifically, under each contingency state, we require that the nodal demands are met and that the synchronized units generating below their limits follow a linear model for primary response. The resulting formulation is a mixed-integer linear program since the primary response model introduces disjunctions to the SCOPF problem. Unfortunately, exact methods relying on traditional Benders' decomposition do not scale well. As an alternative, we propose a decomposition scheme based on the column-and-constraint-generation algorithm where we iteratively add disjunctions and cuts. We provide procedures for preprocessing dedicated cuts and for numerically determining the post-contingency responses based on the master problem solutions. We also discuss heuristics to generate high-quality primal solutions and upper bounds for the method. Finally, we demonstrate the efficiency of the proposed method on large-scale systems.

The contents of this chapter are based on a paper accepted for the *Electric Power Systems Research* [69].

2.1
Introduction

System reliability under contingencies has been widely discussed in the literature. In this context, the goal of the well-known security constrained optimal power flow (SCOPF) problem [77–83] is to produce a pre-contingency (or nominal) schedule for generators at minimal cost, such that it allows for feasible steady-state points of operation for a predefined set of *credible contingencies*. A review of the SCOPF problem, its challenges and trends is available in [80].

The specification of the set of credible contingencies varies in academic works. Generally, a loss of up to one or two elements (generators and/or transmission lines) is considered. Interesting discussions about credible contingencies and reserve requirements can be found in [78, 82] and the

references therein. Security criteria and regulation for reserves also vary across independent system operators. A survey about the requirements for reserves across U.S. ancillary services can be found in [84]. Without loss of generality, we consider the $N-1$ criterion for generators in this paper; that is, the system must operate under the loss of any individual generator.

Variants of the SCOPF problem include the *corrective* case [81] where re-scheduling is possible, and the *preventive* case where no re-dispatch occurs [79, 82]. In this work, we consider preventive SCOPF with *primary response* [82]. In this framework, the synchronized generators must be able to automatically respond to contingencies to restore the balance between loads and generation.

Even though SCOPF is a nonlinear and nonconvex problem [20, 21], for computational purposes, several authors adopt dc approximations [78, 79, 82, 83]. Some authors have dedicated works to address the quality of approximations or relaxations to practical situations [45,51,85,86] or to discuss how to exploit dc SCOPF solutions on more accurate ac SCOPF approaches [87]. Notwithstanding these relevant discussions, the focus of this work is to improve current industry approaches still based on dc SCOPF algorithms. In such models, stability constraints for the system are generally expressed as power flow limits. In practical applications, the solution provided by the dc model can be checked for ac power flow feasibility. Then, iterative and/or heuristic procedures can be applied to further restrict the dc power flow constraints until feasibility is reached.

The primary response of generators is explicitly modeled in [88] for a unit commitment application and in [82, 83], and [89] for SCOPF problems. In [82, 83], and [88] variables that represent the frequency drop in each contingency state were used to generate linear approximations of primary response. These variables are multiplied by parameters that represent the sensitivity of generators to frequency changes. Such frequency regulation parameters are related to *droop coefficients*. We refer the interested reader to the discussions about droop coefficients in [82] (and references therein) where, particularly, the authors argue that the co-optimization of the droop coefficient and the SCOPF might save on costs. In this work, we have also opted for the dc power flow approximation with a linear model for primary response. In summary, for each contingency state, we have substituted the single variable representing frequency drop adopted in [82] and [83] with a single global signal to generators (also a variable).

The SCOPF problem featuring automatic primary response of generators is a mixed-integer linear program (MILP) even under the dc relaxation. This

is because the constraints for the automatic response of generators may lead to power outputs above generator limits [88]. To remedy this, we require binary variables for each generator and for each contingency state to determine whether a generator is producing according to the constraints for automatic response or at its limit. The size of the problem is generally large. It is proportional to the number of contingencies since we are required to represent the network and the power flow variables for each post-contingency state.

The Benders' decomposition approach, which has often been applied to solve energy planning problems [8, 79, 81, 90], is a natural candidate to tackle the preventive SCOPF problem. Generally, in Benders' approaches, the extensive formulation is recast into a master problem and subproblems. The master problem for power systems applications usually solves the nominal dispatch, and the subproblems represent the redispatch or corrective actions under contingencies and/or uncertain scenarios. An iterative procedure that involves solving the master problem and subproblems is performed. During this process, Benders' cuts for the violated subproblems are added into the master problem. The process continues until all subproblems are feasible. A valuable review on the Benders' decomposition method can be found in [91].

Unfortunately, preventive SCOPF imposes challenges for the application of traditional Benders' decomposition since the subproblems are nonconvex. The constraints that enforce the primary response of synchronized generators contain binary variables. Despite such challenges, a solution method inspired by [8] considering nonconvex subproblems was provided in [82]. However, the optimality for this method is not guaranteed. An alternative that ensures optimality is to recast the master problem to include the constraints for the primary response. This modification, however, does not scale well since the number of binary variables increases quadratically with the number of synchronized generators (assuming the $N-1$ security criteria for generators).

In order to remedy the aforementioned limitations, we have devised an exact and scalable algorithm to tackle the preventive SCOPF problem with primary response. The focus of this work is on the computational and practical aspects of the solution methodology. The proposed decomposition scheme differs significantly from previously proposed solution methods. The outline of the method is as follows.

In the master problem we consider a nominal optimal power flow problem that accounts for valid constraints for each contingency state. We initially disregard the network for contingency states and the disjunctions (binary variables) in the master problem. This approach alleviates the computational burden required for solving the master problem. During the iterative process

only a small subset of the disjunctions and network constraints are introduced to the master problem by a column-and-constraint-generation algorithm (CCGA) [68]. In the proposed decomposition approach, the only optimization problem that is solved is the master problem. This is possible since we use: i) preprocessed structures based on the power transfer distribution factors (PTDF) that are useful both as feasibility checkers and as dedicated cuts in the post-contingency states, and ii) a numerical procedure that determines the post-contingency variables based solely on the nominal generation. The aforementioned preprocessed structures allow us to monitor the critical congested areas of the system. As it is necessary, these structures are transformed into constraints (that differ from Benders' cuts) that are added to the master problem. These cuts represent the network for the post-contingency states. Likewise, as it is necessary, we introduce the disjunctions (binary variables) representing the primary response model for a few contingency states into the master problem. We also propose a method to find high-quality primal solutions and a procedure that monitors the upper and lower bounds for the method.

In summary, the main contribution of this work is a decomposition approach that combines a column-and-constraint-generation algorithm with numerical methods to determine exact solutions to the SCOPF problem in such a way that the nonconvex subproblems do not need to be solved directly. We demonstrate that this approach is possible due to the presence of valid post-contingency constraints in the master problem and due to the preprocessed structures derived from a PTDF-based formulation.

The rest of this chapter is organized as follows: The notation is introduced in Section 2.2. In Section 2.3, the SCOPF model is introduced. The solution methodology is presented in Section 2.4. Numerical experiments are reported in Section 2.5. Finally, this paper is concluded in Section 2.6.

2.2 Nomenclature

This section introduces the notation of this chapter. We use bold symbols for matrices (uppercase) and vectors (lowercase). Additional symbols can be interpreted by the following general rules: Symbols with superscript "(j)" denote new variables, parameters or sets corresponding to the j-th iteration of the solution method. The symbols with superscript "$(*)$" denote the optimal value of the associated (iterating) variable.

Sets

$\mathcal{E}, \mathcal{E}_s$	Feasibility sets for the nominal power flow constraints and for the power flow constraints under contingency state s, respectively.
$\mathcal{F}_s$	Feasibility set for primary response constraints under contingency state s.
$\mathcal{G}, \mathcal{L}, \mathcal{N}$	Sets of generators, transmission lines and buses, respectively.
$\mathcal{H}$	Subset of $\mathcal{G}$ for devising primal solutions.
$\mathcal{S}$	Set of contingencies.
$\mathbb{S}$	Subset of $\mathcal{S}$ with disjunctive constraints, used in the column-and-constraint-generation algorithm.
$\mathcal{X}, \mathcal{X}_s$	Sets of power flow-related decision variables for nominal state and for contingency state s.
$\mathcal{Y}_s$	Set of decision variables associated with primary response under contingency state s.

Parameters

α, $\alpha_{s,l}$	Largest transmission line capacity violation and violation for transmission line l, under contingency state s.
β, β_1, β_2	Parameters for selecting preprocessed cuts.
$\boldsymbol{\gamma}$	Vector of parameters for primary response.
γ_i	Parameter for primary response of generator i.
ϵ	Tolerance for transmission line violation.
ε	Tolerance for the binary search procedure.
A, B	Line-bus and Generator-bus incidence matrices.
c	Vector of generation costs.
c_i	Generation cost of generator i.
d	Vector of nodal net loads.
e	Vector of ones with appropriate dimension.
e_s	Total load imbalance for contingency state s.

$\overline{\mathbf{f}}$	Vector of line capacities.
$\underline{\mathbf{g}}, \overline{\mathbf{g}}$	Vectors of lower and upper limits for generators.
$\hat{\mathbf{g}}$	Vector of capacities for generators.
$\overline{g}_i$	Upper limit for generator i.
$\hat{g}_i$	Capacity of generator i.
$\mathbf{K}_0$	Matrix of power transfer distribution factors.
$\mathbf{K}_1, \mathbf{k}_2$	Preprocessed structures for positive flow limits.
$\mathbf{K}_3, \mathbf{k}_4$	Preprocessed structures for negative flow limits.
M	Big-M.
lb, ub	Lower/upper bound for the decomposition method.
p	Parameter for primal solution approach.
$\overline{\mathbf{r}}$	Vector of primary response limits of generators.
$\overline{r}_i$	Primary response limit of generator i, given by $\gamma_i \hat{g}_i$.
$\mathbf{S}$	Angle-to-flow matrix.
z	Objective value of the master problem for the column-and-constraint-generation algorithm.
z_p	Objective value z when using the parameter p.

Nominal-state-related decision variables and vectors

$\boldsymbol{\theta}, \mathbf{f}, \mathbf{g}$	Phase angles, line flows, and nominal generation.
g_i	Generation of generator i in nominal state.

Contingency-state-related decision variables and vectors

$\boldsymbol{\theta}_s$	Vector of phase angles under contingency state s.
$\boldsymbol{\mu}_s$	Vector of dual variables associated with nodal load balance constraint under contingency state s.
$\mathbf{f}_s$	Vector for line flows under contingency state s.

$\mathbf{g}_s$	Vector for generation under contingency state s.
$\mathbf{g}_s^{'}$	Provisional vector for $\mathbf{g}_s$.
$g_{s,i}$	Generation of generator i under contingency state s.
$g_{s,i}^{'}$	Provisional variable for $g_{s,i}$.
n_s	Global signal under contingency state s.
$\mathbf{u}_s^+, \mathbf{u}_s^-$	Vectors of slack variables for line capacities.
$\mathbf{v}_s^+, \mathbf{v}_s^-$	Vectors of slack variables for nodal demand balance.
$\mathbf{x}_s$	Binary vector indicating whether generators reached $\overline{\mathbf{g}}$ under contingency state s.
$x_{s,i}$	Binary variable indicating whether generator i reached $\overline{g}_i$ under contingency state s.

2.3 SCOPF with Primary response Formulation

We assume a generic framework where a bid-based market for energy and reserve and/or unit commitment (UC) procedures have taken place hours before (or in the day before). We assume that, at the time the SCOPF is solved, the operator has precise forecasts for the few-minutes-ahead non-dispatchable generation, and nodal net loads. For notational conciseness we assume that all generators are synchronized.

2.3.1 Power Flow Constraints

We use the following dc power flow constraints:

$$\mathbf{A}\mathbf{f} + \mathbf{B}\mathbf{g} = \mathbf{d} \tag{2-1}$$

$$\mathbf{f} = \mathbf{S}\boldsymbol{\theta} \tag{2-2}$$

$$-\overline{\mathbf{f}} \leq \mathbf{f} \leq \overline{\mathbf{f}} \tag{2-3}$$

$$\underline{\mathbf{g}} \leq \mathbf{g} \leq \overline{\mathbf{g}} \tag{2-4}$$

$$\mathbf{A}\mathbf{f}_s + \mathbf{B}\mathbf{g}_s = \mathbf{d} \qquad \forall s \in \mathcal{S} \tag{2-5}$$

$$\mathbf{f}_s = \mathbf{S}\boldsymbol{\theta}_s \qquad \forall s \in \mathcal{S} \tag{2-6}$$

$$-\overline{\mathbf{f}} \leq \mathbf{f}_s \leq \overline{\mathbf{f}} \qquad \forall s \in \mathcal{S} \tag{2-7}$$

$$\mathbf{g}_s \leq \overline{\mathbf{g}} \qquad \forall s \in \mathcal{S}. \tag{2-8}$$

Constraints (2-1)–(2-4) model the power flow in the nominal state. Expression (2-1) represents nodal power balance under a dc power flow model, while Kirchhoff's second law is accounted for in (2-2). Transmission line limits and generator limits are enforced by (2-3) and (2-4), respectively. In (2-4), we allow generation bounds $\underline{\mathbf{g}}$ and $\overline{\mathbf{g}}$ to be different from the minimum and maximum ($\hat{\mathbf{g}}$) set points for the generators due to commitment and/or operational constraints. Analogously to block (2-1)–(2-4), the set of constraints (2-5)–(2-8) model the power flow under each contingency state s.

2.3.2 Primary Response Model

The primary response under contingency state s is modeled by a global signal[1] n_s sent to all synchronized generators. This approach differs from those of [82] and [83], where variables representing frequency drops under contingency states are considered. We assume that the response of generator i is proportional to its capacity $\hat{g}_i$ and also to a predefined coefficient γ_i that is associated with the droop coefficient. Hence, under s, the automatic response of synchronized generator i is given by $g_{s,i} - g_i = n_s \gamma_i \hat{g}_i$, with the additional constraints that $g_{s,i} \leq \overline{g}_i$. Mathematically, we have

$$g_{s,i} = \min\{g_i + n_s \gamma_i \hat{g}_i,\ \overline{g}_i\} \qquad \forall i \in \mathcal{G}, \forall s \in \mathcal{S}, i \neq s \qquad (2\text{-}9)$$

$$g_{s,s} = 0 \qquad \forall s \in \mathcal{S}. \qquad (2\text{-}10)$$

By using traditional MILP modeling techniques to rewrite (2-9)–(2-10), we obtain

$$|g_{s,i} - g_i - n_s \gamma_i \hat{g}_i| \leq \overline{g}_i(1 - x_{s,i}) \qquad \forall i \in \mathcal{G}, \forall s \in \mathcal{S}, i \neq s \qquad (2\text{-}11)$$

$$g_i + n_s \gamma_i \hat{g}_i \geq \overline{g}_i(1 - x_{s,i}) \qquad \forall i \in \mathcal{G}, \forall s \in \mathcal{S}, i \neq s \qquad (2\text{-}12)$$

$$g_{s,i} \geq \overline{g}_i(1 - x_{s,i}) \qquad \forall i \in \mathcal{G}, \forall s \in \mathcal{S}, i \neq s \qquad (2\text{-}13)$$

$$n_s \in [0, 1] \qquad \forall s \in \mathcal{S} \qquad (2\text{-}14)$$

$$x_{s,i} \in \{0, 1\} \qquad \forall i \in \mathcal{G}, \forall s \in \mathcal{S} \qquad (2\text{-}15)$$

$$g_{s,s} = 0 \qquad \forall s \in \mathcal{S}. \qquad (2\text{-}16)$$

2.3.3

[1] An alternative interpretation is that n_s mimics the system's response which is required for adjusting the power (or frequency) imbalance. The physical interpretation for the limitation of 1 to n_s is that γ_i multiplied by capacity is the maximum deliverable reserve or maximum ramp for a given time frame.

Extensive Formulation for the SCOPF Problem

The SCOPF problem is modeled as a MILP, where we minimize the cost of nominal generation in the objective function subject to constraints (2-1)–(2-8) and (2-11)–(2-16). For conciseness, we define $\mathcal{X} = [\mathbf{g}, \mathbf{f}, \boldsymbol{\theta}]$, $\mathcal{X}_s = [\mathbf{g}_s, \mathbf{f}_s, \boldsymbol{\theta}_s]$, and $\mathcal{Y}_s = [\mathbf{g}, \mathbf{g}_s, \mathbf{x}_s, n_s]$. Let $\mathcal{Y}_s \in \mathcal{F}_s$ denote the disjunctions related to (2-11)–(2-16) while $\mathcal{X} \in \mathcal{E}$ and $\mathcal{X}_s \in \mathcal{E}_s$ denote the power flow constraints in nominal ((2-1)–(2-4)) and contingency states ((2-5)–(2-8)) respectively. The extensive formulation for the SCOPF problem, labeled as EF method, is as follows

$$\min_{\mathcal{X}, [\mathcal{X}_s, \mathbf{x}_s, n_s]_{s \in \mathcal{S}}} \mathbf{c}^\top \mathbf{g} \tag{2-17}$$

subject to:

$$\mathcal{X} \in \mathcal{E} \tag{2-18}$$

$$\mathcal{X}_s \in \mathcal{E}_s \qquad \forall s \in \mathcal{S} \tag{2-19}$$

$$\mathcal{Y}_s \in \mathcal{F}_s \qquad \forall s \in \mathcal{S}. \tag{2-20}$$

2.4 Solution Methodology

In this work we focus on methods that guarantee optimality for the SCOPF problem. A Benders' decomposition with valid post-contingency constraints in the master problem is presented in Section 2.4.1. Preprocessed structures for feasibility checking and cut generation are presented in Section 2.4.2, while a useful binary search is introduced in Section 2.4.3. The CCGA is described in Section 2.4.4. A method for finding high-quality primal solutions is presented in Section 2.4.5.

2.4.1 Modified Benders' Decomposition

The intuitive Benders' decomposition approach for (2-17)–(2-20) is to define the master problem as the nominal schedule, associated with (2-17)–(2-18), and the subproblems as the separable feasibility recourse problems enforcing (2-19)–(2-20) for each $s \in \mathcal{S}$. Unfortunately, this approach introduces nonconvexities to the subproblems [82], and thus, does not guarantee optimality.

In order to ensure the convexity of the subproblems, and thus optimality for the method, we define the subproblems as feasibility-like problems for the constraints in (2-19). As part of the modification, we also add the following

valid post-contingency constraints to the master problem:

$$\mathbf{e}^\top \mathbf{g}_s = \mathbf{e}^\top \mathbf{d} \qquad \forall s \in \mathcal{S}. \tag{2-21}$$

The purpose of (2-21) is to strengthen the master problem with the necessary post-contingency condition that the total generation and the total load are equal. By also enforcing (2-8) we guarantee that post-contingency generation is within bounds. We define the master problem[2] as

$$\min_{\mathcal{X},[\mathbf{g}_s,\mathbf{x}_s,n_s]_{s\in\mathcal{S}}} \mathbf{c}^\top \mathbf{g} \tag{2-22}$$

subject to:

$$(2\text{-}18) \tag{2-23}$$

$$(2\text{-}8), (2\text{-}20), (2\text{-}21) \qquad \forall s \in \mathcal{S}. \tag{2-24}$$

The subproblem for each $s \in \mathcal{S}$, where $\mathbf{g}_s^{(*)}$ is the solution determined in (2-22)–(2-24), is then defined as

$$\min_{\mathbf{v}_s^+,\mathbf{v}_s^-,\mathbf{f}_s,\mathbf{g}_s,\boldsymbol{\theta}} \mathbf{e}^\top(\mathbf{v}_s^+ + \mathbf{v}_s^-) \tag{2-25}$$

subject to:

$$(2\text{-}6), (2\text{-}7) \tag{2-26}$$

$$\mathbf{g}_s = \mathbf{g}_s^{(*)} \qquad : \boldsymbol{\mu}_s \tag{2-27}$$

$$\mathbf{A}\mathbf{f}_s + \mathbf{B}\mathbf{g}_s = \mathbf{d} + \mathbf{v}_s^+ - \mathbf{v}_s^-. \tag{2-28}$$

A feasibility Benders' cut is then added to the master problem at each iteration, for each s that is not feasible; that is, $\forall s \in \mathcal{S}$ such that $\mathbf{e}^\top(\mathbf{v}_s^{+(*)} + \mathbf{v}_s^{-(*)}) > \epsilon$, where ϵ is a tolerance level for the net load imbalance. The Benders' cut for s is as follows: $\mathbf{e}^\top(\mathbf{v}_s^{+(*)} + \mathbf{v}_s^{-(*)}) + \boldsymbol{\mu}^\top(\mathbf{g}_s - \mathbf{g}_s^{(*)}) \leq 0$. We label this approach as the BD method.

2.4.2 Precomputation of Dedicated Cuts

In this subsection, an alternative method named BDDC is introduced. Unlike the BD method that involves subproblems that generate Benders' cuts, the BDDC method uses preprocessed structures as feasibility checkers and to generate cuts. These structures, that are also applied in the CCGA of Section 2.4.4, are based on the PTDF formulation for dc power flow.

[2]There are two main difference with respect to the EF: Line constraints (2-6)–(2-7) are not included, and constraint (2-5) is substituted by (2-21).

In the BDCC method, we have the same master problem (2-22)–(2-24) as the BD method. Thus, $\mathbf{g}_s^{(*)}$ is determined in (2-22)–(2-24), where the primary response constraints (2-20) and the post-contingency generation constraints (2-8) and (2-21) are enforced.

The aforementioned preprocessed structures are constructed directly from the PTDF-based formulation for the dc power flow. This formulation, for contingency state s, is as follows:

$$\min_{\mathbf{u}_s^-, \mathbf{u}_s^+} \mathbf{0} \tag{2-29}$$

subject to:

$$-\overline{\mathbf{f}} + \mathbf{u}_s^- = \mathbf{K}_0(\mathbf{d} - \mathbf{B}\mathbf{g}_s^{(*)}) = \overline{\mathbf{f}} - \mathbf{u}_s^+ \tag{2-30}$$

$$\mathbf{u}_s^-, \mathbf{u}_s^+ \geq \mathbf{0}. \tag{2-31}$$

In (2-30), $\mathbf{g}_s^{(*)}$ is a solution determined by (2-22)–(2-24) and $\mathbf{K}_0$ is the PTDF matrix. A similar description for (2-30) is presented in [92]. We highlight that (2-8) and (2-21) are enforced in the master problem and therefore are not necessary in (2-29)–(2-31). As opposed to the subproblems of the BD method we do not allow nodal imbalance in (2-29)–(2-31). Thus, a given master problem solution $\mathbf{g}_s^{(*)}$ is feasible under contingency state s if there is a feasible solution $\mathbf{u}_s^-$, $\mathbf{u}_s^+$ for (2-29)–(2-31).

In this work we assume that we have more lines $|\mathcal{L}|$ than buses $|\mathcal{N}|$ and that there are no isolated buses. Under these assumptions and because we enforce (2-8) and (2-21) in the master problem, we do not need to solve (2-29)–(2-31) to check for feasibility in post-contingency states or to obtain cuts. Manipulating (2-30), we derive the preprocessed structures:

$$(\mathbf{u}_s^+) : \mathbf{K}_1\mathbf{g}_s + \mathbf{k}_2 \geq \mathbf{0} \tag{2-32}$$

$$(\mathbf{u}_s^-) : \mathbf{K}_3\mathbf{g}_s + \mathbf{k}_4 \geq \mathbf{0}. \tag{2-33}$$

Interestingly, the matrices $\mathbf{K}_1$, $\mathbf{K}_3$ and the vectors $\mathbf{k}_2$, $\mathbf{k}_4$ can be efficiently precomputed[3] and are the same for all $s \in \mathcal{S}$. Another feature is that (2-32) and (2-33) are directly associated with the transmission lines of the system, relating either to the positive (2-32) or negative (2-33) limits. By inspecting solutions $\mathbf{g}_s$ on (2-32)–(2-33) it is possible to verify the existence of violated lines and the intensity of violations (in MW) under each contingency state.

[3]The incorporation of line outages as part of the set of credible contingencies would require the precomputation of different structures for $\mathbf{K}_1$, $\mathbf{K}_3$, $\mathbf{k}_2$, and $\mathbf{k}_4$. This would lead to a linear increase in the size of the precomputed data for the problem (as many as the line contingencies). This would not present a significant computational obstacle.

The algorithm for the BDDC method involves adding rows of (2-32) and (2-33) as lazy constraints to problem (2-22)–(2-24). We do not require that an optimal solution $\mathbf{g}_s$ is found. Whenever a feasible (suboptimal) integer solution is determined by the solver, as a subroutine, we check the feasibility of $\mathbf{g}_s$ using (2-32) and (2-33). We define $\alpha_{s,i}$ as the violation of line l, for contingency state s and α as the largest violation among all transmission lines for all s. We then add to (2-22)–(2-24) as lazy constraints the rows of both (2-32) and (2-33) corresponding to violated lines such that $\alpha_{s,l} > \alpha/\beta_1$, where β_1 is a parameter. We stop the algorithm when α is smaller than a defined tolerance ϵ. This procedure converges in finite steps since adding all rows of (2-32) and (2-33), for every $s \in \mathcal{S}$, to (2-22)–(2-24) results in a problem which is equivalent to (2-17)–(2-20).

Unfortunately, the application of the BDDC method alone is not scalable since its master problem contains all the binary variables. Before proceeding to the proposed CCGA (Section 2.4.4), we introduce next a useful binary search procedure.

2.4.3 Numerical Procedure for Calculating the Global Signal

Under the primary response model, the post-contingency generation for s; that is, $\mathbf{g}_s$, is defined by the combination of the nominal schedule $\mathbf{g}^{(*)}$ and the global signal $n_s^{(*)}$. Namely, given $\mathbf{g}^{(*)}$ and $n_s^{(*)}$, it is straightforward to compute $\mathbf{g}_s^{(*)}$ by applying the relations in (2-11)–(2-16).

Interestingly, $n_s^{(*)}$ can also be calculated from $\mathbf{g}^{(*)}$. This is achieved by a binary search for n_s for each $s \in \mathcal{S}$. The binary search is possible in this case since, for a fixed $\mathbf{g}^{(*)}$, each component of $\mathbf{g}_s$ is monotone with respect to n_s. Thus, despite the presence of the disjunctions, we only need to find the correct $n_s^{(*)}$ that results in a vector $\mathbf{g}_s^{(*)}$ that satisfies the total net demand. Given the fast convergence of the binary search, the tolerance ε can be set to very small values. This procedure is described next.

Algorithm Binary Search(s, ε, $\mathbf{g}^{(*)}$)

Initialization: $j \leftarrow 0$ and $n_s^{(0)} \leftarrow 0.5$
for $i \in \mathcal{G}, i \neq s$ **do**
  if $g_i^{(*)} + n_s^{(j)} \gamma_i \hat{g}_i \geq \overline{g}_i$ **then:** $g_{s,i}^{(j)} \leftarrow \overline{g}_i$
  else: $g_{s,i}^{(j)} \leftarrow g_i^{(*)} + n_s^{(j)} \gamma_i \hat{g}_i$
  end if
end for
$g_{s,s}^{(j)} \leftarrow 0$; $e_s \leftarrow (\mathbf{e}^\top \mathbf{g}_s - \mathbf{e}^\top \mathbf{d})$.
if $|e_s| \leq \varepsilon$ **then:** $n_s^{(*)} \leftarrow n_s^{(j)}$, $g_{s,i}^{(*)} \leftarrow g_{s,i}^{(j)}, \forall i \in \mathcal{G}$ and **BREAK**
else if: $e_s > 0$ **then:** $n_s^{(j+1)} \leftarrow n_s^{(j)}/2$
else: $n_s^{(j+1)} \leftarrow (1 + n_s^{(j)})/2$
end if
$j \leftarrow j + 1$; Go to step 2.

2.4.4 Column-and-Constraint-Generation Algorithm

We define the master problem for the CCGA as follows

$$z = \min_{\mathcal{X}, [\mathbf{g}_s']_{s\in\mathcal{S}}, [\mathbf{x}_s, n_s]_{s\in\mathbb{S}}} \mathbf{c}^\top \mathbf{g} \tag{2-34}$$

subject to:

$$(2\text{-}18) \tag{2-35}$$

$$\mathbf{g}_s' - \mathbf{g} \leq \overline{\mathbf{r}} \qquad \forall s \in \mathcal{S} \tag{2-36}$$

$$(2\text{-}8), (2\text{-}16), (2\text{-}21) \qquad \forall s \in \mathcal{S} \tag{2-37}$$

$$(2\text{-}20) \qquad \forall s \in \mathbb{S}. \tag{2-38}$$

Note that, as opposed to the BDDC method, in (2-38) we define a different set of contingency states $\mathbb{S}$ for the disjunctive constraints (starting with $\mathbb{S} = \emptyset$). We also abuse notation by using $\mathbf{g}_s'$ as a provisional variable for the post-contingency generation replacing $\mathbf{g}_s$ in (2-36) and (2-37). We performed this substitution to make explicit that $\mathbf{g}_s$ is not determined in (2-34)–(2-38) for the entire iterative process. The determination of $\mathbf{g}_s$ in (2-34)–(2-38) would only be possible in the presence of the disjunctive constraints (2-20) for s. These disjunctive constraints are not initially present in (2-34)–(2-38) for computational purposes. In fact, the determination of $\mathbf{g}_s$ is performed by the binary search algorithm, which requires only $\mathbf{g}$ and tolerance as inputs. The purpose of $\mathbf{g}_s'$ in (2-36) and (2-37) is to guarantee that $\mathbf{g}$ is determined in such a way that the binary search algorithm is capable of enforcing the primary response compatibility to $\mathbf{g}_s$, while meeting the global demand. That is, for each s, $|\mathbf{e}^\top \mathbf{g}_s - \mathbf{e}^\top \mathbf{d}| \leq \epsilon$.

In order to verify the above claim, note that by (2-36) and (2-8), $g'_{s,i} \leq \min\{\overline{g}_i, g_i + \gamma_i \hat{g}_i\}$ for each i and s, where $g'_{s,i}$ is the i-th element of $\mathbf{g}'_s$. Fixing $n_s = 0$ in the binary search algorithm implies $\mathbf{g}_s = \mathbf{g}$, except for $g_{s,s} = 0$. If instead we set $n_s = 1$ then $g_{s,i} = \min\{\overline{g}_i, g_i + \gamma_i \hat{g}_i\} \geq g'_{s,i}$ for each i and s, with $i \neq s$. For $i = s$, we have that $g'_{s,s} = g_{s,s} = 0$. Thus, since $\mathbf{g}'_s$ meets the global demand, it is always the case that $\mathbf{e}^\top \mathbf{g}_s \geq \mathbf{e}^\top \mathbf{g}'_s = \mathbf{e}^\top \mathbf{d}$ by choosing $n_s = 1$. By the monotonicity and continuity of $g_{s,i}$ with respect to n_s for a given g_i, there is a value $n_s^{(*)}$ that results in $\mathbf{g}_s^{(*)}$ that satisfies the global demand and preserves the primary response model.

At each iteration j of the CCGA, we solve the master problem (2-34)–(2-38) to obtain $\mathbf{g}^{(j)}$ and $z^{(j)}$. Then, for each $s \in \mathcal{S}$, we perform the binary search algorithm to define $\mathbf{g}_s^{(j)}$ according to the primary response model. Next, for all s, we check feasibility of the solutions $\mathbf{g}_s^{(j)}$ using (2-32) and (2-33). We use $\alpha_{s,i}^{(j)}$ to define the violation of each line l, for each contingency state s and we use $\alpha^{(j)}$ as the largest violation among all transmission lines for all s. We identify the contingency state $s^{(j)}$ that contains the most violated line. If $s^{(j)} \in \mathbb{S}$ we skip the rest of this step. Otherwise we set $\mathbb{S} = \mathbb{S} \cup s^{(j)}$ which means including the disjunctions (2-20) for $s^{(j)}$ into (2-34)–(2-38).

We also add to (2-34)–(2-38) the rows of both (2-32) and (2-33) corresponding to violated lines using two criteria: i) For the post-contingency states $s \in \mathbb{S}$ we include the lines where $\alpha_{s,l}^{(j)} > \alpha^{(j)}/\beta_1$. ii) For the post-contingency states $s \notin \mathbb{S}$ we include the lines where $\alpha_{s,l}^{(j)} > \alpha^{(j)}/\beta_2$. The objective of this step is to enforce the network constraints for critical lines in post-contingency states. Typically, $\beta_1 > \beta_2$. We are stricter with the states $s \in \mathbb{S}$ since defining tight parameters for contingency states without corresponding disjunctions may lead to the inclusion of many constraints at a time. A user defined tolerance ϵ (in MW) for maximum line violation is used to stop the iterative process. The CCGA is described next.

Algorithm CCGA(ε, ϵ, β_1, β_2)

Initialization: $j \leftarrow 0$, $\mathbb{S} \leftarrow \emptyset$.
Solve master problem (2-34)–(2-38) to obtain $\mathbf{g}^{(j)}$
for $s \in \mathcal{S}$ **do**
    Apply Binary Search(s, ε, $\mathbf{g}^{(*)}$) to obtain: $z^{(j)}$, $\mathbf{g}_s^{(j)}, n_s^{(j)}$
    for $\forall l \in \mathcal{L}$ **do**
        Compute $\alpha_{s,l}^{(j)}$ as the maximum between violation of (2-32) and violation of (2-33)
    end for
end for
Compute $\alpha^{(j)}$ as the maximum among all $\alpha_{s,l}^{(j)}$
Identify the state $s^{(j)}$ associated with $\alpha^{(j)}$
if $s^{(j)} \notin \mathbb{S}$ **then:** $\mathbb{S} \leftarrow \mathbb{S} \cup s^{(j)}$ (add (2-20) for $s^{(j)}$ to (2-34)–(2-38))
end if
for $s \in \mathcal{S}$ **do**
    if $s \in \mathbb{S}$ **then:** $\beta \leftarrow \beta_1$
    else: $\beta \leftarrow \beta_2$
    end if
    for $l \in \mathcal{L}$ **do**
        if $\alpha_{s,l}^{(j)} > \alpha^{(j)}/\beta$
            if cuts (2-32)–(2-33) for the pair (l,s) are not yet added to master problem
                then: add cuts (2-32)–(2-33) for contingency state s, line l to master problem
        end if
    end for
end for
if $\alpha^{(j)} < \epsilon$ **then:** $z^{(*)} \leftarrow z^{(j)}$, $\mathbf{g}^{(*)} \leftarrow \mathbf{g}^{(j)}$; **BREAK**
else: $j \leftarrow j + 1$; Go to step 2.
end if.

2.4.5 Finding High-Quality Primal Solutions and Monitoring the Optimality Gap using the CCGA

Because very large cases might still impose computational challenges, we propose a procedure for finding feasible primal solutions. This procedure restricts the disjunctions in (2-20) to a subset of synchronized generators $\mathcal{H} \subset \mathcal{G}$. The generators in $\mathcal{G} \setminus \mathcal{H}$ respond with $g_{s,i} - g_i = n_s \gamma_i \hat{g}_i$; that is, we define $x_{s,i} = 1, \forall s \in \mathcal{S}, \forall i \in \mathcal{G} \setminus \mathcal{H}, i \neq s$.

The following criterion is used for defining $\mathcal{H}$. We rank the synchronized generators according to a "cost/limit" index ($c_i/\overline{g}_i$) and define $\mathcal{H}$ as the $p\%$ generators with lowest ranks, where p is a parameter. The objective value of the problem using this approach is denoted as $z_p^{(*)}$. Note that $z_{100}^{(*)} = z^{(*)}$.

This approach reduces the number of binary variables and thus the complexity of the problem. It is then a tool for finding upper bounds for (2-17)–(2-20). If we apply CCGA(ε, ϵ, β_1, β_2) using the proposed primal

method; i.e., setting $x_{s,i} = 1, \forall s \in \mathcal{S}, \forall i \in \mathcal{G} \setminus \mathcal{H}$ in (2-34)–(2-38) we obtain $ub = z_p^{(*)}$ as a valid upper bound. If the problem is infeasible for p then $z_p^{(*)} \leftarrow \inf$.

Note, however, that a procedure that monitors the optimality gap is still required. A lower bound for (2-17)–(2-20) is not obtained for $p < 100$. Conversely, solving for $p = 100$ generates upper bounds only after a feasible solution is found. This typically occurs in the later iterations when the tolerance ϵ for all lines in every contingency state is achieved.

We propose a simple strategy that monitors the bounds. Note that solving the SCOPF with the CCGA for low values of p tends to be faster than for high values of p. Thus, we start $p = 0$ and increase it sequentially. The solution for each $p < 100$ provides an upper bound for (2-17)–(2-20). As a parallel procedure, we solve for $p = 100$ to obtain valid lower bounds. Namely, for each iteration j of the CCGA for $p = 100$, a valid lower bound is defined as the best bound provided by the solver. This procedure monitors the gap efficiently.

2.5 Computational Experiments

We compared the proposed CCGA with two solution methods: EF and BDDC described in Sections 2.3.3 and 2.4.2.

We performed simulations for various values of $\boldsymbol{\gamma}$, β_1, and β_2. Our results indicate that varying the parameters may impact the performance of the CCGA. However, the dominance of the CCGA over other methods (EF and BDDC) was a constant, despite the parameterization. We have reported results for $\beta_1 = 5$, $\beta_2 = 1.2$, and $\gamma_i = 0.05$ for all $i \in \mathcal{G}$.

We used Gurobi 8.1.1 under the modeling package JuMP 0.18.5 for Julia Language 0.6.4 on a Xeon E5-2680 processor at 2.5 GHz and 128 GB of RAM. We set the optimality gap of Gurobi to 0.5% for the EF method and BDDC method as well as for the master problem of the CCGA. The maximum line violation was set to $\epsilon = 0.05$ MW and the precision for the binary search algorithm to $\varepsilon = 10^{-10}$ MW.

The data are based on modified versions of the benchmark systems presented in [93]. The size of the instances for the EF method, after Gurobi's presolve, are reported in Table 3.1.

2.5.1 Solution Method Comparison

Table 2.2 provides the computational times for selected methods and the number of iterations for the CCGA method in parentheses. The CCGA

System	Continuous Variables	Binary Variables	Linear Constraints
118 IEEE	10,604	2,862	19,137
1354 PEGASE	323,571	63,455	513,677
1888 RTE	387,979	79,032	624,780
1951 RTE	563,273	149,370	1,010,994
2848 RTE	1,104,192	276,822	1,934,115
2868 RTE	1,284,568	348,036	2,328,081
6468 RTE	5,067,009	1,563,640	9,756,668

Table 2.1: Instance Size for the EF method after Presolve

System	Solution Method		
	EF	BDDC	CCGA
118 IEEE	46.2	27.6	8.0 (4)
1354 PEGASE	T	T	138.0 (12)
1888 RTE	T	2,899.0	14.0 (4)
1951 RTE	T	T	16.2 (4)
2848 RTE	T	T	26.6 (4)
2868 RTE	T	T	31.0 (3)
6468 RTE	T	T	7,881.6 (18)

T - Time limit of 4 hours exceeded.

Table 2.2: Comparative CPU times (s) and number of iterations

dominates the other methods, which were only able to solve the 118 IEEE case within a reasonable time limit. For this instance, the CCGA required less than one third of the time of the BDDC method and less than one fifth of the time of the EF mehod. The only other instance that the BDDC method was able to solve in less than 4 hours was the 1888 RTE. The CCGA was more than 200 times faster for this instance. Interestingly, the number of iterations required by the CCGA is generally small, implying that the CCGA solved far less complex MILPs than the other methods. The only instance that posed difficulties for the CCGA was the 6468 RTE that contains more than 6,000 buses, 1,200 generators, and 9,000 transmission lines. Nevertheless, a solution for the optimality gap of 0.5% was achieved in less than 3 hours.

Interestingly, as reported next, it is possible to determine high-quality solutions in competitive computational times for large systems by applying the primal method of Section 2.4.5.

2.5.2

p	Cost (10^3 \$)	Cost Gap (%)	Time (s)	Iter. (#)
100	1624.8	0.00	7881.6	18
10	1625.8	0.02	813.5	17
0	1628.7	0.25	481.2	16

Table 2.3: Primal Approach for the 6468 RTE System

p	Cost (10^3 \$)	Cost Gap (%)	Time (s)	Iter. (#)
100	1190.6	0.00	138.0	12
50	1192.6	0.17	64.7	11
10	1195.4	0.40	21.1	11
0	1208.3	1.49	9.4	10

Table 2.4: Primal Approach for the 1354 PEGASE System

Finding Primal Solutions and Determining Bounds

The method of Section 2.4.5 for defining primal solutions was applied for the 6468 RTE and 1354 PEGASE systems. CCGA was used to solve the SCOPF problem for different values of p to an optimality gap of 0.5%. The results are summarized in Tables 2.3 and 2.4. Columns 1 and 2 present the cost and the relative cost gap for each p with respect to the cost achieved by $p = 100$. Columns 3 and 4 report the required computational time and number of iterations.

For the 6468 RTE system (Table 2.3) the result is quasi-optimal even for $p = 0$. For the 1354 PEGASE system (Table 2.4) the solution for $p = 0$ is already competitive, and required 9.4 seconds only. By increasing the complexity of the problem to $p = 10$, the cost gap is reduced by more than 1% for a reasonable solution time of 21.1 seconds. For $p = 50$, the CCGA required 64.7 seconds to converge, achieving a negligible cost gap of 0.17.

Despite the good results for small values of p, the cost gap is not observable before solving for $p = 100$. Thus, we adopted the strategy of Section 2.4.5 for obtaining bounds. We used multi-threading to solve problems in parallel. In the first thread we solved a sequence of problems for increasing values of p, starting with $p = 0$. We have stored the costs and times for the solutions of each p. In the second thread we solved for $p = 100$ and recorded solving time and the best bound of each iteration provided by Gurobi. A convergence plot from applying this method to the 1354 PEGASE system is

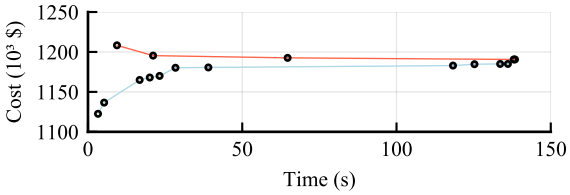

Figure 2.1: Bounds for the 1354 PEGASE system.

illustrated in Fig. 2.1. The proposed strategy yields the true optimality gap and is a useful decision-making tool for system operators.

2.6 Conclusion

We presented an exact and scalable column-and-constraint-generation algorithm for the SCOPF problem with primary response of generators. Under the proposed framework, we add the disjunctions as necessary in an iterative process that does not involve subproblems. This is possible by a scheme that involves a master problem with valid post-contingency constraints, preprocessed structures that serve both as feasibility checkers and delayed cuts, and a numerical procedure that reduces the complexity of the master problem by exogenously calculating the nonconvex primary response. We also proposed a procedure for finding high-quality primal solutions that helps monitor the bounds for the method. As shown by the computational experiments, this approach scales to large instances of the SCOPF problem with primary response.

In future works we will generalize these techniques. As a first step, convexifications of ac power flow, such as those studied in the recent works of Coffrin and Van Hentenryck [45, 51], will be used to model the system's response after contingencies.

3
Combining Deep Learning and Optimization for Security-Constrained Optimal Power Flow

The security-constrained optimal power flow (SCOPF) is fundamental in power systems and connects the automatic primary response (APR) of synchronized generators with the short-term schedule. Every day, the SCOPF problem is repeatedly solved for various inputs to determine robust schedules given a set of contingencies. Unfortunately, the modeling of APR within the SCOPF problem results in complex large-scale mixed-integer programs, which are hard to solve. To address this challenge, leveraging the wealth of available historical data, this chapter proposes a novel approach that combines deep learning and robust optimization techniques. Unlike recent machine-learning applications where the aim is to mitigate the computational burden of exact solvers, the proposed method predicts directly the SCOPF implementable solution. Feasibility is enforced in two steps. First, during training, a Lagrangian dual method penalizes violations of physical and operations constraints, which are iteratively added as necessary to the machine-learning model by a Column-and-Constraint-Generation Algorithm (CCGA). Second, another different CCGA restores feasibility by finding the closest feasible solution to the prediction. Experiments on large test cases show that the method results in significant time reduction for obtaining feasible solutions with an optimality gap below 0.1%.

3.1
Introduction

3.1.1
Motivation

Power systems operations require constant equilibrium between nodal loads and generation. At the scale of seconds, this balance is achieved by *Automatic Primary Response* (APR) mechanisms that govern the *synchronized generators*. For longer time scales, ranging from a few minutes to hours or even days ahead, this balance is obtained by solving mathematical optimization problems, as independent system operators seek consistent and efficient

schedules satisfying complex physical and operational constraints. The need to solve these optimization problems in a timely manner is driving intense research about new models and algorithms, both in industry and academia. In this vein, this work aims at speeding up solution times of security-constrained optimal power flow (SCOPF) problem [77–83] by combining deep learning and robust optimization methods. The SCOPF is solved by operators every few minutes for different sets of bus loads. The high penetration of renewable sources of energy has increased the frequency of these optimizations. The SCOPF problem considered in this work links the APR to the very short-term schedule. It is also relevant to mention that the SCOPF problem is directly or indirectly present in many other power system applications, including security-constrained unit commitment [94], transmission switching [95], and expansion planning [96]. Thus, a reduction in the computational burden would allow system operators to introduce important modeling improvements to many applications.

3.1.2 Contextualization and Related Work

The SCOPF problem determines a least-cost pre-contingency generator dispatch that allows for feasible points of operation for a set of *contingencies*, e.g., individual failures of main lines and/or generators. The SCOPF problem may refer to the *corrective* case [81] where re-scheduling is deemed possible and to the *preventive* case where no re-dispatch occurs [69, 79, 82], i.e., the system must be able to achieve a feasible steady-state point without a new schedule. A valuable review of the SCOPF problem and solution methods is available in [80]. Interesting discussions about credible contingencies, reserve requirements, security criteria, and regulation for reserves can be found in [78, 82, 84] and the references therein. Without loss of generality, the $N-1$ security criterion for generators is adopted in this chapter, i.e., the system must operate under the loss of any single generator.

The SCOPF is a nonlinear and nonconvex problem based on the AC optimal power flow (OPF) equations. Extensive reviews can be found in [20] and [21]. The DC formulation of the SCOPF has been widely used in both academia and industry [78, 79, 82, 83]. Interesting discussions regarding the quality of approximations and relaxations of the OPF problem can be found in [45, 51, 85, 86]. The DC-SCOPF can also be used to improve AC-SCOPF approaches [87]. It is not within the scope of this work to discuss the quality of aforementioned approximations or relaxations to the optimal power flow. Instead, this research offers a new approach that improves current industry

practices, which is still strongly based on DC-SCOPF.

The APR of synchronized generators is essential for stability. These generators respond automatically to frequency variations, caused by power imbalances for instance, by adjusting their power outputs until frequency is normalized and the power balance is restored. Unfortunately, the APR deployment, which is bounded by generators limits only, may result in transmission line overloads [69, 82, 97]. Therefore, this work co-optimizes the APR of synchronized generators within the (preventive) SCOPF problem. Even though the APR behavior is nonlinear, linear approximations are used in practice [98]. In [69, 82, 83, 88, 89], the APR is modeled by a single variable representing frequency drop (or power loss) for each contingency state and by a participation factor for each generator.

The DC-SCOPF problem with APR is referred to as the SCOPF problem for conciseness in this chapter. It admits an exact *extensive formulation* (with all variables and constraints for nominal state and contingency states) as a mixed-integer linear program (MILP) [69, 82]. Nevertheless, this formulation is generally very large because the APR constraints require binary variables for each generator and for each contingency state to determine whether generators are producing according to the linear response model or are at their limits [69, 82]. Thus, the number of binary variables increases quadratically with the number of generators, which makes the extensive form of the SCOPF impractical. Better modeling strategies and decomposition schemes are required.

The robust optimization framework has been widely applied in power systems due to its interesting tradeoff between modeling capability and tractability. See [99] for a review of robust optimization applications in power systems. The SCOPF problem can be modeled as a two-stage robust optimization or adaptive robust optimization (ARO) and tackled by two main decomposition methods: Benders decomposition [8] and the column-and-constraint-generation algorithm (CCGA) [68]. Both approaches rely on iterative procedures that solve a *master problem* and *subproblems*. The master problem is basically the nominal OPF problem with additional cuts/constraints and variables representing feasibility or optimality information on the subproblems. Whereas Benders decomposition provides dual information about the subproblems through valid cuts restricting the master problem, the CCGA adds primal contraints and variables from the subproblems to the master problem.

Unfortunately, the SCOPF problem is not suitable for a traditional Benders decomposition since the subproblems are nonconvex due to the APR

constraints (which feature binary variables). Despite such challenges, inspired by [8], an interesting heuristic method was proposed in [82] but it does not guarantee optimality. In contrast, the CCGA algorithm proposed in [69] is an exact solution method which was used to produce optimal solutions to power network with more than 2,000 buses. Notwithstanding aforementioned contributions, both approaches still require significant computational effort to obtain near-optimal solutions.

Machine learning (ML) approaches have been advocated to address the computational burden associated with the hard and repetitive optimization problems in the power sector, given the large amounts of historical data (i.e., past solutions). Initial attempts date back to the early 1990s, when, for example, artificial neural networks were applied to predict the on/off decisions of generators for an unit commitment problem [100, 101]. More recently, ML was used to identify partial warm-start solutions and/or constraints that can be omitted, and to determine affine subspaces where the optimal solution is likely to lie [71]. Artificial neural network and decision tree regression were also used to learn sets of high-priority lines to consider for transmission switching [72], while the k-nearest neighbors approach was used to select previously optimized topologies directly from data [28]. As for the security and reliability aspects of the network, the security-boundary detection was modeled with a neural network to simplify stability constraints for the optimal power flow [102], while decision trees were applied to determine security boundaries (regions) for controllable variables for a coupled natural gas and electricity system [103]. Machine learning was also applied for identifying the relevant sets of active constraints for the OPF problem [70].

Unlike these applications, where the main purpose of machine learning is to enhance the solver performance by classifying sets, eliminating constraints, and/or by modeling specific parts of the problems, the machine-learning approach in [48] directly predicts the generator dispatch for the OPF by combining deep learning and Lagrangian duality. This approach produces significant computational gains but is not directly applicable to the SCOPF problem which features an impractical number of variables and constraints. This work remedies this limitation.

3.1.3 Contributions

The chapter assumes the existence of historical SCOPF data, i.e., pairs of inputs and outputs [28, 48, 70–72] The proposed approach uses a deep neural network (DNN) to approximate the mapping between loads

and optimal generator dispatches. To capture the physical, operational, and APR constraints, the chapter applies the Lagrangian dual scheme of [48] that penalizes constraint violations at training time. Moreover, to ensure computational tractability, the training process, labeled as CCGA-DNN, mimics a dedicated CCGA algorithm that iteratively adds new constraints for a few critical contingencies. In these constraints, an approximation for the post-contingency generation is adopted to keep the size of the DNN small. The resulting DNN provides high-quality approximations to the SCOPF in milliseconds and can be used to seed another dedicated CCGA to find the nearest feasible solution to the prediction. The resulting approach may bring two orders of magnitude improvement in efficiency compared to the original CCGA algorithm.

In summary, the contributions can be summarized as follows: i) a novel DNN that maps a load profile onto a high-quality approximation of the SCOPF problem, ii) a new training procedure, the CCGA-DNN, that mimics a CCGA, where the master optimization problem is replaced by a DNN prediction, iii) an approximation for the post-contingency generation which keeps the DNN size small, and iv) an dedicated CCGA algorithm seeded with the DNN evaluation to obtain high-quality feasible solutions fast. Of particular interest is the tight combination of machine learning and optimization proposed by the approach.

3.1.4 Chapter Organization

This chapter is organized as follows. Section introduces the notation. Section 3.3 introduces the SCOPF problem. Section 3.4 presents the properties of the SCOPF problem and the CCGA for SCOPF. Section 3.5 introduces the deep learning models in stepwise refinements. Section 3.6 describes the CCGA for feasibility recovery. Section 3.7 reports the case studies and the numerical experiments and Section 3.8 concludes the chapter.

3.2 Nomenclature

This section introduces the main notation. Bold symbols are used for matrices (uppercase) and vectors (lowercase). Additional symbols are either explained in the context or interpretable by applying the following general rules: Symbols with superscript "j", "k", or "l" denote new variables, parameters or sets corresponding to the j-th, k-th, or l-th iteration of the associated method. Symbols with superscript "$*$" denote the optimal value of the associated (iterating) variable. Symbols with superscript "t" are associated

with the data set for the t-th past solve. Dotted symbols are associated with predictors for the corresponding variable.

Sets

$\mathcal{E}, \mathcal{E}_s$	Feasibility sets for variables associated with the nominal state and contingent state s, respectively.
$\mathcal{F}_s$	Feasibility set for primary response variables under contingent state s.
$\mathcal{C}$, $\mathbb{C}$	Full set and subset of constraints.
$\mathcal{G}, \mathcal{L}, \mathcal{N}$	Sets of generators, transmission lines and buses, respectively.
$\mathcal{S}$, $\mathbb{S}$	Full set and subset of contingencies, respectively.
$\mathcal{T}$, $\mathbb{T}$	Full set and subset of past solves, respectively.
$\mathbb{U}^+$, $\mathbb{U}^-$	Subsets of line–contingent state pairs.
$\mathcal{Y}_s$	Set of decision variables associated with automatic primary response under contingent state s.

Parameters

α, ρ	Learning rate and Lagragian dual step size.
β, β_1, β_c	Parameters for selecting constraints.
$\boldsymbol{\gamma}$	Vector of parameters for primary response.
γ_i	Parameter for primary response of generator i.
ϵ	Tolerance for transmission line violation.
$\boldsymbol{\lambda}, \lambda_c$	Vectors for all Lagrangian multipliers and Lagrangian multipliers for constraint c.
$\boldsymbol{\nu}, \nu_c, \tilde{\nu}_c$	Vector for violations, violation for constraint c, and median violation for c among past solves $\mathcal{T}$.
$\mathbf{A}$, $\mathbf{B}$	Line-bus and Generator-bus incidence matrices.
$\boldsymbol{\omega}$	Vector of weights for deep neural network.
$\mathbf{d}$	Vector of nodal net loads.

$\mathbf{e}$	Vector of ones with appropriate dimension.
$\overline{\mathbf{f}}$	Vector of line capacities.
$\underline{\mathbf{g}}, \overline{\mathbf{g}}$	Vectors of lower and upper limits for generators.
$\overline{g}_i$	Upper limit for generator i.
$\hat{\mathbf{g}}$	Vector of capacities for generators.
$\hat{g}_i$	Capacity of generator i.
$h(\cdot)$	Piecewise linear generation costs.
$\mathbf{K}_0$	Matrix of power transfer distribution factors.
$\mathbf{K}_1$	Preprocessed matrix for flow limits.
$\mathbf{k}_2, \mathbf{k}_3$	Preprocessed vectors for flow limits.
$\overline{\mathbf{r}}$	Vector of primary response limits of generators.
$\overline{r}_i$	Element of $\overline{\mathbf{r}}$ related to generator i, given by $\gamma_i \hat{g}_i$.
$\mathbf{S}$	Angle-to-flow matrix.

Nominal-state-related decision variables and vectors

$\boldsymbol{\theta}, \mathbf{f}, \mathbf{g}$	Phase angles, line flows, and nominal generation.
g_i	Generation of generator i in nominal state.

Contingent-state-related decision variables and vectors

$\boldsymbol{\theta}_s$	Vector of phase angles under contingent state s.
$\boldsymbol{\tau}_s^+, \boldsymbol{\tau}_s^-$	Vectors of line violation under contingent state s.
ϕ, s_ϕ	Highest line violation and related contingent state.
$\tilde{\phi}$	Median highest line violation among instances $\mathcal{T}$.
$\mathbf{f}_s$	Vector for line flows under contingent state s.
$\mathbf{g}_s$	Vector for generation under contingent state s.
$\mathbf{g}_s'$	Provisional vector for $\mathbf{g}_s$.

$g_{s,i}$	Generation of generator i under contingent state s.
$g'_{s,i}$	Provisional variable for $g_{s,i}$.
n_s	Global signal under contingent state s.
$\mathbf{x}_s$	Binary vector indicating whether generators reached $\overline{\mathbf{g}}$ under contingency state s.
$x_{s,i}$	Element of $\mathbf{x}_s$ corresponding to generator i.

3.3 SCOPF Problem

In this chapter, it is assumed that, at the time the SCOPF problem is solved, the operator has precise forecasts for the few-minutes-ahead non-dispatchable generation and loads. For simplicity, all generators are regarded as synchronized.

3.3.1 Power Flow Constraints

The SCOPF formulation uses traditional security-constrained DC power flow constraints over the vectors for generation $\mathbf{g}$, flows $\mathbf{f}$, and phase angles $\boldsymbol{\theta}$. In matrix notations, these constraints are represented as follows:

$$\mathbf{A}\mathbf{f} + \mathbf{B}\mathbf{g} = \mathbf{d} \quad (3\text{-}1) \qquad \mathbf{A}\mathbf{f}_s + \mathbf{B}\mathbf{g}_s = \mathbf{d} \quad \forall s \in \mathcal{S} \quad (3\text{-}5)$$

$$\mathbf{f} = \mathbf{S}\boldsymbol{\theta} \quad (3\text{-}2) \qquad \mathbf{f}_s = \mathbf{S}\boldsymbol{\theta}_s \quad \forall s \in \mathcal{S} \quad (3\text{-}6)$$

$$-\overline{\mathbf{f}} \leq \mathbf{f} \leq \overline{\mathbf{f}} \quad (3\text{-}3) \qquad -\overline{\mathbf{f}} \leq \mathbf{f}_s \leq \overline{\mathbf{f}} \quad \forall s \in \mathcal{S} \quad (3\text{-}7)$$

$$\underline{\mathbf{g}} \leq \mathbf{g} \leq \overline{\mathbf{g}} \quad (3\text{-}4) \qquad \mathbf{g}_s \leq \overline{\mathbf{g}} \quad \forall s \in \mathcal{S} \quad (3\text{-}8)$$

Equations (3-1)–(3-4) model the DC power flow in pre-contingency state and capture the nodal power balance (3-1), Kirchhoff's second law (3-2), transmission line limits (3-3), and generator limits (3-4). Analogously, equations (3-5)–(3-8) model the power flow for each post-contingency state s. The bounds $\overline{\mathbf{g}}$ in (3-4) and (3-8) may be different from capacity $\hat{\mathbf{g}}$ due to commitment and/or operational constraints.

3.3.2 Automatic Primary Response

The APR is modeled as in [69, 82, 83]: under contingent state s, a global variable n_s is used to mimic the level of system response required for adjusting the power imbalance. The APR of generator i under contingency s, $g_{s,i} - g_i$, is proportional to its capacity $\hat{g}_i$ and to the parameter γ_i associated with the droop coefficient, i.e.,

$$g_{s,i} = \min\{g_i + n_s \gamma_i \, \hat{g}_i, \ \overline{g}_i\} \qquad \forall i \in \mathcal{G}, \forall s \in \mathcal{S}, i \neq s \qquad (3\text{-}9)$$

$$g_{s,s} = 0 \qquad \forall s \in \mathcal{S}. \qquad (3\text{-}10)$$

These equations are nonconvex and can be linearized by introducing binary variables $x_{s,i}$ to denote whether generator i in scenario s is not at its limit, i.e.,

$$|g_{s,i} - g_i - n_s \gamma_i \, \hat{g}_i| \leq \overline{g}_i (1 - x_{s,i}) \qquad \forall i \in \mathcal{G}, \forall s \in \mathcal{S}, i \neq s \qquad (3\text{-}11)$$

$$g_i + n_s \gamma_i \, \hat{g}_i \geq \overline{g}_i (1 - x_{s,i}) \qquad \forall i \in \mathcal{G}, \forall s \in \mathcal{S}, i \neq s \qquad (3\text{-}12)$$

$$g_{s,i} \geq \overline{g}_i (1 - x_{s,i}) \qquad \forall i \in \mathcal{G}, \forall s \in \mathcal{S}, i \neq s \qquad (3\text{-}13)$$

$$n_s \in [0, 1] \qquad \forall s \in \mathcal{S} \qquad (3\text{-}14)$$

$$x_{s,i} \in \{0, 1\} \qquad \forall i \in \mathcal{G}, \forall s \in \mathcal{S} \qquad (3\text{-}15)$$

$$g_{s,s} = 0 \qquad \forall s \in \mathcal{S}. \qquad (3\text{-}16)$$

3.3.3 Extensive Formulation for the SCOPF Problem

The extensive formulation for the SCOPF problem using variables for generation, flows, and phase angles is as follows:

$$\min_{\boldsymbol{\theta}, \mathbf{f}, \mathbf{g}, [\boldsymbol{\theta}_s, \mathbf{f}_s, \mathbf{g}_s, n_s, \mathbf{x}_s]_{s \in \mathcal{S}}} \quad h(\mathbf{g}) \qquad (3\text{-}17)$$

$$\text{s.t.:} \quad (3\text{-}1) - (3\text{-}4) \qquad (3\text{-}18)$$

$$(3\text{-}5) - (3\text{-}16) \qquad \forall s \in \mathcal{S}. \qquad (3\text{-}19)$$

Using power transfer distribution factors (PTDF), constraints (3-1)–(3-8) can be replaced by the following constraints:

$$\mathbf{e}^\top \mathbf{g} = \mathbf{e}^\top \mathbf{d} \qquad (3\text{-}20)$$

$$-\overline{\mathbf{f}} \leq \mathbf{K}_0 (\mathbf{d} - \mathbf{B}\mathbf{g}) \leq \overline{\mathbf{f}} \qquad (3\text{-}21)$$

$$(3\text{-}4) \qquad (3\text{-}22)$$

$$\mathbf{e}^\top \mathbf{g}_s = \mathbf{e}^\top \mathbf{d} \qquad \forall s \in \mathcal{S} \qquad (3\text{-}23)$$

$$-\overline{\mathbf{f}} \leq \mathbf{K}_0(\mathbf{d} - \mathbf{B}\mathbf{g}_s) \leq \overline{\mathbf{f}} \qquad \forall s \in \mathcal{S} \qquad (3\text{-}24)$$

$$(3\text{-}8) \qquad \forall s \in \mathcal{S}. \qquad (3\text{-}25)$$

Constraints (3-20)–(3-25) that involve the PTDF matrix $\mathbf{K}_0$ are from [92]. The total demand balance for the nominal and contingent states are enforced by (3-20) and (3-23) respectively. In constraints (3-21) and (3-24), the PTDF matrix translates the power injected by each generator at its bus into its contribution to the flow of each line. These constraints also bound the flows from above and below. Observe that $\mathbf{g}$ and $\mathbf{g}_s$ are the only variables in this formulation.

For conciseness, denote the power flow constraints (3-20)–(3-22) and (3-23)–(3-25) by $\mathbf{g} \in \mathcal{E}$ and $\mathbf{g}_s \in \mathcal{E}_s$ respectively. Similarly, denote the APR constraints (3-11)–(3-16) by $\mathcal{Y}_s = [\mathbf{g}, \mathbf{g}_s, \mathbf{x}_s, n_s] \in \mathcal{F}_s$. The extensive SCOPF formulation then becomes

$$\min_{\mathbf{g},[\mathbf{g}_s,\mathbf{x}_s,n_s]_{s\in\mathcal{S}}} \quad h(\mathbf{g}) \qquad (3\text{-}26)$$

$$\text{s.t.:} \quad \mathbf{g} \in \mathcal{E} \qquad (3\text{-}27)$$

$$\mathbf{g}_s \in \mathcal{E}_s \qquad \forall s \in \mathcal{S} \qquad (3\text{-}28)$$

$$\mathcal{Y}_s \in \mathcal{F}_s \qquad \forall s \in \mathcal{S}. \qquad (3\text{-}29)$$

Note that the number of binary variables above grows quadratically with the number of generators. Hence, solving (3-26)–(3-29) becomes impractical for large-scale systems.

3.4 SCOPF Properties and CCGA

This section introduces key properties of the SCOPF problem and summarizes the CCGA proposed in [69]. These properties are necessary for the CCGA and the ML models. The CCGA serves both as a benchmark for evaluation and is used as part of the feasibility recovery scheme proposed in Section 3.6.

Property 1: *For $s \in \mathcal{S}$, given values $\mathbf{g}^*$ and n_s^* for $\mathbf{g}$ and n_s, there exists a unique value $\mathbf{g}_s^*$ for $\mathbf{g}_s$ that can be computed directly using constraints* (3-11)–(3-16).

Property 2: *Consider $s \in \mathcal{S}$ and a value $\mathbf{g}^*$ for $\mathbf{g}$. If there exists a value n_s^* for n_s that admits a feasible solution to constraints* (3-11)–(3-16) *and* (3-23)*, then this value n_s^* is unique and can be computed by a simple bisection method [69].*

Property 2 holds since, for a given $\mathbf{g}^*$, each component of $\mathbf{g}_s$ is continuous and monotone with respect to n_s. Hence the value n_s^* and its associated vector $\mathbf{g}_s^*$ that satisfy constraint (3-23) can be found by a simple bisection search over n_s.

Property 3: *Constraint* (3-24) *can be formulated as:*

$$\mathbf{K}_1\mathbf{g}_s + \mathbf{k}_2 \geq \mathbf{0} \tag{3-30}$$

$$\mathbf{K}_1\mathbf{g}_s + \mathbf{k}_3 \geq \mathbf{0}, \tag{3-31}$$

using matrix operations to obtain $\mathbf{K}_1$*,* $\mathbf{k}_2$*, and* $\mathbf{k}_3$*.*
Note that each row of $\mathbf{K}_1$ and each element of $\mathbf{k}_2$ and $\mathbf{k}_3$ are associated with a specific transmission line. Therefore, for each $s \in \mathcal{S}$ and for each line, the (positive and negative) violation of the thermal limit of the line can be obtained by inspecting (3-30)–(3-31) for the proposed value $\mathbf{g}_s^{(*)}$.

3.4.1 Column-and-Constraint-Generation Algorithm

The CCGA, which relies on the above properties, alternates between solving a master problem to obtain a nominal schedule $\mathbf{g}$ and a bisection method to obtain the state variables of each contingency. The master problem is specified as follows:

$$\min_{\mathbf{g},[\mathbf{g}_s']_{s\in\mathcal{S}},[\mathbf{x}_s,n_s]_{s\in\mathbb{S}}} \quad h(\mathbf{g}) \tag{3-32}$$

$$\text{s.t.:} \quad \mathbf{g} \in \mathcal{E} \tag{3-33}$$

$$\mathbf{g}_s' - \mathbf{g} \leq \overline{\mathbf{r}} \qquad \forall s \in \mathcal{S} \tag{3-34}$$

$$(3\text{-}8), (3\text{-}23), (3\text{-}16) \qquad \forall s \in \mathcal{S} \tag{3-35}$$

$$\mathcal{Y}_s \in \mathcal{F}_s \qquad \forall s \in \mathbb{S} \tag{3-36}$$

$$\mathbf{K}_1^l\mathbf{g}_s' + \mathbf{k}_2^l \geq \mathbf{0} \qquad \forall (l,s) \in \mathbb{U}^+ \tag{3-37}$$

$$\mathbf{K}_1^l\mathbf{g}_s' + \mathbf{k}_3^l \geq \mathbf{0} \qquad \forall (l,s) \in \mathbb{U}^- \tag{3-38}$$

Constraints (3-32)–(3-38) uses variables $\mathbf{g}_s'$ to denote a "guess" for the post-contingency generation: the actual vector $\mathbf{g}_s$ is not determined by the master problem but by the aforementioned bisection method. Constraint (3-33) enforces the nominal state constraints. Constraint (3-34) imposes a valid bound for post-contingency generation. For all contingencies, constraint (3-35) enforces the generation capacity (3-8), total demand satisfaction (3-23), and the absence of generation for a failed generator (3-16). The APR is enforced

"on-demand" in (3-36) for a reduced set of contingent states $\mathbb{S}$. Initially, $\mathbb{S} = \emptyset$. Inequalities (3-37)–(3-38) are also the "on-demand" versions of (3-30)–(3-31) for (a few) pairs of transmission lines and contingencies. Initially, $\mathbb{U}^+$ and $\mathbb{U}^-$ are empty sets.

The CCGA algorithm is specified in Algorithm 1. At iteration j, the master problem (3-32)–(3-38) computes $\mathbf{g}^j$. The bisection method then determines the contingent state variables $[\mathbf{g}_s^j, \mathbf{x}_s^j, n_s^j]_{s\in\mathcal{S}}$. The vectors $\boldsymbol{\tau}_s^+$ and $\boldsymbol{\tau}_s^-$ of non-negative numbers represent the positive and negative violations of transmission lines for contingent state s: they are calculated for all $s \in \mathcal{S}$ by inspecting constraints (3-30)–(3-31) for $[\mathbf{g}_s^j]_{s\in\mathcal{S}}$. The algorithm then computes the highest single line violation ϕ among all contingent states and uses s_ϕ to denote the contingent state associated with ϕ. The pairs lines/contingencies featuring violations above a predefined threshold β are added to the master problem by updating sets $\mathbb{U}^+$ and $\mathbb{U}^-$. Likewise, s_ϕ is added to $\mathbb{S}$. As a result, the variables and APR constraints associated with s_ϕ are added to the master problem during the next iteration. The CCGA terminates when $\phi < \epsilon$, where ϵ is the tolerance for line violation.

Algorithm 1 CCGA

1: Initialization: $j \leftarrow 0, \mathbb{S} \leftarrow \emptyset$, $\mathbb{U}^+ \leftarrow \emptyset$, $\mathbb{U}^- \leftarrow \emptyset$
2: **for** $j = 0, 1, \ldots$ **do**
3: Solve: (3-32)–(3-36) to obtain $\mathbf{g}^j$
4: $n_s^j \leftarrow$ apply bisection method on all $s \in \mathcal{S}$
5: $\mathbf{g}_s^j \leftarrow$ enforce (3-11)–(3-16) on all $s \in \mathcal{S}$
6: $\boldsymbol{\tau}_s^-, \boldsymbol{\tau}_s^+ \leftarrow$ get the line violations of $\mathbf{g}_s^j$ using (3-30)–(3-31) for all $s \in \mathcal{S}$
7: $\phi \leftarrow$ compute the highest line violation among all $s \in \mathcal{S}$
8: $s_\phi \leftarrow$ select the contingent state associated with ϕ
9: $\mathbb{S} \leftarrow \mathbb{S} \cup \{s_\phi\}$
10: $\mathbb{U}^+ \leftarrow \mathbb{U}^+ \cup \{\, (l, s) \,|\, \boldsymbol{\tau}_s^+[l] > \beta\}$
11: $\mathbb{U}^- \leftarrow \mathbb{U}^+ \cup \{\, (l, s) \,|\, \boldsymbol{\tau}_s^-[l] > \beta\}$
12: **BREAK** if $\phi \leq \epsilon$.
13: **end for**

The following result from [69] ensures the correctness of CCGA: It shows that a solution to the master problem produces a nominal generation for which there exists a solution to each contingency that satisfies the APR and total demand constraints. Since the CCGA adds at least one violated line constraint and, possibly, a set of violated APR constraints for one contingency to the master problem at each iteration, it is guaranteed to converge after a finite number of iterations.

Theorem 1: *For each solution* $\mathbf{g}^*$ *to the master problem, there exist values* n_s^* *and* $\mathbf{g}_s^*$ *that satisfy the demand constraint* $\mathbf{e}^\top \mathbf{g}_s^* = \mathbf{e}^\top \mathbf{d}$ *and the APR constraints*

(3-11)–(3-16) for each contingency s.

Proof: By (3-8) and (3-34), $g'_{s,i} \leq \min\{\overline{g}_i, g_i + \gamma_i \hat{g}_i\}$ for each i and s, where $g'_{s,i}$ is the i-th element of $\mathbf{g}'_s$. When $n_s = 0$, $\mathbf{g}_s = \mathbf{g}$, except for $g_{s,s} = 0$. When $n_s = 1$, $g_{s,i} = \min\{\overline{g}_i, g_i + \gamma_i \hat{g}_i\} \geq g'_{s,i}$ for each i and s, with $i \neq s$. Since, by (3-23), $\mathbf{g}'_s$ meets the global demand, $\mathbf{e}^\top \mathbf{g}_s \geq \mathbf{e}^\top \mathbf{g}'_s = \mathbf{e}^\top \mathbf{d}$ when $n_s = 1$. By the monotonicity and continuity of $g_{s,i}$ with respect to n_s (for a given g_i), there is a value n^*_s whose associated $\mathbf{g}^*_s$ satisfies the demand constraint in (3-23) and preserves the APR constraints □.

3.5 Deep Neural Networks for SCOPF

This section describes the use of supervised learning to obtain DNNs that map a load vector into a solution of the SCOPF problem. A DNN consists of many layers, where the input for each layer is typically the output of the previous layer [104]. This work uses fully-connected DNNs.

3.5.1 Specification of the Learning Problem

For didactic purposes, the specification of the learning problem uses the extensive formulation (3-26)–(3-29). The training data is a collection of instances of the form

$$\{\mathbf{d}^t; \mathbf{g}^t, [\mathbf{g}^t_s, n^t_s, \mathbf{x}^t_s]_{s\in\mathcal{S}}\}_{t\in\mathcal{T}}$$

where $(\mathbf{g}^t, [\mathbf{g}^t_s, n^t_s, \mathbf{x}^t_s]_{s\in\mathcal{S}})$ is the optimal solution (ground truth) to the SCOPF problem for input $\mathbf{d}^t$. The DNN is a parametric function $\mathrm{O}[\boldsymbol{\omega}](\cdot)$ whose parameters are the network $\boldsymbol{\omega}$: It maps a load vector $\mathbf{d}$ into an approximation $\mathrm{O}[\boldsymbol{\omega}](\mathbf{d}) = \{\dot{\mathbf{g}}, [\dot{n}_s, \dot{\mathbf{x}}_s, \dot{\mathbf{g}}_s]_{s\in\mathcal{S}}\}$ of the optimal solution to the SCOPF problem for load $\mathbf{d}$. The goal of the machine-learning training to find the optimal weights $\boldsymbol{\omega}^*$, i.e.,

$$\boldsymbol{\omega}^* = \arg\min_{\boldsymbol{\omega}} \sum_{t\in\mathcal{T}} \mathbb{L}^t_0(\dot{\mathbf{g}}^t) + \sum_{s\in\mathcal{S}} \mathbb{L}^t_s(\dot{\mathbf{g}}^t_s, \dot{\mathbf{x}}^t_s, \dot{n}^t_s) \tag{3-39}$$

$$\text{s.t.: } O[\boldsymbol{\omega}](\mathbf{d}^t) = (\dot{\mathbf{g}}^t, [\dot{\mathbf{g}}^t_s, \dot{n}^t_s, \dot{\mathbf{x}}^t_s]) \qquad \forall t \in \mathcal{T} \tag{3-40}$$

$$\dot{\mathbf{g}}^t \in \mathcal{E}^t \qquad \forall t \in \mathcal{T} \tag{3-41}$$

$$\dot{\mathbf{g}}^t_s \in \mathcal{E}^t_s \qquad \forall t \in \mathcal{T}, \forall s \in \mathcal{S} \tag{3-42}$$

$$\dot{\mathcal{Y}}^t_s \in \mathcal{F}^t_s \qquad \forall t \in \mathcal{T}, \forall s \in \mathcal{S} \tag{3-43}$$

where the loss functions are defined as

$$\mathbb{L}_0^t(\dot{\mathbf{g}}^t) = ||\mathbf{g}^t - \dot{\mathbf{g}}^t||_2$$
$$\mathbb{L}_s^t(\dot{\mathbf{g}}_s^t, \dot{\mathbf{x}}_s^t, \dot{n}_s^t) = ||\mathbf{g}_s^t - \dot{\mathbf{g}}_s^t||_2 + ||\mathbf{x}_s^t - \dot{\mathbf{x}}_s^t||_2 + ||n_s^t - \dot{n}_s^t||_2$$

and minimize the distance between the prediction and the ground truth. There are two difficulties in this learning problem: the large number of scenarios, variables, and constraints, and the satisfaction of constraints (3-41)–(3-43). This section examines possible approaches.

3.5.2 The Baseline Model

The baseline model is a parsimonious approach that disregards constraints (3-41)–(3-43) and predicts the nominal generation only, i.e.,

$$\begin{aligned} \boldsymbol{\omega}^* = \ & \operatorname{argmin}_{\boldsymbol{\omega}} \sum_{t \in \mathcal{T}} \mathbb{L}_0^t(\dot{\mathbf{g}}^t) \\ & \text{s.t.: } O[\boldsymbol{\omega}](\mathbf{d}^t) = (\dot{\mathbf{g}}^t) \qquad \forall t \in \mathcal{T} \end{aligned}$$

It uses a DDN model with 5 linear layers, interspersed with 5 nonlinear layers that use the softplus activation function. The sizes of the input and output of each layer are linearly parameterized by $|\mathcal{L}|$ and $|\mathcal{G}|$. A high-level algebraic description of layers of the DNN follows:

$$\mathbf{l}_i = \gamma(\mathbf{W}_i \mathbf{l}_{i-1} + \mathbf{b}_i), \text{for each layer } \mathbf{l}_i$$
$$\mathbf{l}_1 = \gamma(\mathbf{W}_1 \mathbf{d} + \mathbf{b}_1)$$

The elements of vector $\boldsymbol{\omega}$ are rearranged as matrices $\mathbf{W}_i$ and vector of biases $\mathbf{b}_i$. Note that the demand vector $\mathbf{d}$ is the input for the first layer. The symbol γ denotes a nonlinear activation function. Unfortunately, training the baseline model tends to produce predictors violating the problem constraints [48, 70].

3.5.3 A Lagrangian Dual Model for Nominal Constraints

This section extends the baseline model to include constraints on the nominal state (3-41). Constraints (3-42)–(3-43) on the contingency cases are not considered in the model. To capture physical and operational constraints, the training of the DNN adopts the Lagrangian dual approach from [48].

The Lagrangian dual approach relies on the concept of constraint violations. The violations of a constraint $f(x) = 0$ is given by $|f(x)|$, while

the violations of $f(x) \geq 0$ are specified by $\max(0, -f(x))$. Although these expressions are not differentiable, they admit subgradients. Let $\mathbb{C}$ represent the set of nominal constraints and $\nu_c(\mathbf{g})$ be the violations of constraint c for generation dispatch $\mathbf{g}$. The Lagrangian dual approach introduces a term $\lambda_c \nu_c^t(\mathbf{g}^t)$ in the objective function for each $c \in \mathbb{V}$ and each $t \in \mathcal{T}$, where λ_c is a Lagrangian multiplier. The optimization problem then becomes

$$LR(\boldsymbol{\lambda}) = \min_{\boldsymbol{\omega}} \quad \sum_{t \in \mathcal{T}} (\mathbb{L}_0^t(\dot{\mathbf{g}}^t) + \sum_{c \in \mathcal{C}} \lambda_c \nu_c^t(\dot{\mathbf{g}}^t)) \tag{3-44}$$

$$\text{s.t.} \quad O[\boldsymbol{\omega}](\mathbf{d}^t) = (\dot{\mathbf{g}}^t) \qquad \forall t \in \mathcal{T} \tag{3-45}$$

and the Lagrangian dual is simply

$$LD = \max_{\boldsymbol{\lambda}} \; LR(\boldsymbol{\lambda}) \tag{3-46}$$

Problem (3-46) is solved by iterating between training for weights $\boldsymbol{\omega}$ and updating the Lagrangian multipliers. Iteration j uses Lagrangian multiplier $\boldsymbol{\lambda}^j$ and solves $LR(\boldsymbol{\lambda}^j)$ to obtain the optimal weights $\boldsymbol{\omega}^j$. It then updates the Lagrangian multipliers using the constraint violations. The overall scheme is presented in Algorithm 2. Lines 3–10 train weights $\boldsymbol{\omega}^j$ for a fixed vector of Lagrangian multipliers $\boldsymbol{\lambda}^j$, using minibatches and a stochastic gradient descent method with learning rate α. For each minibatch, the algorithm computes the predictions (line 6), the constraint violations (line 7), and updates the weights (line 9). Lines 2–13 describe the solving of Lagrangian dual. It computes the Lagrangian relaxation described previously and updates the Lagrangian multipliers in line 11 using the median violation $\tilde{\nu}_c$ for each nominal constraint c.

Algorithm 2 Lagrangian Dual Model ($\mathcal{T}$, $\mathbb{C}$, α, ρ, *Jmax*, $\boldsymbol{\lambda}^0$, $\boldsymbol{\omega}^0$)

1: $j \leftarrow 0$.
2: **for** $j = 0, 1, \ldots$ *Jmax* **do**
3: **for** $k = 0, 1, \ldots$ **do**
4: Sample minibatch: $\mathbb{T}_k \subset \mathcal{T}$
5: **for** $t \in \mathbb{T}_k$ **do**
6: Compute: $\mathrm{O}[\boldsymbol{\omega}^j](\mathbf{d}^t) = \dot{\mathbf{g}}^t$ and $\mathbb{L}_0^t(\dot{\mathbf{g}}^t)$
7: Compute $\nu_c^t(\dot{\mathbf{g}}^t)$ $\forall c \in \mathbb{C}$
8: **end for**
9: $\boldsymbol{\omega}^j \leftarrow \boldsymbol{\omega}^j - \alpha \nabla_{\boldsymbol{\omega}^j} [\sum_{t \in \mathcal{T}} (\mathbb{L}_0^t(\dot{\mathbf{g}}^t) + \sum_{c \in \mathcal{C}} \lambda_c \nu_c^t(\dot{\mathbf{g}}^t))]$
10: **end for**
11: $\lambda_c^{j+1} \leftarrow \lambda_c^j + \rho\, \tilde{\nu}_c \; \forall c \in \boldsymbol{C}$
12: $\boldsymbol{\omega}^{j+1} \leftarrow \boldsymbol{\omega}^j$
13: **end for**

3.5.4 CCGA-DNN Model

This section presents the final ML model, the CCGA-DNN, which mimics a CCGA algorithm. In particular, the CCGA-DNN combines the Lagrangian dual model with an outer loop that adds constraints for the contingent states on-demand.

Observe first that a direct Lagrangian dual approach to the SCOPF would require an outer loop to add predictors $[\dot{\mathbf{g}}_s, \dot{\mathbf{x}}_s, \dot{n}_s]_{s\in\mathcal{S}}$ and constraints (3-42)–(3-43) for selected contingency states s. Unfortunately, the addition of new predictors structurally modifies the DNN output $\mathrm{O}[\boldsymbol{\omega}](\cdot)$ and induces a considerable increase in the DNN size.

The key idea to overcome this difficulty is to mimic the CCGA closely, replacing the master problem with the prediction $O[\boldsymbol{\omega}^l](\mathbf{d}^t)$ at iteration l. Moreover, constraints (3-43) are replaced by constraints of the form

$$\dot{g}^t_{s,i} = \max\{0, \min\{\dot{g}^t_i + \dot{n}^t_s \gamma_i \, \hat{g}_i \, , \overline{g}_i\}\}, \tag{3-47}$$

where $\dot{n}^t_s$ is obtained by the bisection method on the prediction. Again, these constraints are not differentiable but admit subgradients and hence can be dualized in the objective function. The CCGA-DNN is summarized in Algorithm 3. At each iteration l, the Lagrangian dual model (Algorithm 2) produces updated weights $\boldsymbol{\omega}^l$ and multipliers $\boldsymbol{\lambda}^l$ (line 5). The inner loop (lines 6–12) applies the bisection method to find $\dot{n}^t_s$ for all t and constraints (3-11)–(3-16) to obtain $\dot{\mathbf{g}}^t_s$ (lines 8–9). These values are then used to compute the highest line violation ϕ^t among all states and the associated contingent state s^t_ϕ (line 10). The inner loop also increases the element of the counter vector $\mathbf{p}$ associated with s^t_ϕ whenever the highest violation for solve t is above tolerance ϵ (line 11). Then, in the main loop, contingency states with high frequencies of violated lines are identified (line 13) using a threshold β_1. The algorithm is terminated if $\mathbb{S}'$ is empty and median relative violations for nominal constraints in (3-41) are within tolerances β_c (line 14). Otherwise, the set of constraints is updated by adding constraints (3-30)–(3-31) and (3-47) for added contingent states (line 15). The Lagrangian multipliers for added constraints (3-30)–(3-31) $\forall s \in \mathbb{S}'$ are initialized in line 16. Finally, constraints (3-30)–(3-31) $\forall s \in \mathbb{S}$ are updated with the median violation $\tilde{\phi}$ for those lines associated with some ϕ^t (line 17). Note that the process of updating Lagrangian multipliers for (3-30)–(3-31) $\forall s \in \mathbb{S}$ is different and much stricter than that for nominal constraints in Algorithm 2.

Algorithm 3 SC Lagrangian Dual Model ($\mathcal{T}$, α, ρ, β_1, β_c, ϵ, jMax)

$\mathbb{C} \leftarrow \{(3\text{-}41)\}$, $\mathbb{S} \leftarrow \emptyset$, $\boldsymbol{\lambda}^0 \leftarrow \mathbf{0}$, $\boldsymbol{\omega}^0 \leftarrow \mathbf{0}$
Create a counter vector $\mathbf{p}$ of size $|\mathcal{S}|$
for $l = 1, 2, \ldots$ **do**
  $\mathbf{p} \leftarrow \mathbf{0}$
  $\boldsymbol{\lambda}^l, \boldsymbol{\omega}^l \leftarrow$ Lagrangian Dual Model($\mathcal{T}$, $\mathbb{C}$, α, ρ, *Jmax*, $\boldsymbol{\lambda}^{l-1}$,$\boldsymbol{\omega}^{l-1}$)
  for $t \in \mathcal{T}$ **do**
    $\dot{\mathbf{g}}^t \leftarrow \mathrm{O}[\boldsymbol{\omega}^l](\mathbf{d}^t)$
    $\dot{n}_s^t \leftarrow$ bisection method, $\forall s \in \mathcal{S}$
    $\dot{\mathbf{g}}_s^t \leftarrow$ enforce (3-11)–(3-16), $\forall s \in \mathcal{S}$
    Compute: ϕ^t and identify s_ϕ^t
    if $\phi^t > \epsilon$ **then** increase (s_ϕ^t)-th element of $\mathbf{p}$ by 1
  end for
  $\mathbb{S}' \leftarrow \{s \,|\, \mathbf{p}[s] \,/\, |\mathcal{T}| > \beta_1\}$
  BREAK if $\mathbb{S}' \equiv \emptyset$ and $\tilde{\nu_c} \leq \beta_c, \forall c \in (3\text{-}41)$.
  $\mathbb{C} \leftarrow \mathbb{C} \cup \{(3\text{-}30) - (3\text{-}31), (3\text{-}47), \forall s \in (\mathbb{S}' \setminus \mathbb{S})\}$
  $\lambda^l_{(3\text{-}30)}$, $\lambda^l_{(3\text{-}31)} \leftarrow 0$, $\forall s \in (\mathbb{S}' \setminus \mathbb{S})$
  $\lambda^l_{(3\text{-}30)}$, $\lambda^l_{(3\text{-}31)}$ += $\rho\, \tilde{\phi}$, $\forall s \in \mathbb{S}$
end for

3.6 Feasibility Recovery and Optimality Gap

The training step produces a set of weights $\boldsymbol{\omega}^*$ and the associated DNN produces, almost instantly, a dispatch prediction $\dot{\mathbf{g}} = O[\boldsymbol{\omega}^*](\mathbf{d})$ for an input load vector $\mathbf{d}$. However, the prediction $\dot{\mathbf{g}}$ may violate the nominal and contingency constraints. To restore feasibility, this chapter proposes a feasibility-recovery CCGA, denoted by FR-CCGA, that finds the feasible solution closest to $\dot{\mathbf{g}}$. The master problem for FR-CCGA is similar to (3-32)–(3-38) but it uses a different objective function, i.e.,

$$\min_{\mathbf{g},[\mathbf{g}'_s]_{s\in\mathcal{S}},[\mathbf{x}_s,n_s]_{s\in\mathbb{S}}} \quad \|\dot{\mathbf{g}} - \mathbf{g}\| \tag{3-48}$$

$$\text{s.t.:} \quad (3\text{-}33)\text{–}(3\text{-}38) \qquad \forall\, \mathcal{S},\, \mathbb{S},\, \mathbb{U}^+,\, \mathbb{U}^- \tag{3-49}$$

Note that $\dot{\mathbf{g}}$ is a constant vector in FR-CCGA. While CCGA and FR-CCGA are similar in nature, FR-CCGA is significantly faster because $O[\boldsymbol{\omega}^*](\mathbf{d})$ is often close to feasibility.

The FR-CCGA and CCGA can be run in parallel to provide upper and lower bounds to the SCOPF respectively. This may be useful for operators to assess the quality of the prediction and the associated FR-CCGA solution and decide whether to commit to the FR-CCGA solutions or wait until a better solution is found or the optimality gap is sufficiently small.

System	$\|\mathcal{G}\|$	$\|\mathcal{L}\|$	$\|\mathcal{N}\|$	Total Variables	Binary Variables	Linear Constraints
118-IEEE	54	186	118	13,466	2,862	19,137
1354-PEG	260	1,991	1,354	387,026	63,455	513,677
1888-RTE	297	2,531	1,888	467,011	79,032	624,780

Table 3.1: Instance Size for the SCOPF Problem (3-26)–(3-29) after Presolve

System	Iterations	Contingent States $\mathbb{S}$ added (by generator numbers)
118-IEEE	3	{4}
1354-PEG	3	{23, 65, 74, 112, 126, 163, 222}
1888-RTE	2	{152, 153}

Table 3.2: Training Summary for Algorithm 3

3.7 Computational Experiments

3.7.1 Data

The test cases are based on modified versions of 3 system topologies from [93]. Table 3.1 shows the size of a single instance for each topology. For each topology, the training and testing data is given by the inputs and solutions of many instances that are constructed as follows. For each instance, the net demand of each bus has a deterministic component and a random component. The deterministic component varies across instances from 82% of the nominal net load to near-infeasibility values by small increments of 0.002%. The random component is independently and uniformly distributed ranging from -0.5% to 0.5% of the corresponding nominal nodal net load for each bus and instance. Algorithm 1 was applied to solve each instance for a maximum line violation of $\epsilon = 0.05$ MW and an optimality gap of 0.25%.

3.7.2 Training Aspects

The training set $\mathcal{T}$ is composed by a random sample containing 70% of the generated instances. Algorithm 3 was applied with ϵ set to 1 MW, β_1 to 5%, β_c to $1.5 \cdot 10^{-2}$, and ρ to 10^5. The inner loop of Algorithm 2 (lines 4–11) is executed $1.5 \cdot 10^5$ times with a learning rate α varying from 10^{-4} to 10^{-10} and *Jmax* was set to 1. The DNN models were implemented using PyTorch package with Python 3.0. The training was performed using NVidia Tesla V100 GPUs and 2 GHz Intel Cores. Table 3.2 presents a training summary. In the following, the baseline model is denoted by $\mathcal{M}_b$ and the CCGA-DNN by $\mathcal{M}_{ccga}$. Note that the first iteration of Algorithm 3 returns the weights of the baseline model.

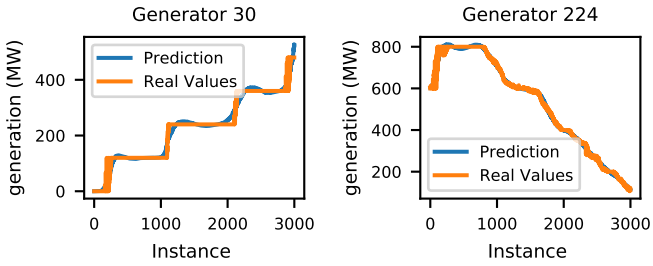

Figure 3.1: $\mathcal{M}_{ccga}$ prediction for selected generators for the 1354-PEG system.

System	Model	Generation Range (MW) 10 50	50 100	100 250	250 500	500 1000	1000 2000	2000 5000
118-IEEE	$\mathcal{M}_b$	2.3	2.8	0.7	0.3	N/A	N/A	N/A
	$\mathcal{M}_{ccga}$	2.5	3.0	0.7	0.4	N/A	N/A	N/A
1354-PEG	$\mathcal{M}_b$	2.4	1.3	1.1	0.9	0.4	0.2	0.1
	$\mathcal{M}_{ccga}$	5.0	1.8	1.2	1.0	0.4	0.3	0.2
1888-RTE	$\mathcal{M}_b$	1.3	1.2	0.7	0.4	0.3	0.1	N/A
	$\mathcal{M}_{ccga}$	1.4	1.1	0.6	0.4	0.3	0.1	N/A

Table 3.3: Prediction Mean Absolute Errors (%)

3.7.3 Prediction Quality

Accurate predictions were obtained for all DNN models and topologies. Figure 3.1 illustrates how $\mathcal{M}_{ccga}$ can learn complex generator patterns arising in the 1354-PEG system. Table 3.3 reports the mean absolute errors for predictions $\dot{\mathbf{g}}^t$, segmented by generation range: $\mathcal{M}_b$ achieves a slightly better accuracy which is expected since it is the less constrained model.

Table 3.4 reports selected indicators of violations: the relative violation $\lambda_{(3\text{-}20)}$ of the total load constraint and the relative violation RLV of the lines associated with ϕ. The results report median values as well as lower and upper bounds for intervals that capture 95% of the instances. Both models achieve the desired tolerance of $\beta_c = 1.5 \cdot 10^{-2}$ for $\lambda_{(3\text{-}20)}$ (the tolerance β_c does not apply to RLV). Model $\mathcal{M}_{ccga}$ produces lower overall violations and has a major effect on RLV.

3.7.4 Comparison with Benchmark CCGA

The previous sections reported on the accuracy of the predictors. This section shows how FR-CCGA leverages the predictors to find near-optimal primal solutions significantly faster than CCGA. More precisely, it compares, in terms of cost and CPU time, CCGA and FR-CCGA when seeded with

		$\lambda_{(3\text{-}20)}$			RLV		
System	Model	Median	95%-Interval		Median	95%-Interval	
118-IEEE	$\mathcal{M}_b$	0.016	0.001	0.055	0.099	0.000	0.467
	$\mathcal{M}_{ccga}$	0.003	0.000	0.011	0.000	0.000	0.548
1354-PEG	$\mathcal{M}_b$	0.018	0.001	0.062	0.259	0.086	1.256
	$\mathcal{M}_{ccga}$	0.010	0.000	0.040	0.005	0.000	0.117
1888-RTE	$\mathcal{M}_b$	0.012	0.001	0.047	0.205	0.021	1.418
	$\mathcal{M}_{ccga}$	0.005	0.000	0.027	0.007	0.000	0.057

$\lambda_{(3\text{-}20)}$ – Net load constraint violation divided by total load.
RLV – Relative violation for line associated with ϕ.

Table 3.4: Selected Indicators of Violation Across Instances (%)

System	Model	Median	95%-Interval	
118-IEEE	$\mathcal{M}_b$	0.05	0.01	0.12
	$\mathcal{M}_{ccga}$	0.18	0.05	0.47
1354-PEG	$\mathcal{M}_b$	0.05	0.01	0.13
	$\mathcal{M}_{ccga}$	0.09	0.05	0.14
1888-RTE	$\mathcal{M}_b$	0.04	0.00	0.10
	$\mathcal{M}_{ccga}$	0.04	0.01	0.07

Table 3.5: Distance between Prediction and Feasible Solution (%)

$\mathcal{M}_b$ and $\mathcal{M}_{ccga}$, for 200 randomly selected instances for each system topology. Each instance was solved with the same tolerances as in the training. They were solved using Gurobi 8.1.1 under JuMP package for Julia 0.6.4 on a laptop Dell XPS 13 9380 featuring a i7-8565U processor at 1.8 GHz and 16 GB of RAM. Tables 3.5, 3.6, and 3.7 summarize the experiments. Table 3.5 reports the distances in percentage between the predictions and the feasible solutions obtained by FR-CCGA when seeded with the predictions. For instance, for $\mathcal{M}_b$, this distance is $\sum_i |g_i^b - g_i^f| / \sum_i g_i^f$, where g_i^b is $\mathcal{M}_b$'s prediction for generator i and g_i^f is i's generation computed by FR-CCGA seeded with $\boldsymbol{g}^b$. As should be clear, the predictions are very close to feasibility. Table 3.6 reports the computation times which show significant increases in performance by FR-CCGA especially when seeded with $\mathcal{M}_{ccga}$ and on the 1354-PEG system, the most challenging network. FR-CCGA is about 160 times faster than CCGA on this test case. FR-CCGA is also significantly more robust when using $\mathcal{M}_{ccga}$ instead of $\mathcal{M}_b$. Table 3.7 indicates that the cost/objective increase of FR-CCGA over CCGA is very small for both $\mathcal{M}_b$ and $\mathcal{M}_{ccga}$.

Figure 3.2 illustrates the behavior of the algorithms on a randomly chosen instance of the 1354-PEG system. The red line represents the upper bound (feasible solution) generated in 1.87 seconds by the FR-CCGA seeded with $\mathcal{M}_{ccga}$. The blue line represents a sequence of true lower bounds (infeasible solutions) generated by Algorithm 1.

System	Model	Median	Mean	Min.	Max.	Std.
118-IEEE	CCGA	0.210	0.214	0.101	3.717	0.305
	$\mathcal{M}_b$	0.024	0.057	0.021	1.580	0.160
	$\mathcal{M}_{ccga}$	0.026	0.068	0.023	1.372	0.171
1354-PEG	CCGA	321.746	327.210	75.585	741.798	127.101
	$\mathcal{M}_b$	5.335	8.434	1.320	133.366	13.505
	$\mathcal{M}_{ccga}$	1.521	2.168	0.768	8.449	1.740
1888-RTE	CCGA	5.479	7.406	3.110	30.923	7.073
	$\mathcal{M}_b$	5.316	5.501	1.224	18.074	3.348
	$\mathcal{M}_{ccga}$	2.120	1.945	0.911	4.543	0.919

Table 3.6: CPU Time Comparison

System	Model	Median	Mean	Min.	Max.	Std.
118-IEEE	$\mathcal{M}_b$	0.021	0.019	-0.073	0.055	0.014
	$\mathcal{M}_{ccga}$	0.027	0.030	-0.010	0.112	0.020
1354-PEG	$\mathcal{M}_b$	0.020	0.021	-0.007	0.051	0.012
	$\mathcal{M}_{ccga}$	0.067	0.067	0.032	0.091	0.017
1888-RTE	$\mathcal{M}_b$	0.026	0.024	-0.003	0.070	0.011
	$\mathcal{M}_{ccga}$	0.033	0.033	0.004	0.070	0.013

Table 3.7: FR-CCGA Cost Increase over CCGA (%)

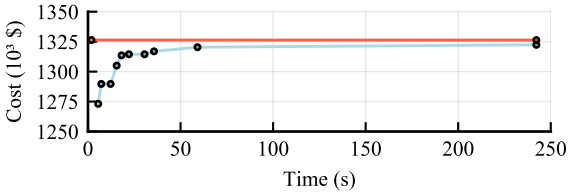

Figure 3.2: Convergence plot for the $\mathcal{M}_{ccga}$ for the 1354-PEG system.

Conclusion

This chapter proposed a tractable methodology that combines deep learning models and robust optimization for generating solutions for the SCOPF problem. The considered SCOPF modeled generator contingencies and the automatic primary response of synchronized units. Computational results over two large test cases demonstrate the practical relevance of the methodology as a scalable, easy to specify, and cost-efficient alternative tool for managing short-term scheduling.

4
Two-Stage Robust Unit Commitment for Co-Optimized Electricity Markets: An Adaptive Data-Driven Approach for Scenario-Based Uncertainty Sets

Two-stage robust unit commitment (RUC) models have been widely used for day-ahead energy and reserve scheduling under high renewable integration. The current state of the art relies on budget-constrained polyhedral uncertainty sets to control the conservativeness of the solutions. The associated lack of interpretability and parameter specification procedures, as well as the high computational burden exhibited by available exact solution techniques call for new approaches. In this chapter, we use an alternative scenario-based framework whereby uncertain renewable generation is characterized by a polyhedral uncertainty set relying on the direct specification of its vertexes. Moreover, we present a simple, yet efficient, adaptive data-driven procedure to dynamically update the uncertainty set vertexes with observed daily renewable-output profiles. Within this setting, the proposed data-driven RUC ensures protection against the convex hull of realistic scenarios empirically capturing the complex and time-varying intra-day spatial and temporal interdependences among renewable units. The resulting counterpart features advantageous properties from a computational perspective and can be effectively solved by the column-and-constraint generation algorithm until ϵ-global optimality. Out-of-sample experiments reveal that the proposed approach is capable of attaining efficient solutions in terms of cost and robustness while keeping the model tractable and scalable.

The contents of this chapter are based on the paper published in the *IEEE Transactions on Sustainable Energy* [73].

4.1
Introduction

Non-dispatchable renewable energy generation (REG) has undergone a sharp increase in the last decades and is already one of the major components in some electricity markets. High integration of these intermittent and variable energy sources brings additional challenges to short-term power system operation that are well known and have been widely discussed [6–17].

Briefly, REG variability, especially from wind power units, is driven by complex time-varying spatial and temporal dynamics [18]. In order to benefit from REG resources, a mix of conventional generation and expensive operational actions are both needed to constantly deploy (up and down) reserves in a fast and reliable way. For this reason, the uncertainty inherent to REG should be precisely accounted for in the scheduling and dispatch models used to determine appropriate levels of energy and reserves, such as those adopted in currently implemented co-optimized electricity markets [11,16,17,90,105–108].

Due to the appealing tradeoff between tractability and accuracy, two-stage adaptive robust optimization has been used to deal with uncertainty in day-ahead generation scheduling [7–17]. The interested reader is referred to [99] for a detailed literature review. In such robust unit commitment (RUC) models, a trilevel optimization problem is built to characterize the min(decision)-max(uncertainty)-min(decision) structure. Within such a scheme, the first-level problem determines, before the observation of the uncertain parameters, the day-ahead commitment for each generator. In the second-level problem, the worst-case scenario of uncertainties is selected within a given polyhedral uncertainty set as a function of the first-level decisions. Finally, in the third level, the best operational reaction (redispatch) is obtained for the second-level scenario within the first-level scheduled resources.

4.1.1 State-of-the-art literature in RUC

A key aspect in RUC is the way that uncertainties are represented. The success of an RUC model mainly depends on the selection of an uncertainty set that is capable of capturing the main patterns present in the uncertain parameters while keeping model tractability. Valuable and thorough discussions on the subject can be found in [99] and [109].

Most previously reported two-stage RUC models [7–17] rely on the budget-constrained polyhedral uncertainty set presented in [57]. The specification of a budget-constrained uncertainty set is made through linear inequality constraints defining the boundaries of a polyhedron. Such boundaries are set up by componentwise box-like limits and linear (budget) constraints limiting the number of components deviating from their nominal scenario. In this framework, each vertex of the polyhedron representing the uncertainty set is indirectly determined by the intersection of constraints, which may hinder the physical interpretation of the scenarios.

Variants of conventional budget-constrained uncertainty sets have been proposed in [61] and applied in [10–15] to better model the variability of

renewable power generation. In [10], an interesting approach based on linear models was proposed to improve the dynamics of REG scenarios. The use of parametric linear models was also described in [11]. For those cases, the polyhedral uncertainty sets were defined based on affine constraints representing linear models for renewable injections. In addition, budget constraints were applied to the residuals of the models to control the conservativeness of solutions. In [12], An and Zeng introduced variants of robust models based on linear expected-value operators (averages) applied to multiple worst-case operational costs. In such a work, each worst case resulted from a different budget-constrained uncertainty set centered on an exogenously generated scenario. Multiple spatial and temporal budget constraints were presented in [13] to increase the modeling capability. In [14], a flexible uncertainty set was characterized in terms of a user-defined parameter to capture the risk of misestimating the box-like limits for REG levels. In [15], a flexible uncertainty set was adjusted over time to provide a tradeoff between economics and robustness of the generation schedule. Notwithstanding, the approaches presented in [10–15] rely on budget-constrained uncertainty sets. Therefore, the modeling choices for describing REG variability, which features complex, nonlinear, and time-varying dynamics [18], are restricted to linear models due to tractability issues.

From a computational perspective, another drawback associated with the use of budget-constrained uncertainty sets is the combinatorial growth of the number of vertexes of the polyhedron with respect to the number of uncertain parameters. The resulting RUC models based on budget-constrained uncertainty sets are challenging instances of trilevel programming that are generally addressed through decomposition-based methods. The state-of-the-art techniques such as the column-and-constraint generation algorithm (CCGA) [68] and Benders decomposition [8] involve the iterative solution of a master problem and a subproblem, also known as oracle subproblem. In the related literature, the oracle subproblem represents the worst-case-scenario search procedure corresponding to the two lowermost optimization levels of the trilevel counterpart. Hence, the oracle is an instance of bilevel programming, which, in the presence of budget-constrained uncertainty sets, is NP-hard [8]. Solution techniques available to tackle the oracle subproblem can be categorized in two groups. On the one hand, heuristic yet efficient methods, such as variants of the outer-approximation algorithm [110], were applied in [7–10] and [13]. On the other hand, in [11, 12, 14–17], well-known linearization procedures, relying on the binary representation of the vertexes of the polyhedron characterizing the uncertainty set, were

used to obtain exact yet computationally expensive single-level equivalents based on mixed-integer linear programming (MILP). Thus, existing solution methodologies for RUC models with budget-constrained uncertainty sets either efficiently provide a solution without being able to acknowledge optimality or rely on exact MILP-based NP-hard models that are challenging to solve in practice.

4.1.2 Contributions

Motivated by the above issues of existing works [7–17] and the wide availability of REG data, the objective of this chapter is to propose an alternative to the use of budget-constrained uncertainty sets in RUC. In this work, we consider the RUC for co-optimized electricity markets, i.e., the centralized robust joint scheduling of energy and reserves targeting total cost minimization. Here, as suggested in [111], the uncertainty characterization is directly connected to data. To that end, we propose modeling the REG uncertainty in day-ahead RUC by an alternative scenario-based polyhedral uncertainty set that is built through a novel data-driven approach. Based on the general scenario-based uncertainty set description provided in [112], we define a new polyhedral uncertainty set as the convex hull of a set of exogenously generated multivariate points, or scenarios, capturing relevant information regarding the uncertainty process over a given time window. Thus, differently from [12], each vertex of the polyhedron representing the uncertainty set is defined as one of these exogenous scenarios. In the proposed data-driven framework, scenarios represent observed daily renewable-generation profiles, i.e., matrices whose dimension is given by the number of renewable units and the number of time periods of the scheduling horizon, typically 24 hours. Hereinafter, the proposed data-driven scenario-based uncertainty set is referred to as DDUS.

Two recent examples of successful application of the scenario-based uncertainty sets first proposed in [112] can be found in [113] and [114]. Within a finance context, the vertexes of the uncertainty set were generated directly from most recent observed data in [113]. Using a general mathematical setting, in [114], sampled points were endogenously selected to belong to the uncertainty set through embedded statistical hypothesis tests. In the context of RUC, however, this alternative framework has not been explored yet despite its relevant benefits.

From a modeling perspective, the use of the proposed uncertainty characterization for RUC is advantageous in several aspects as compared

with previous models relying on budget-constrained uncertainty sets [7–17]. First, the true underlying uncertainty process drives the construction of the polyhedron representing the uncertainty set, which is made up of vertexes with high physical interpretability. As a consequence, the resulting RUC features relevant information about the complex and time-varying temporal and spatial dependences found in REG within the scheduling horizon. Moreover, the novel data-driven procedure devised to build polyhedral uncertainty sets through their vertexes is an entirely exogenous adaptive and nonparametric process. Therefore, the proposed approach paves the way for the use of a wide range of existing scenario-generation methods as alternatives to the proposed data-driven procedure. For instance, any nonlinear model or data-processing scheme useful for defining or preprocessing the scenarios, such as clustering, data categorization, or filtering processes based on weather-related and real-time dispatch information, can be used to generate vertexes for the uncertainty set.

The incorporation of the proposed DDUS in RUC is also beneficial from a methodological perspective. Similar to existing models [7–17], the resulting data-driven formulation, denoted by DDRUC, is suitable for the state-of-the-art CCGA. In addition, as a salient feature, the proposed scenario-based robust framework is characterized by a relevant property: one of the multivariate points within the given time window of observed data is the worst-case vertex provided by the optimal solution of the oracle subproblem. This property results in an oracle that is solvable in polynomial time [114], unlike the oracle subproblems described in [7–17]. It is also worth mentioning that, according to our empirical findings, which are consistent with those reported in [113], the use of DDUS typically requires a narrow time window to attain high-quality solutions. This aspect is particularly relevant for the practical adoption by system operators to schedule generation in electricity markets.

The contributions of this chapter are threefold:

1. To raise awareness of the modeling capability and computational advantages of the scenario-based polyhedral uncertainty sets proposed in [112] to address REG uncertainty in RUC problems. Within this general framework, we propose defining scenarios as matrices representing the hourly generation profiles of all renewable units within a day. Hence, for the first time in the RUC literature, REG variability is described by a polyhedral uncertainty set relying on the convex hull of a polynomial set of multivariate points.

2. To propose a nonparametric data-driven procedure that defines the vertexes of the resulting polyhedral uncertainty set directly from observed data, thereby embedding the true complex and time-varying interdependences among renewable units.

3. To present a novel data-driven two-stage robust unit commitment model that is scalable, easy to specify, and suitable for the exact CCGA due to the resulting computationally inexpensive and polynomial-time-solvable oracle subproblem.

4.1.3 Chapter Organization

The rest of this chapter is organized as follows. The nomenclature in introduced in Section 4.2. In Section 4.3, the alternative uncertainty set is described. The proposed RUC model is formulated in Section 4.4. The solution methodology is presented in Section 4.5. An evaluation procedure for assessing the devised model and numerical experience are reported in Section 4.6. Finally, this chapter is concluded in Section 4.7.

4.2 Nomenclature

This section lists the notation. Bold symbols are reserved to matrices (uppercase) and vectors (lowercase). Additional symbols with superscript "(k)" denote new variables corresponding to the k-th scenario selected by the solution method.

4.2.1 Sets

$\mathcal{F}$	Feasible set for the decision variables associated with thermal generators.
$\mathcal{H}$	Set of time periods.
$\mathcal{R}$	Set of renewable energy generators.
$\mathcal{S}$	Set of renewable energy generation scenarios.
$\mathcal{S}_j$	Subset of $\mathcal{S}$ including the scenarios selected until iteration j.
$\mathcal{U}$	Uncertainty set defined as the convex hull of $\mathcal{S}$.
$\mathcal{X}$	Set of first-stage generation-related variables.

4.2.2 Constants

Γ, Λ	Spatial and temporal budgets used in the budget-constrained uncertainty set formulation.
$\Delta^{+}_{ih}, \Delta^{-}_{ih}$	Upper and lower deviation bounds for renewable generator i and period h used in the budget-constrained uncertainty set formulation.
ϵ	Feasibility tolerance.
$\mathbf{A}$	Line-bus incidence matrix.
$\mathbf{B}$	Thermal generator-bus incidence matrix.
$\mathbf{c}^{g}$	Vector of fuel costs of thermal generators.
$\mathbf{c}^{dn}, \mathbf{c}^{up}$	Vectors of cost rates for down- and up-spinning reserves.
$\mathbf{d}_h$	Vector of nodal consumptions in period h.
$\mathbf{e}$	Vector of ones with appropriate dimension.
$\overline{\mathbf{f}}$	Vector of line capacities.
$\overline{\mathbf{G}}, \underline{\mathbf{G}}$	Diagonal matrices of maximum and minimum generation limits of thermal units.
$\overline{G}_i$	Capacity of thermal unit i.
K	Number of days for observed renewable energy generation data.
$\mathbf{P}$	Renewable generator-bus incidence matrix.
RD_i, RU_i	Ramp-down and ramp-up limits of thermal unit i within two consecutive periods.
$\mathbf{R}^{dn}, \mathbf{R}^{up}$	Diagonal matrices of downward and upward limits for corrective actions of thermal units within each period.
$\mathbf{S}$	Angle-to-flow matrix.
SD_i, SU_i	Shut-down and start-up ramp rates for thermal unit i.
$\mathbf{u}_{hk}$	Vector of renewable energy generation in period h for scenario k.
$\mathbf{U}_k$	Scenario k of $\mathcal{S}$.

$\hat{\mathbf{u}}_h$	Vector of expected day-ahead renewable energy generation levels in period h.
$\hat{u}_{ih}$	Expected day-ahead power output of renewable generator i in period h.

4.2.3 First-Level Decision Vectors

$\boldsymbol{\theta}_h$	Phase angles in period h.
$\mathbf{c}_h^{sd}, \mathbf{c}_h^{su}$	Shut-down and start-up costs in period h.
$\mathbf{f}_h$	Line power flows in period h.
$\mathbf{g}_h$	Nominal generation levels in period h.
$\mathbf{r}_h^{dn}, \mathbf{r}_h^{up}$	Down- and up-spinning reserves in period h.
$\mathbf{v}_h$	Binary on/off statuses in period h.

4.2.4 Second- and Third-Level Decision Variables

α_k	Second-level decision variable representing the convex combination weight of scenario $\mathbf{U}_k$ used in the scenario-based uncertainty set $\mathcal{U}$.
$\boldsymbol{\theta}_h^{wc}$	Third-level decision vector representing the worst-case nodal phase angles in period h.
$\mathbf{f}_h^{wc}$	Third-level decision vector representing the worst-case line power flows in period h.
$\mathbf{g}_h^{wc}$	Third-level decision vector representing the worst-case generation redispatch in period h.
$\mathbf{s}_h^+, \mathbf{s}_h^-$	Third-level decision vectors representing the renewable energy spillage and load shedding in period h.
$\mathbf{U}$	Second-level decision matrix representing the generation levels for all renewable units across the day-ahead scheduling horizon.
$\mathbf{u}_h$	Second-level decision vector representing the h-th column of $\mathbf{U}$.
u_{ih}	Second-level decision variable representing the i-th element of $\mathbf{u}_h$.

z_{ih}^{+}, z_{ih}^{-} Second-level decision variables, used in the budget-constrained uncertainty set formulation, representing upward and downward deviations from the expected value for renewable generator i in period h.

4.2.5 Dual Variables

$\boldsymbol{\beta}_h$ Vector of dual variables associated with the power balance equations in period h.

$\boldsymbol{\gamma}_h, \boldsymbol{\tau}_h$ Vectors of dual variables associated with generation redispatch limits in period h.

$\boldsymbol{\zeta}_h, \boldsymbol{\kappa}_h$ Vectors of dual variables associated with ramping-up and ramping-down constraints in period h.

$\boldsymbol{\sigma}_h, \boldsymbol{\pi}_h$ Vectors of dual variables associated with the power flow capacity constraints in period h.

$\boldsymbol{\varsigma}_h, \boldsymbol{\xi}_h$ Vectors of dual variables associated with load shedding and renewable energy spillage limits in period h.

$\boldsymbol{\omega}_h$ Vector of dual variables associated with Kirchhoff's second law constraints in period h.

4.2.6 Functions

$\Phi(\cdot)$ Worst-case system power imbalance.

$\mathbf{a}(\cdot), \mathbf{b}(\cdot)$ Vector functions used to enforce ramping limits.

4.3 Uncertainty Set Characterization

In generation scheduling under high penetration of renewable-based generation, uncertain data comprise the day-ahead power output for each renewable generator $i \in \mathcal{R}$ and each time period $h \in \mathcal{H}$. Thus, we represent uncertainty by a renewable generator-by-time matrix, $\mathbf{U} \in \mathbb{R}^{|\mathcal{R}|\times|\mathcal{H}|}$, where $\mathbf{U} = [\mathbf{u}_1, ..., \mathbf{u}_h, ..., \mathbf{u}_{|\mathcal{H}|}]$ and $\mathbf{u}_h \in \mathbb{R}^{|\mathcal{R}|}$ is the uncertainty vector whose components u_{ih} correspond to the available generation of each renewable generator i in period h. Note that generation levels of different REG units may present spatial, temporal, and cross-lagged dependences.

In robust optimization, uncertainty is modeled through uncertainty sets. Before presenting the proposed DDUS, a general formulation for conventional budget-constrained uncertainty sets is provided based on the above matrix characterization.

4.3.1 Conventional Budget-Constrained Uncertainty Sets

In robust generation scheduling, uncertainty sets typically rely on fluctuation intervals representing the support of the uncertainties [7–9, 16, 17], and spatial and/or temporal budget constraints modeling the conservativeness or risk aversion of the decision maker [7–9, 13, 16, 17]. Thus, conventional budget-constrained uncertainty sets can be defined as the set of matrices $\mathbf{U}$ such that:

$$u_{ih} = \hat{u}_{ih} + \Delta^{+}_{ih} z^{+}_{ih} - \Delta^{-}_{ih} z^{-}_{ih} \qquad \forall i \in \mathcal{R},\ \forall h \in \mathcal{H} \qquad (4\text{-}1)$$

$$0 \leq z^{+}_{ih}, z^{-}_{ih} \leq 1 \qquad \forall i \in \mathcal{R},\ \forall h \in \mathcal{H} \qquad (4\text{-}2)$$

$$\sum_{i\in\mathcal{R}} z^{+}_{ih} + z^{-}_{ih} \leq \Gamma|\mathcal{R}| \qquad \forall h \in \mathcal{H} \qquad (4\text{-}3)$$

$$\sum_{h\in\mathcal{H}} z^{+}_{ih} + z^{-}_{ih} \leq \Lambda \qquad \forall i \in \mathcal{R}. \qquad (4\text{-}4)$$

As per (4-1) and (4-2), decision variables z^{+}_{ih} and z^{-}_{ih} determine the available generation for renewable generator i in period h, represented by u_{ih}. The lower and upper box-like limits, $\hat{u}_{ih} - \Delta^{-}_{ih}$ and $\hat{u}_{ih} + \Delta^{+}_{ih}$, are, respectively, the minimum and maximum possible values for u_{ih}. The first budget constraint (4-3) limits, for each period, the number of renewable generating units that may deviate from their expected value by parameter Γ, which can vary from 0 to 100%. As in [57], this constraint means that up to $\lfloor \Gamma|\mathcal{R}| \rfloor$ generators[1] can

[1] In cases where $\Gamma|\mathcal{R}|$ is not an integer, an additional renewable generator is allowed to deviate to make up for the residual fraction, $\Gamma|\mathcal{R}| - \lfloor \Gamma|\mathcal{R}| \rfloor$.

simultaneously change their production from their expected values $\hat{u}_{ih}$ to their upper or lower bounds in the same period. The second budget constraint (4-4) limits the number of periods in which each renewable generator $i \in \mathcal{R}$ can deviate from its expected production. For the sake of simplicity, parameter Λ represents an integer number of periods ranging between 0 and $|\mathcal{H}|$.

4.3.2 Scenario-Based Uncertainty Sets Driven by Data

In order to build a flexible, easy to specify, and practical uncertainty set that allows scalability for the available exact solution techniques for RUC, we propose a scenario-based polyhedral uncertainty set [112–114] to model REG uncertainty. To that end, the uncertainty set is defined as the convex hull of a set of multivariate points representing scenarios, i.e., REG profiles. Among the various exogenous approaches that could be used to generate the scenarios, we propose the use of a data-driven scheme. Historical daily profiles are therefore directly used as scenarios, thereby embedding relevant information about the true underlying uncertainty process in each vertex of the uncertainty set. Mathematically, the proposed DDUS, $\mathcal{U}$, is cast as follows:

$$\mathcal{U} = \left\{ \mathbf{U} \in \mathbb{R}^{|\mathcal{R}|\times|\mathcal{H}|} \middle| \mathbf{U} = \sum_{k=1}^{K} \alpha_k \mathbf{U}_k, \sum_{k=1}^{K} \alpha_k = 1, \alpha_k \geq 0 \right\} \tag{4-5}$$

where $\{\mathbf{U}_k\}_{k=1,\ldots,K}$ is the set of daily REG profiles corresponding to K previous days, which is hereinafter referred to as $\mathcal{S}$. Note that $\mathcal{U}$ is the convex hull of $\mathcal{S}$, thereby representing the smallest convex set that contains every scenario in $\mathcal{S}$. Moreover, by definition, the vertexes of the polyhedral uncertainty set $\mathcal{U}$ are in $\mathcal{S}$ [44]. Additionally, it is worth highlighting that the conservativeness level of the proposed DDUS is solely modeled by K. As a consequence, this parameter must be adjusted based on an out-of-sample test according to the decision maker's preference on cost and reliability.

The capability of DDUS to capture temporal and spatial dependences is illustrated in Figs. 4.1 and 4.2, where two-dimensional projections of the multidimensional DDUS are shown for the data of the second case study examined in Section 4.6, for the period between 10/31/2012 and 12/15/2012. Fig. 4.1 shows a high-dependence pattern, exhibited in bus 5 for 12:00 p.m. and 1:00 p.m., and a low-dependence pattern, observed in the same bus for 12:00 p.m. and 6:00 p.m. Likewise, different spatial dependences can be visualized in Fig. 4.2 for 9:00 a.m.

An interesting interpretation for the use of observed generation profiles as vertexes of the uncertainty set is that we are implicitly performing an endogenous stress test for each feasible solution of the RUC problem whereby

relevant multidimensional dependences found in the true hourly REG within a day are empirically accounted for. Furthermore, by using the proposed DDUS within an adaptive decision-making scheme, the evolution of the REG dependences across time can be dynamically updated. Hence, strong assumptions about the nature of the true model behind data are not required.

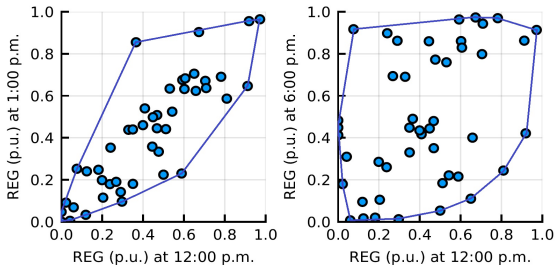

Figure 4.1: Examples of temporal dependences.

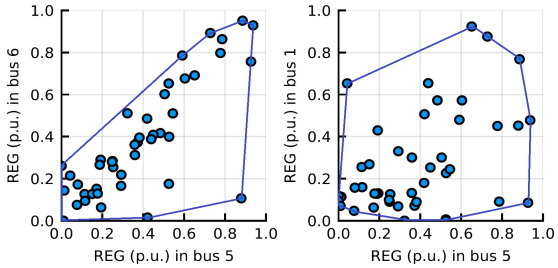

Figure 4.2: Examples of spatial dependences.

Moreover, note that the proposed framework can be adapted to consider sophisticated REG forecasts. As an example, any exogenous day-ahead forecasting procedure could be used to detrend/deseasonalize historical data and generate forecast errors. The errors computed for the K previous days could thus be added to an updated day-ahead forecast to generate data-driven adjusted scenarios to build $\mathcal{S}$. With this simple preprocessing scheme, the shaping capability of the proposed data-driven approach could be straightforwardly combined with state-of-the-art forecasting methods.

It is also worth mentioning that, if, instead of using real data, our data-driven model were built based on a Monte Carlo simulation of a time-series model, as done under a stochastic programming framework, our model can be viewed as a sampled version of a chance-constrained model. For instance, according to Calafiore [115], if the number of scenarios K (generated through Monte Carlo sampling methods) in DDUS is greater than $|\mathcal{R}||\mathcal{H}|/\varepsilon - 1$, where $\varepsilon \in (0, 1)$ is a user-defined parameter that can be made arbitrarily small, the expected probability of violations (shedding load or curtailing REG) remains below ε. As per our numerical experiments, the CCGA, in practice,

converges with a much smaller subset of the K sampled scenarios. Hence, in the case where our model is used to reproduce sample-based chance-constrained problems as done in [115], our robust approach would be a computationally efficient solution methodology.

4.4 Two-Stage Robust Unit Commitment Model

For expository purposes, we use a standard two-stage robust optimization framework with a single uncertainty set [99], which is a particular instance of the general notion of stochastic robust optimization presented in [12] and [116]. This model is simpler to describe and analyze yet bringing out the main features of the proposed data-driven approach. Based on previous works on robust energy and reserve scheduling [11,16,17] and industry practice [105,117], a base-case dispatch for energy is considered while ensuring ϵ-feasibility for all realizations within the uncertainty set. The mathematical formulation for the proposed DDRUC problem is as follows:

$$\min_{\mathcal{X},[\boldsymbol{\theta}_h,\mathbf{f}_h]_{h\in\mathcal{H}}} \sum_{h\in\mathcal{H}} \left\{ \mathbf{e}'(\mathbf{c}_h^{sd}+\mathbf{c}_h^{su}) + \ (\mathbf{c}^g)'\mathbf{g}_h + \ (\mathbf{c}^{up})'\,\mathbf{r}_h^{up} + \ (\mathbf{c}^{dn})'\mathbf{r}_h^{dn} \right\} \tag{4-6}$$

subject to:

$$\mathbf{A}\mathbf{f}_h + \mathbf{B}\mathbf{g}_h + \mathbf{P}\hat{\mathbf{u}}_h = \mathbf{d}_h \qquad \forall h\in\mathcal{H} \tag{4-7}$$

$$-\overline{\mathbf{f}} \le \mathbf{f}_h \le \overline{\mathbf{f}} \qquad \forall h\in\mathcal{H} \tag{4-8}$$

$$\mathbf{f}_h = \mathbf{S}\boldsymbol{\theta}_h \qquad \forall h\in\mathcal{H} \tag{4-9}$$

$$\underline{\mathbf{G}}\mathbf{v}_h + \mathbf{r}_h^{dn} \le \mathbf{g}_h \le \overline{\mathbf{G}}\mathbf{v}_h - \mathbf{r}_h^{up} \qquad \forall h\in\mathcal{H} \tag{4-10}$$

$$\mathbf{0} \le \mathbf{r}_h^{up} \le \mathbf{R}^{up}\,\mathbf{v}_h \qquad \forall h\in\mathcal{H} \tag{4-11}$$

$$\mathbf{0} \le \mathbf{r}_h^{dn} \le \mathbf{R}^{dn}\,\mathbf{v}_h \qquad \forall h\in\mathcal{H} \tag{4-12}$$

$$-\mathbf{b}(\mathbf{v}_h,\mathbf{v}_{h-1}) \le \mathbf{g}_h - \mathbf{g}_{h-1} \le \mathbf{a}(\mathbf{v}_h,\mathbf{v}_{h-1}) \qquad \forall h\in\mathcal{H} \tag{4-13}$$

$$\{\mathbf{c}_h^{sd},\mathbf{c}_h^{su},\mathbf{v}_h\}_{h\in\mathcal{H}} \in \mathcal{F} \tag{4-14}$$

$$\Phi(\mathcal{X}) \le \epsilon \tag{4-15}$$

$$\Phi(\mathcal{X}) = \max_{\mathbf{U}\in\mathcal{U}} \left\{ \min_{\substack{[\boldsymbol{\theta}_h^{wc},\mathbf{f}_h^{wc},\\ \mathbf{g}_h^{wc},\mathbf{s}_h^{+},\\ \mathbf{s}_h^{-}]_{h\in\mathcal{H}}}} \sum_{h\in\mathcal{H}} \mathbf{e}'(\mathbf{s}_h^{+}+\mathbf{s}_h^{-}) \right. \tag{4-16}$$

subject to:

$$\mathbf{A}\mathbf{f}_h^{wc} + \mathbf{B}\mathbf{g}_h^{wc} + \mathbf{P}\mathbf{u}_h = \mathbf{d}_h + \mathbf{s}_h^{+} - \mathbf{s}_h^{-} \quad : (\boldsymbol{\beta}_h) \qquad \forall h\in\mathcal{H} \tag{4-17}$$

$$-\overline{\mathbf{f}} \le \mathbf{f}_h^{wc} \le \overline{\mathbf{f}} \quad : (\boldsymbol{\sigma}_h,\boldsymbol{\pi}_h) \qquad \forall h\in\mathcal{H} \tag{4-18}$$

$$\mathbf{f}_h^{wc} = \mathbf{S}\boldsymbol{\theta}_h^{wc} \quad : (\boldsymbol{\omega}_h) \qquad \forall h\in\mathcal{H} \tag{4-19}$$

$$\mathbf{g}_h^{wc} - \mathbf{g}_{h-1}^{wc} \le \mathbf{a}(\mathbf{v}_h,\mathbf{v}_{h-1}) \quad : (\boldsymbol{\zeta}_h) \qquad \forall h\in\mathcal{H} \tag{4-20}$$

$$\mathbf{g}^{wc}_{h-1} - \mathbf{g}^{wc}_{h} \leq \mathbf{b}(\mathbf{v}_h, \mathbf{v}_{h-1}) \quad : (\boldsymbol{\kappa}_h) \quad \forall h \in \mathcal{H} \quad (4\text{-}21)$$

$$\mathbf{g}_h - \mathbf{r}^{dn}_h \leq \mathbf{g}^{wc}_h \leq \mathbf{g}_h + \mathbf{r}^{up}_h \quad : (\boldsymbol{\gamma}_h, \boldsymbol{\tau}_h) \quad \forall h \in \mathcal{H} \quad (4\text{-}22)$$

$$\mathbf{0} \leq \mathbf{s}^{-}_h \leq \mathbf{d}_h \quad : (\boldsymbol{\varsigma}_h) \quad \forall h \in \mathcal{H} \quad (4\text{-}23)$$

$$\mathbf{0} \leq \mathbf{s}^{+}_h \leq \mathbf{P}\mathbf{u}_h \quad : (\boldsymbol{\xi}_h) \quad \forall h \in \mathcal{H}\Big\}, \quad (4\text{-}24)$$

where $\mathcal{X}$ is the set of first-level variables related to generation, i.e., $\mathcal{X} = [\mathbf{c}^{sd}_h, \mathbf{c}^{su}_h, \mathbf{g}_h, \mathbf{r}^{dn}_h, \mathbf{r}^{up}_h, \mathbf{v}_h]_{h\in\mathcal{H}}$, and third-level dual variables are shown in parentheses.

The two-stage DDRUC (4-6)–(4-24) is formulated as a (min-max-min) trilevel optimization problem. The first optimization level (4-6)–(4-15) determines the on/off statuses of generating units, as well as the energy and reserve scheduling. The objective function (4-6) comprises shut-down costs, start-up costs, production costs, and up- and down-reserve costs. Constraint (4-7) represents nodal power balance under a dc power flow model. Expression (4-8) represents transmission line power flow limits, while Kirchhoff's second law is accounted for through (4-9). The limits for generation levels and up- and down-spinning reserves are imposed in expressions (4-10)–(4-12). Inter-period ramping limits are modeled by (4-13), where the components of the auxiliary vector functions $\mathbf{a}(\cdot)$ and $\mathbf{b}(\cdot)$ are [16]: $a_i(v_{ih}, v_{ih-1}) = RU_i v_{ih-1} + SU_i(v_{ih} - v_{ih-1}) + \overline{G}_i(1 - v_{ih})$ and $b_i(v_{ih}, v_{ih-1}) = RD_i v_{ih} + SD_i(v_{ih-1} - v_{ih}) + \overline{G}_i(1 - v_{ih-1})$. Following [22], equation (4-14) represents constraints related to shut-down costs, start-up costs, and minimum up and down times. Equation (4-15) ensures redispatch capability within a feasibility tolerance, ϵ, under the set $\mathcal{X}$ for all plausible realizations within the uncertainty set.

The second-level problem comprises the outer maximization problem in (4-16). The goal of the second-level problem is to find the weights $\{\alpha_k\}_{k=1,\ldots,K}$ in (4-5) corresponding to the worst-case uncertainty realization $\mathbf{U} \in \mathcal{U}$ for a given value of $\mathcal{X}$. The measure of worst case is given by the minimum power imbalance function, which receives as inputs the values of the first- and second-level variables, $\mathcal{X}$ and $\mathbf{U}$, respectively. The third-level problem, i.e., the inner minimization problem (4-16)–(4-24), plays the role of the minimum power imbalance function. The objective of this problem is to find a redispatch solution that minimizes the total sum of the mismatch variables artificially introduced in the power balance constraint (4-17). The mismatch variables, $\mathbf{s}^{-}_h$ and $\mathbf{s}^{+}_h$, can be interpreted as load shedding and REG spillage, respectively. Constraints (4-17)–(4-21) are analogous to first-level expressions (4-7)–(4-9) and (4-13). The maximum operational deviation from nominal scheduled generation is controlled by constraint (4-22), whereby generation redispatch

levels $\mathbf{g}_h^{wc}$ are limited by up- and down-reserves.

Within this approach, by ensuring ϵ-feasibility for a given set of observed data points, the proposed DDRUC provides solutions that are optimized and tight for a given stress test setup. Therefore, the resulting reserve procurement can be interpreted as the least-cost schedule that allows reserve deliverability for realistic system-stress conditions. The proposed approach differs from current industry practice, where stress tests are applied *ex post* as offline validation procedures.

4.5 Solution Methodology

This work leverages from the fact that the two lowermost levels (4-16)–(4-24) correspond to a maximization, within a polyhedral uncertainty set $\mathcal{U}$, of a convex function given by the output of the inner minimization in (4-16) as a function of $\mathbf{U}$. Therefore, from standard results of convex analysis, one of the vertexes belongs to the optimal solution set [44]. In other words, at the optimal solution, all α_k are equal to 0 except that corresponding to the worst-case vertex, which is equal to 1, thereby being binary valued. Hence, we can replace the continuous polyhedral uncertainty set $\mathcal{U}$ in the outer maximization of (4-16) with the discrete set of scenarios $\mathcal{S}$. By doing so, problem (4-6)–(4-24) can be cast as a single-level MILP-based equivalent wherein expressions (4-16)–(4-24) are replaced with one set of redispatch constraints (4-17)–(4-24) for each one of the K scenarios in $\mathcal{S}$. Such a scenario-based model is structurally similar to that presented in [118] for a different problem, namely stochastic unit commitment. Unfortunately, addressing such a full-scenario-based equivalent by the branch-and-cut algorithm may lead to intractability.

Alternatively, problem (4-6)–(4-24), and its single-level equivalent, likewise, are suitable for the CCGA [68], which ensures finite convergence to global optimality by iteratively solving a master problem and an oracle subproblem. At each iteration, the master problem, which is a relaxed version of the full-scenario-dependent equivalent problem, finds a trial solution that is evaluated in terms of operational feasibility by the oracle procedure. The oracle returns to the master problem violated constraints that will change the master problem solution at the next iteration. The algorithm terminates when the oracle does not find any violated constraint, thereby certifying the incumbent trial solution as globally optimal.

4.5.1

Master Problem

The master problem is a relaxed version of problem (4-6)–(4-24). Thus, at each iteration j of the CCGA, the master problem is an instance of MILP as follows:

$$\min_{\substack{\mathcal{X},[\boldsymbol{\theta}_h,\mathbf{f}_h]_{h\in\mathcal{H}} \\ [\boldsymbol{\theta}_h^{(k)},\mathbf{f}_h^{(k)},\mathbf{g}_h^{(k)},\mathbf{s}_h^{+(k)}, \\ \mathbf{s}_h^{-(k)}]_{h\in\mathcal{H},k=1,\ldots,|\mathcal{S}_j|}}} \sum_{h\in\mathcal{H}} \left\{ \mathbf{e}'(\mathbf{c}_h^{sd}+\mathbf{c}_h^{su}) + (\mathbf{c}^g)'\mathbf{g}_h + \quad (\mathbf{c}^{up})'\mathbf{r}_h^{up} + (\mathbf{c}^{dn})'\mathbf{r}_h^{dn} \right\} \quad (4\text{-}25)$$

subject to:

$$\text{Constraints (4-7)–(4-14)} \quad (4\text{-}26)$$

$$\text{Redispatch constraints for scenario } k, \qquad k=1,\ldots,|\mathcal{S}_j| \quad (4\text{-}27)$$

$$\sum_{h\in\mathcal{H}} \mathbf{e}'(\mathbf{s}_h^{+(k)} + \mathbf{s}_h^{-(k)}) \le \epsilon, \qquad k=1,\ldots,|\mathcal{S}_j| \quad (4\text{-}28)$$

where set $\mathcal{S}_j$ comprises the scenarios of $\mathcal{S}$ selected by the oracle subproblem until iteration j of the CCGA.

Expressions (4-25)–(4-26) are identical to (4-6)–(4-14). As per (4-27), a set of redispatch constraints is iteratively added. Such redispatch constraints correspond to (4-17)–(4-24) where variables $\boldsymbol{\theta}_h^{wc}, \mathbf{f}_h^{wc}, \mathbf{g}_h^{wc}, \mathbf{s}_h^{+}$, and $\mathbf{s}_h^{-}$ are respectively replaced with new variables $\boldsymbol{\theta}_h^{(k)}, \mathbf{f}_h^{(k)}, \mathbf{g}_h^{(k)}, \mathbf{s}_h^{+(k)}$, and $\mathbf{s}_h^{-(k)}$, whereas $\mathbf{u}_h$ is replaced with the corresponding scenario of $\mathcal{S}_j$ selected at previous iterations by the oracle subproblem. Finally, in (4-28), the system power imbalance under every scenario in $\mathcal{S}_j$ is bounded by the threshold ϵ.

4.5.2 Oracle Subproblem

The oracle subproblem corresponds to the two lowermost optimization levels (4-16)–(4-24) for given upper-level decisions provided by the preceding master problem. This bilevel program can be solved in two different ways:

1. By the enumeration of all feasible values for variables α_k. This solution approach, hereinafter referred to as the *inspection-based oracle*, consists in the serial or parallel evaluation of the imbalance through the solution of the third-level problem for all K scenarios in $\mathcal{S}$. The inspection-based oracle is thus equivalent to searching through all vectors $\{\alpha_k\}_{k=1,\ldots,K}$ that are candidates for optimality, i.e., those with one entry equal to 1 and all other entries equal to 0. Note that each optimization problem is a linear program, which runs in polynomial time with interior point methods. As the value of K is not related to the instance size, the inspection-based oracle can be easily implemented as a computational

routine that receives a pair $(\mathcal{X}^*, \mathcal{S})$ and returns the worst-case scenario $\mathbf{U}^*$ in $\mathcal{S}$ and the associated power imbalance $\Phi(\mathcal{X}^*)$ in polynomial time [114].

2. By the application of branch-and-cut algorithms (readily available in off-the-shelf MILP solvers) to a single-level MILP-based equivalent subproblem. Based on a discrete representation of $\mathcal{S}$, this solution approach consists in casting the original bilevel subproblem as a single-level MILP equivalent, denoted by *MILP-based oracle* subproblem. Such an equivalent requires modeling variables α_k as binary, using the dual of the lower level of the subproblem, and applying well-known integer algebra results [119] to recast the resulting bilinear terms as linear expressions. The MILP-based oracle subproblem is thus a linearized version (relying on standard disjunctive constraints) of this mixed-integer nonlinear problem:

$$\begin{aligned}\Phi(\mathcal{X}) = \max_{\substack{[\alpha_k]_{k\in\mathcal{K}},\\ [\boldsymbol{\beta}_h,\boldsymbol{\gamma}_h,\boldsymbol{\zeta}_h,\boldsymbol{\kappa}_h,\boldsymbol{\xi}_h,\boldsymbol{\pi}_h,\\ \boldsymbol{\sigma}_h,\boldsymbol{\varsigma}_h,\boldsymbol{\tau}_h,\boldsymbol{\omega}_h,\mathbf{u}_h]_{h\in\mathcal{H}}}} \sum_{h\in\mathcal{H}} \Big\{ & \boldsymbol{\beta}_h'(\mathbf{d}_h - \mathbf{P}\mathbf{u}_h) \\ & - \boldsymbol{\pi}_h'\overline{\mathbf{f}} - \boldsymbol{\sigma}_h'\overline{\mathbf{f}} \\ & + \boldsymbol{\gamma}_h'(\mathbf{g}_h - \mathbf{r}_h^{dn}) \\ & - \boldsymbol{\tau}_h'(\mathbf{g}_h + \mathbf{r}_h^{up}) \\ & - \boldsymbol{\zeta}_h'\mathbf{a}(\mathbf{v}_h, \mathbf{v}_{h-1}) \\ & + \boldsymbol{\kappa}_h'\mathbf{b}(\mathbf{v}_h, \mathbf{v}_{h-1}) \\ & - \boldsymbol{\varsigma}_h'\mathbf{d}_h - \boldsymbol{\xi}_h'\mathbf{P}\mathbf{u}_h \Big\} \end{aligned} \tag{4-29}$$

subject to:

$$\mathbf{u}_h = \sum_{k\in\mathcal{S}} \alpha_k \mathbf{u}_{hk} \qquad \forall h \in \mathcal{H} \tag{4-30}$$

$$\sum_{k\in\mathcal{S}} \alpha_k = 1 \tag{4-31}$$

$$\alpha_k \in \{0,1\} \qquad \forall k \in \mathcal{S} \tag{4-32}$$

$$\boldsymbol{\beta}_h - \boldsymbol{\varsigma}_h \leq \mathbf{e} \qquad \forall h \in \mathcal{H} \tag{4-33}$$

$$-\boldsymbol{\beta}_h - \boldsymbol{\xi}_h \leq \mathbf{e} \qquad \forall h \in \mathcal{H} \tag{4-34}$$

$$-\mathbf{A}'\boldsymbol{\beta}_h + \boldsymbol{\pi}_h - \boldsymbol{\sigma}_h - \boldsymbol{\omega}_h = \mathbf{0} \qquad \forall h \in \mathcal{H} \tag{4-35}$$

$$-\mathbf{S}'\boldsymbol{\omega}_h = \mathbf{0} \qquad \forall h \in \mathcal{H} \tag{4-36}$$

$$\begin{aligned} -\boldsymbol{\gamma}_h + \boldsymbol{\tau}_h - \mathbf{B}'\boldsymbol{\beta}_h + \boldsymbol{\zeta}_h \\ - \boldsymbol{\zeta}_{h+1} - \boldsymbol{\kappa}_h + \boldsymbol{\kappa}_{h+1} \geq \mathbf{0} \end{aligned} \qquad \forall h \in \mathcal{H} \tag{4-37}$$

$$\boldsymbol{\pi}_h, \boldsymbol{\sigma}_h, \boldsymbol{\tau}_h, \boldsymbol{\gamma}_h, \boldsymbol{\zeta}_h, \boldsymbol{\kappa}_h, \boldsymbol{\varsigma}_h, \boldsymbol{\xi}_h \geq \mathbf{0} \qquad \forall h \in \mathcal{H}. \tag{4-38}$$

In (4-29)–(4-38), the objective function (4-29) and constraints (4-33)–(4-38) represent, respectively, the objective function and constraints of the dual formulation for the third-level problem presented in (4-16)–(4-24). The proposed DDUS is equivalently modeled by constraints (4-30)–(4-32), where $\mathbf{u}_{hk}$ stands for the h-th column of the k-th data point, $\mathbf{U}_k$. According to (4-5) and the aforementioned results of convex analysis, $\mathcal{U}$ is replaced with $\mathcal{S}$ in (4-30) and (4-31), whereas variables α_k are characterized as binary in (4-32). Note that problem (4-29)–(4-38) is a mixed-integer nonlinear optimization problem with bilinear terms in the objective function (4-29). Such nonlinearities involve products of $\mathbf{u}_h$ and third-level dual variables. As is customary in the literature [11, 16, 17], an equivalent MILP formulation for (4-29)–(4-38), i.e., the MILP-based oracle, is achieved by applying standard integer algebra results [119] that allow recasting the nonlinear products in (4-29) as linear expressions.

4.5.3 Algorithm

For given $\mathcal{S}$ and ϵ, the proposed CCGA works as follows:

Algorithm CCGA($\mathcal{S}$, ϵ)

1: Initialization: $j \leftarrow 0$ and $\mathcal{S}_j \leftarrow \emptyset$.
2: Solve the master problem (4-25)–(4-28) to obtain $\mathcal{X}^*$.
3: Solve the subproblem for ($\mathcal{X}^*$, $\mathcal{S}$) to obtain $\Phi(\mathcal{X}^*)$ and the worst-case scenario $\mathbf{U}^*$.
4: **if** $\Phi(\mathcal{X}^*) \leq \epsilon$ **then :** STOP
5: **else:** $j \leftarrow j + 1$, $\mathcal{S}_j \leftarrow \mathcal{S}_{j-1} \cup \{\mathbf{U}^*\}$, and go to step 2
6: **end if**.

The algorithm iteratively adds violated constraints into the master problem and terminates when infeasibility is within ϵ.

In order to reduce the search space, vertex-identification algorithms [120] could be implemented *ex ante* to determine the subset of $\mathcal{S}$ comprising the vertexes of $\mathcal{U}$. However, in a high-dimensional case, it is very unlikely to find a point in $\mathcal{S}$ that is not a vertex of $\mathcal{U}$. Hence, the use of vertex-identification procedures, in practice, may deteriorate the performance of the CCGA as only an insignificant number of points of $\mathcal{S}$, most likely none, would be excluded for being in the interior of the DDUS.

4.6 Numerical Results

This section reports results from an illustrative 4-bus system and the IEEE 118-bus test system over a 24-hour time span. For the sake of reproducibility, data for both test systems can be downloaded from [121]. For expository purposes, wind-related uncertainty is considered. The source of data for wind power generation is the Global Energy Competition (GEFCom) [122, 123].

As explained in the next section, the proposed DDRUC has been assessed with two benchmark models based on two-stage robust optimization and two-stage stochastic programming. Such an assessment has been conducted through backtesting on historical data observed over a given set of days.

The benchmark RUC model, hereinafter referred to as BRUC, relies on the budget-constrained uncertainty set formulated in Section 4.3.1. DDRUC has been implemented for different time windows, i.e., for different values of K, whereas different combinations of budgets Γ and Λ were considered for BRUC. For quick reference, the instances of both models are denoted by DDRUC(K) and BRUC(Γ,Λ), respectively. For a given day d, the uncertainty set for DDRUC(K) is directly defined using the REG profiles observed in the K previous days, i.e., considering $\mathcal{S}$ as $\{\mathbf{U}_k\}_{k=d-K,\ldots,d-1}$.

For the sake of a fair comparison, BRUC is also adaptively adjusted across the rolling-horizon study, similarly to DDRUC, in order to prevent over-conservative solutions. This is done through a moving window of previous observed days within which the lower and upper box-like limits used in the budget-constrained uncertainty sets are defined according to the corresponding hourly minimum and maximum production limits for each renewable unit. Our tests indicated that the length of such a moving window is not as relevant for BRUC as the selection of K is for DDRUC. Hence, based on trial and error, the budget-constrained uncertainty sets for BRUC(Γ,Λ) were built using the previous 35 days.

The instances of DDRUC were addressed by the CCGA with both the inspection- and the MILP-based oracle subproblems. In contrast, BRUC was solved by the CCGA with a modified version of the MILP-based oracle subproblem, as done in [16]. To that end, expressions (4-30) and (4-31) in problem (4-29)–(4-38), representing the uncertainty set constraints, were replaced with (4-1)–(4-4), whereas the linearization scheme mentioned in Section 4.5.2 was applied to the resulting bilinear terms.

Additionally, in order to provide a comparison between the proposed data-driven robust approach and stochastic programming, a benchmark

stochastic unit commitment model, hereinafter referred to as BSUC, was analyzed. BSUC is a mixed-integer linear program structurally similar to the DDRUC master problem (4-25)–(4-28). Three differences characterize BSUC, namely 1) an expected imbalance cost term is added to the objective function (4-25), 2) the set of scenarios in (4-27) comprises uncertainty realizations obtained from a scenario-generation procedure using probabilistic information, and 3) imbalance requirements are eliminated by dropping constraint (4-28). The value of the imbalance cost was set to \$500/MWh, which corresponds approximately to 25 times the average value (or 13 times the highest value) of the fuel costs, $\mathbf{c}^g$, for the thermal generators.

The scenario-generation procedure for BSUC was based on a multivariate lognormal distribution inferred from the previous 100 days. First, the historical data were normalized and a logarithmic transformation was applied. Then, a multivariate normal distribution was estimated and 500 independent and equally distributed scenarios were generated based on the expected value vector and the covariance matrix. Finally, the inverse transformations were applied to rescale the scenarios. As for the solution methodology, BSUC was tackled by the branch-and-cut algorithm, which was initialized with the previous day's solution for binary scheduling variables and reserve contributions.

Simulations were run using Gurobi 7.0.2 under JuMP (Julia 0.5) on a Xeon E5-2680 processor at 2.5 GHz and 128 GB of RAM.

4.6.1 Evaluation Methodology

The performances of DDRUC(K), BRUC(Γ,Λ), and BSUC have been compared in terms of their tradeoff between cost and robustness. The evaluation methodology consists in conducting a rolling-horizon out-of-sample backtest over a set of days for which realistic REG data are available.

For each day d within the backtest horizon, the instances under assessment are solved using available historical REG data for past days, i.e., excluding day d. The solution of such instances of DDRUC, BRUC, and BSUC yields the corresponding values of the total cost for that day. Subsequently, solution robustness is quantified by computing the infeasibility of the generation dispatch associated with the resulting generation schedules and the actual REG scenario observed for day d. To that end, based on industry practice, a single-period version of the inner minimization problem in (4-16)–(4-24) is solved for each hour of this day. Hence, based on the resulting hourly levels of load shedding and REG spillage, out-of-sample statistics for robustness are devised.

Instance	Avg. time (s)	Avg. iter. no.	Avg. cost ($)	LOLP (%)	PWS (%)
DDRUC(42)	20.0 (34.7)	13.4	62122	1.56	2.67
DDRUC(35)	17.7 (28.8)	12.8	61894	1.85	3.53
DDRUC(28)	15.2 (23.2)	12.0	61592	2.33	4.15
DDRUC(20)	11.9 (17.0)	10.9	61121	3.91	5.43
BRUC(90,24)	157.7	6.2	66256	4.13	1.00
BRUC(90,1)	688.7	71.5	63401	5.36	1.09
BRUC(70,24)	115.9	6.5	62349	12.44	2.86
BRUC(50,24)	13.0	6.2	60571	21.60	5.25
BSUC	1494.0	–	61967	9.78	2.96

Table 4.1: 4-Bus System –Results from DDRUC, BRUC, and BSUC

4.6.2 Illustrative 4-Bus System

First, we consider an illustrative test system consisting of 4 buses, 4 transmission lines, 14 thermal generators, and 2 wind farms [121]. Wind generation data were rescaled from buses 2 and 5 from [122]. The optimality gap of Gurobi was set at 0% and the CCGA was implemented until no imbalance was found for the instances of DDRUC and BRUC. Hence, such simulations were run to optimality for $\epsilon = 0$. As for BSUC, a time limit of 1,500 seconds was considered. The evaluation backtest was conducted for 336 days of realistic wind power generation data. Table 4.1 and Fig. 4.3 summarize the results from the backtest for several instances of DDRUC, BRUC, and BSUC.

Columns 2–4 of Table 4.1 respectively provide the average computing times, iteration numbers, and costs over the 336 runs of the models being examined. For the instances of DDRUC, the first figure in column 2 corresponds to the method using the inspection-based oracle subproblem, whereas the second figure in parentheses is associated with the approach relying on the solution of the MILP-based equivalent for the oracle subproblem. Column 5 presents a reliability index referred to as loss of load probability (LOLP), which is defined as the fraction of hours with load shedding exceeding 0.1% of the system load. Analogously, column 6 reports the probability of wind spillage (PWS), defined as the fraction of hours in which wind spillage exceeds 0.1% of the available wind power generation. Thus, the values of LOLP and PWS listed in Table 4.1 represent valuable statistical information on the robustness of the solutions provided by each model.

Table 4.1 shows the impact of K on the computational effort required by DDRUC. It should be emphasized that the number of iterations of the

CCGA grows at a less than linear rate with K whereas computing times behave similarly. As a relevant result, the impact of K on computing times is lower when the subproblem is solved by the vertex inspection, which outperforms the MILP solver for all instances.

As compared with BRUC, DDRUC is in general more effective from a computational perspective. For the instances with no temporal budget constraints ($\Lambda = 24$), the average numbers of iterations for BRUC are approximately half of those required to solve the instances of DDRUC. However, such reduced numbers of iterations do not imply shorter computing times because the MILP-based oracle for BRUC is computationally expensive. Moreover, for $\Lambda = 1$, which is far less conservative, BRUC requires significantly more iterations to converge on average, thereby increasing the computational burden. An exception is the instance BRUC(50, 24), which is a particular case with no temporal budget constraints and a spatial budget corresponding to precisely a single renewable generator deviating from the expected production. Interestingly, this was the case for which BRUC achieved the worst solution robustness in terms of LOLP, which is 5.5 times higher than the worst level attained by DDRUC. Regarding BSUC, its required computational effort is considerably greater than those of DDRUC and BRUC. The 1,500-s time limit was reached almost every day of the rolling-window study.

As can also be observed in Table 4.1, as K grows from 20 to 42, both LOLP and PWS decrease. Note also that, in comparison with BRUC and BSUC, all solutions provided by DDRUC gave rise to acceptably small LOLP values ranging between 1.56% and 3.91%, while keeping the average cost at reasonable levels within a narrow 1.6% band. The superiority of DDRUC over BRUC and BSUC is thus evidenced in terms of the tradeoff between cost and robustness. Such a tradeoff is further illustrated in Fig. 4.3, where robustness is expressed in terms of the out-of-sample reliability index LOLP. Note that the solutions to DDRUC dominate in Pareto sense (lower cost and lower LOLP) almost all solutions provided by BRUC. The only non-dominated BRUC instance is the aforementioned BRUC(50, 24), which, albeit incurring the lowest average cost, leads to an unreasonably high LOLP. Analogously, despite featuring a reasonable average cost, the solution provided by BSUC gave rise to a very high value of LOLP, namely 9.78%, which was substantially outperformed by all instances of DDRUC. Hence, the BSUC solution was dominated by the instances DDRUC(20), DDRUC(28), and DDRUC(35).

A breakdown of the average costs provided in column 4 of Table 4.1 is presented in Table 4.2 for representative instances of DDRUC, BRUC, and BSUC models. Thus, average production costs, average reserve costs, and

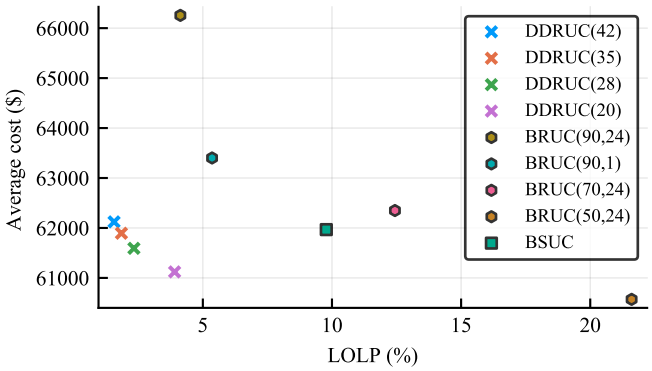

Figure 4.3: Average cost vs. LOLP for the 4-bus system.

Instance	Total	Production	Reserve	Start-up and shut-down
DDRUC(35)	61.9	55.7	6.1	0.1
DDRUC(20)	61.1	55.5	5.5	0.1
BRUC(90,24)	66.3	57.2	9.0	0.1
BRUC(90,1)	63.4	56.2	7.1	0.1
BSUC	62.0	55.7	6.2	0.1

Table 4.2: 4-Bus System – Average Cost Breakdown (10^3 $)

average start-up and shut-down costs are reported. It can be observed that the largest cost component is the average production cost, representing between 86% and 91% of the average total cost for all instances. However, the average reserve cost, which amounts to between 9% and 14% of the average total cost, is the most relevant in terms of cost difference for any pair of instances. Overall, reserve costs for DDRUC and BSUC are considerably lower than those for BRUC. For further details, daily reserve costs are shown in Fig. 4.4. As compared to BRUC, DDRUC and BSUC were able to address the next-day REG profile with lower levels of reserves. Moreover, daily reserve costs for DDRUC are less variable than those for BSUC due to the inherent stochastic nature of the scenario-generation procedure.

For illustration purposes, Fig. 4.5 depicts two two-dimensional projections of the scenarios in $\mathcal{S}$ for the 43^{rd} day of the rolling window. The 8 scenarios colored in red correspond to the scenarios selected by the CCGA for DDRUC(35). Not surprisingly, some of the selected scenarios present very high or very low REG profiles. Such scenarios are more likely to yield higher imbalance costs (from either wind spillage or load shedding) at intermediate iterations of the CCGA. Salient features of the selected scenarios are also characterized by the scatter plot in Fig. 4.6, which shows the total 24-hour REG and the largest absolute variation of renewable generation between two consecutive hours of each scenario. Note that the two scenarios

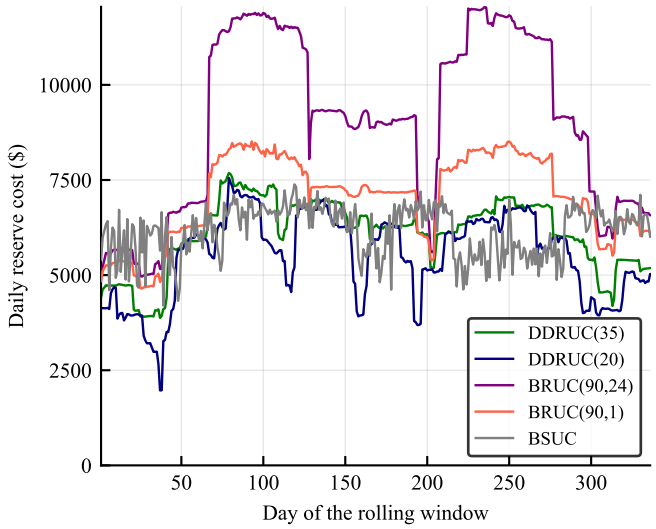

Figure 4.4: Daily reserve costs for the 4-bus system.

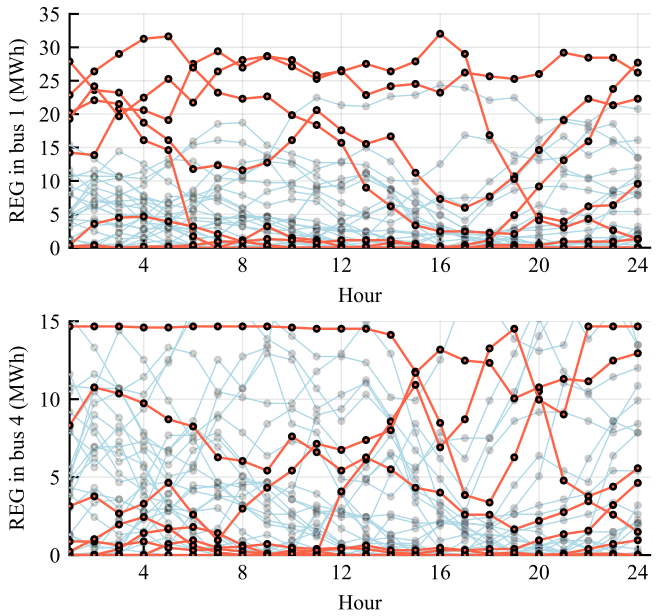

Figure 4.5: Scenarios in $\mathcal{S}$ for the 43^{rd} day of the rolling window for the 4-bus system.

with the largest absolute REG variation between two consecutive periods were also selected. These scenarios also represent a challenge to the system as they stress its ramping capability and require higher reserve levels.

4.6.3 118-Bus System

The second case study is a modified version of the IEEE 118-bus test system with 10 wind farms. The optimality gap of Gurobi was set at 0.05% for the master problem, the subproblem was solved to optimality through the vertex inspection, and ϵ was equal to 0.1% of the total system demand.

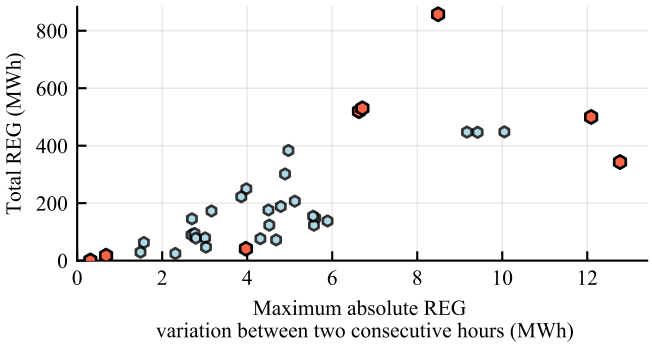

Figure 4.6: Scatter plot for the scenarios selected by DDRUC(35) in the 43^{rd} day of the rolling window for the 4-bus system.

	DDRUC(35)	DDRUC(35+10)
Average time (s)	774	792
Maximum time (s)	1752	2220
Average number of iterations	8.5	8.4
Average cost (10^4 \$)	110.4	110.5
LOLP (%)	3.2	2.7
PWS (%)	5.8	4.6

Table 4.3: 118-Bus System – Results from the 214-Day Backtest

For this case study, we first assessed the performance of DDRUC(35) with a second instance, denoted by DDRUC(35+10), whereby intra-day dynamics of wind power generation for the same period in the previous year were considered. Thus, the scenarios for DDRUC(35+10) were associated with the previous 35 days and a ten-day period from the year before, beginning five days prior to the date corresponding to the day under analysis in the backtest scheme. For both instances, the backtest was performed for 214 days under realistic wind power generation data [123]. The results listed in Table 4.3 indicate that the proposed DDRUC can provide a robust and cost-effective generation schedule. Moreover, it is interesting to note that the cost increase due to the consideration of 10 additional vertexes from the previous year is negligible, while the values of LOLP and PWS respectively drop from 3.2% and 5.8% to 2.7% and 4.6%.

It is also relevant to highlight the low computational burden exhibited by both DDRUC instances. The significance of such a result was validated by performing the 214-day backtest with BRUC, which was the only benchmark model used for this case study due to the poor computational behavior featured by BSUC for the illustrative example. Unfortunately, for BRUC, the CCGA failed to converge in practical computing times.

DDRUC has been further assessed with BRUC through a reduced backtest relying on a randomly selected sequence of 10 days. Simulations were

Instance	Avg. time (s)	Avg. iter. no.	Avg. cost (10^4 \$)	LOLP (%)	PWS (%)
DDRUC(42)	494	5.0	110.2	1.67	0.83
DDRUC(35+10)	696	5.7	110.2	1.67	0.83
DDRUC(35)	378	5.6	110.1	1.67	1.25
DDRUC(28)	804	6.6	109.6	1.25	5.00
BRUC(70,24)	3847	3.0	109.6	8.33	1.67
BRUC(50,24)	3741	3.0	108.3	19.17	5.83

Table 4.4: 118-Bus System – Results from the 10-Day Backtest

run for a feasibility tolerance ϵ of 0.1% of the system demand and a practical 1-hour time limit. For the instances of BRUC examined, the time limit was reached during the solution of the master problem. For such instances, the CCGA was allowed to run until the corresponding iteration was completed. Table 4.4 summarizes the results from the 10-day backtest. The reported results suggest that the proposed DDRUC is a scalable alternative for RUC.

4.7 Conclusion

This chapter has described a new, comprehensive, and parsimonious method to characterize REG uncertainty in day-ahead RUC. The proposed method relies on an alternative scenario-based polyhedral uncertainty set that is built through a novel data-driven approach. Unlike conventional budget-constrained uncertainty sets, the proposed polyhedral uncertainty set is characterized directly from data through the convex hull of a set of previously observed REG profiles. Thus, relevant empirical information regarding the existing complex and time-varying dynamics of REG sources is embedded in the vertexes of the polyhedron. In addition, a salient feature of the proposed uncertainty set is its capability to consider any exogenous model (or scheme) for adjusting, including or excluding (filtering or clustering) scenarios based on existing methods used in industry. Moreover, the resulting robust counterpart for generation scheduling can be efficiently solved by the CCGA until ϵ-global optimality. This relevant practical aspect stems from the reduced complexity of the oracle subproblem, which is solvable in polynomial time. For the case studies analyzed in the chapter, a relatively small number of past renewable generation profiles were required by the proposed data-driven approach to outperform two benchmarks, namely an RUC model based on a conventional budget-constrained uncertainty set and a stochastic unit commitment model. Numerical results indicate that the proposed method might be a practical,

scalable, easy to specify, and cost-efficient alternative tool for managing wind power variability in the unit commitment problem.

Future research will consider 1) exogenous day-ahead forecasting methods for nominal scenarios, and 2) data-processing schemes based on forecasting errors to generate the vertexes for the uncertainty set. In addition, alternative budget-constrained uncertainty sets will be analyzed. Another relevant avenue of research is the extension of the proposed data-driven approach within a stochastic robust optimization framework.

5
Distributionally Robust Transmission Expansion Planning: a Multi-scale Uncertainty Approach

We present a distributionally robust optimization (DRO) approach for the transmission expansion planning problem, considering both long- and short-term uncertainties on the system demand and non-dispatchable renewable generation. On the long-term level, as is customary in industry applications, we address the deep uncertainties arising from social and economic transformations, political and environmental issues, and technology disruptions by using long-term scenarios devised by experts. In this setting, many exogenous long-term scenarios containing partial information about the random parameters, namely, the average and the support set, can be considered. For each long-term scenario, a conditional ambiguity set models the incomplete knowledge about the probability distribution of the uncertain parameters in the short-term operation. Consequently, the mathematical problem is formulated as a DRO model with multiple conditional ambiguity sets. The resulting infinite-dimensional problem is recast as an exact, although very large, finite mixed-integer linear programming problem. To circumvent scalability issues, we propose a new enhanced-column-and-constraint-generation (ECCG) decomposition approach with an additional Dantzig–Wolfe procedure. In comparison to existing methods, ECCG leads to a better representation of the recourse function and, consequently, tighter bounds. Numerical experiments based on the benchmark IEEE 118-bus system are reported to corroborate the effectiveness of the method.

The contents of this chapter are based on the paper accepted for the *IEEE Transactions on Power Systems* [74].

5.1
Introduction

The transmission expansion planning (TEP) problem is generally related to strategic policies, as the outcome of a transmission plan extends far beyond providing a simple least-cost connection between the generation and loads. For example, it may directly or indirectly shape the economic development

for covered regions [43], or even facilitate policies for fostering innovation in various generation technologies. As for electrical aspects, the system reliability, operational flexibility, reserves deliverability, and long-run adaptability [43] are key concepts that are significantly affected by the selected transmission capacity updates. On the uncertainty side, planners have been dealing with several deep uncertainties arising from social and economic transformations, political and environmental issues, and technology disruptions, among others. In this context, the definition of coherent future scenarios is a necessary step for defining the TEP [124].

Practical TEP applications generally rely on demand growth and renewable integration scenarios. These scenarios, hereinafter referred to as long-term scenarios, are projections that are based on hypotheses about long-term drivers. The definition of the drivers that are relevant for the construction of the long-term scenarios frequently involves stakeholders and experts in various fields. In terms of modeling, the projections of long-term scenarios are generally provided by econometric models with many explanatory variables representing the long-term drivers. In this setting, a long-term scenario is a description of the future state of the system; that is, a conditional expectation on a specific set of beliefs and hypotheses (priors) that were used to parameterize the drivers. Notwithstanding, in practice, system planners want to consider multiple long-term scenarios [65, 125]. Therefore, different hypotheses about the drivers are conceived, where these hypotheses draw distinct consistent narratives of the economic, political, technological, and environmental factors. [124]. A coherent long-term scenario for demand growth and renewable integration is then built on each of these hypotheses.

5.1.1 Motivation and literature review

Despite the ability to consider many long-term profiles for the unknown parameters, the traditional deterministic "what-if" approach, labeled in this chapter as D-TEP, may not be sufficient for addressing all layers of uncertainty in modern power systems. For example, the large increase in renewable generation (RG) has introduced new levels of intermittency and unpredictability to electrical systems. These new aspects have motivated a change in numerous paradigms for short-term operation as well as for the planning of transmission networks (see [63, 126] and references therein).

In this context, it may be reasonable to consider both the long- and short-term effects of the uncertainty. For instance, a long-term scenario with high integration of wind-related sources would exhibit significantly more

short-term variability than another where a reduced expansion of the wind power technology occurs. Thus, the representation of multi-scale uncertainty in TEP models has been receiving attention in the recent literature across various approaches (stochastic, robust, and distributionally robust). We refer the interest reader to [65], [126], [127], [128], and [67] for further details.

The most popular framework for decision-making under uncertainty is the stochastic optimization (SO) approach, which considers scenarios drawn from a predefined probability distribution function (PDF) [125, 129]. Unfortunately, the PDF of short-term uncertainty is considered difficult to estimate, specially in long-term studies, where the market and system structure may experience deep changes. This fact has motivated the use of the adaptive robust optimization (ARO) framework to address TEP problems, which we label as the ARO-TEP approach. In ARO-TEP problems, uncertainties are, in general, represented by polyhedral uncertainty sets relying on few assumptions about the uncertainty factors (see [63] and [64]). Under this framework, the solution is that which performs the best in the worst-case scenario.

It is worth mentioning that while part of the recent literature on ARO has considered probability agnostic models (see [65], [63], and [64]), relevant efforts have been made to account for the information extracted from data to devise more realistic descriptions of the short-term uncertainty. We refer the interested reader to [66,73], and [12] for applications in short-term operational models and to [67] for a hybrid-robust-and-stochastic approach applied to the TEP problem. Nevertheless, in long-term TEP applications, the use of scenario-based approaches relying on current data may be questionable, as the structure of the uncertainties in the target period may significantly differ from that found via data [125].

As an alternative to SO and ARO approaches, the distributionally robust optimization (DRO) framework, first introduced in [130], has been developed within a broad mathematical and operations research context in the 2010s (see [131–134] and references therein). Unlike the SO approach that requires full PDF specification, the assumption for DRO-based models is that only partial information about the distributions of the uncertain parameters is available. The DRO framework is a robust approach, which is based on the worst-case expected cost. This contrasts with the more conservative ARO framework, which considers the single worst-case scenario. Therefore, the DRO framework produces ambiguity-averse models; that is, models that are robust against predefined sets of probability distributions, the so-called ambiguity sets.

More recently, DRO approaches have been applied to model uncertainty in power system problems such as congestion line management [135], economic

dispatch [136], security-constrained optimal power flow [137], risk-based optimal power flow with dynamic line rating [138], investment decisions in wind farms [139], and unit commitment [140–142]. Regarding the application of DRO to TEP (DRO-TEP), to the best of the authors' knowledge only a few works have been published so far. The network security was addressed in [143] and a data-driven ambiguity set was applied in [144] to account for the estimation uncertainty of empirical probability distributions. In both works, notwithstanding the relevant contributions to the DRO-TEP literature, the multi-scale nature of the uncertainty is not addressed.

Most of the aforementioned works under robust approaches (ARO and DRO) are characterized by the traditional two-stage decision framework involving first-stage decision, uncertainty realization, and second-stage decision. The second-stage decision is modeled by a *recourse function*, which in power system applications frequently represents the system's redispatch or corrective actions after uncertainty realization. Even though they provide flexibility in decision-making under uncertainty, two-stage robust models are generally hard to solve, requiring decomposition techniques.

The column-and-constraint-generation (CCG) algorithm, developed in [68], has been largely applied to tackle two-stage models in power system applications under both ARO and DRO frameworks. The CCG method is a decomposition technique that relies on an iterative process that alternates between a master problem and an oracle subproblem. In many applications, each block of constraints and variables of the master problem is associated with one possible realization (scenario) of the uncertain parameter. In summary, the master problem is a relaxed version of the problem's extensive formulation where only a small subset of scenarios (and their respective constraints and variables) is represented. The oracle subproblem is a search procedure that, for a given first-stage trial solution determined by the master problem, finds the scenario that, according to some metric, produces the highest cost (or the largest violation for a specific set of constraints) for the recourse function. The constraints and variables associated with the new scenario are then represented in the master problem, which becomes more constrained.

The CCG method is tailored to the ARO framework, since the first-stage solution and the single scenario determined by the oracle subproblem are sufficient to compute, at each iteration, the exact worst-case value for the recourse function. However, in the DRO framework, the recourse function is not completely determined by a single scenario, as it deals with worst-case expected values. As a consequence, recent applications of the CCG algorithm to solve problems under the DRO framework have relied on loose upper bounds

for the recourse function. Moreover, many iterations of the CCG algorithm may be required until all the relevant scenarios are determined and introduced to the master problem. Hence, to further develop the DRO approach, new tailored uncertainty models and new solution methods are needed.

5.1.2 Contributions

In this chapter, we extend the ideas and developments of [127] and present a new DRO-TEP model. We assume that the true joint distribution of the uncertain parameters is difficult to estimate. Nevertheless, according to industry practices, we assume that partial information regarding the random parameters is available. In the designed framework, such partial information; that is, the characterization of the conditional expected values and support sets for the short-term net demand, is extracted from the long-term scenarios, which are projected by experts [65, 124, 125]. It is relevant to emphasize that, in this setting, the full specification of the conditional probability distribution for the short-term uncertainty is not required and that multiple exogenous long-term scenarios can be considered.

In terms of modeling, in order to couple long- and short-term uncertainties, we propose an extension of the traditional two-stage DRO framework to consider multiple ambiguity sets. This extension requires the introduction of the concept of conditional ambiguity set, which is formalized in this chapter. Therefore, current industry practices, involving the consideration of multiple long-term scenarios, are accommodated within the proposed multiple conditional ambiguity set parametrization for the DRO-TEP model[1].

As for the solution approach, we propose a decomposition algorithm tailored for DRO problems where the ambiguity set is parameterized by first moment information. The new method is referred to as the enhanced column-and-constraint-generation (ECCG) algorithm. The proposed scheme differs from the CCG method by an inner loop, which is based on a Dantzig-Wolfe procedure (DWP) that determines more than one scenario at each main iteration of the algorithm. As a result, the proposed ECCG method provides a better representation of the recourse function and consequently a tighter *Dantzig-Wolfe-like* upper bound, which is also mathematically formalized. Finally, as opposed to the CCG algorithm, more than one scenario is included to the master problem at each main iteration, resulting in higher

[1]The proposed extension finds parallels in recent advances in robust optimization. The Stochastic Robust Optimization model in [66] and the Extended Robust Model in [12] propose extensions to the robust optimization framework to consider multiple uncertainty sets.

lower bounds. In order to determine the scenarios to be added to the master problem, we propose a procedure that ranks the new scenarios based on their contribution to the recourse function value and selects only those of best rank. The combination of tighter lower and upper bounds results in fewer iterations and reduced computational burden as compared to the benchmark CCG algorithm.

In summary, the contributions of this chapter are twofold:

1. A new multi-scale DRO-TEP that is based on the concept of multiple conditional ambiguity sets. This is a novelty in the literature of DRO and suitable to current industry practices in TEP.

2. A new decomposition method (ECCG algorithm) that provides better approximations for the distributionally robust recourse function than the CCG algorithm, resulting in tighter bounds.

5.1.3 Chapter Organization

The rest of the chapter is organized as follows. In Section 5.2 the nomenclature is introduced. In Section 5.3, the multi-scale uncertainty modeling is described and formalized. The proposed DRO-TEP model is formulated in Section 5.4. The solution methodology (ECCG algorithm) is presented in Section 5.5. The case study and numerical experiments are reported in Section 5.6. Finally, conclusions are addressed in Section 5.7.

5.2 Nomenclature

This section lists the main notation used in this chapter. Additional symbols are explained in the text or are interpretable in the context using the following general rules. The symbols with superscript "(j)" denote variables, sets or results corresponding to the j-th iteration of the solution method. The symbols with superscript "k" denote variables, parameters, and results associated with the k-th extreme point (or scenario) of a given support set. The symbols with subscript "ω" refer to variables, parameters or sets related to the long-term scenario ω. The symbols with subscript "t" refer to variables, functions or sets related to the t-th time period. Finally, the superscript "*" indicates an optimal value of objective functions or variables.

5.2.1 Sets and Indices

Ξ, Ξ_ω	Support set of the random vector and conditional support set of the random vector under the long-term scenario ω.
Ω	Set of long-term scenarios.
$\mathcal{D}_\omega$	Conditional ambiguity set under the long-term scenario ω.
$\mathcal{E}_\omega$	Set of the extreme points of Ξ_ω.
K_ω	Set of indices of the extreme points of Ξ_ω.
$\mathcal{P}_\omega$	Set of probability measures conditioned on the long-term scenario ω.
$\mathcal{S}, \mathcal{S}_\omega$	Sample space, and subset of the sample space associated with the long-term scenario ω.
$\mathbb{S}, \mathbb{S}_\omega$	Appropriate sigma-algebras for $\mathcal{S}$ and $\mathcal{S}_\omega$, respectively.
$\mathcal{T}$	Set of time periods t.
$\mathcal{X}$	Set of feasible investment plans.

5.2.2 Functions

$\tilde{\boldsymbol{\xi}}$	Measurable function (or random vector) modeling the uncertainty in the net demand.
$\tilde{\boldsymbol{\xi}}_t$	Subvector of $\tilde{\boldsymbol{\xi}}$ related to period t.
$\tilde{\boldsymbol{\xi}}(s)$	Realization of $\tilde{\boldsymbol{\xi}}$ for scenario s.
$g(\mathbf{x}, \boldsymbol{\xi}, \omega)$	Minimum-cost dispatch function for investment $\mathbf{x}$, realization $\boldsymbol{\xi}$, and long-term scenario ω.
$H_{DR}(\mathbf{x}, \omega)$	Distributionally robust recourse function for investment $\mathbf{x}$, under the long-term scenario ω.
$\overline{H}_{DR}(\mathbf{x}, \omega)$	Upper bound associated with $H_{DR}(\mathbf{x}, \omega)$.
$\underline{H}_{DR}(\mathbf{x}, \omega)$	Lower bound associated with $H_{DR}(\mathbf{x}, \omega)$.

5.2.3 Constants and Parameters

ϵ, ε Tolerances for the inner and main loops (in monetary and percentage units, respectively).

$\boldsymbol{\lambda}_{\omega}^{(-)}, \boldsymbol{\lambda}_{\omega}^{(+)}$ Vectors of imbalance costs for the long-term scenario ω.

$\underline{\boldsymbol{\mu}}_{\omega}, \overline{\boldsymbol{\mu}}_{\omega}$ Lower and upper bounds for the expected value of $\tilde{\boldsymbol{\xi}}$ for the long-term scenario ω.

ρ_{ω} Probability or multi-objective weight of the long-term scenario ω.

$\boldsymbol{\xi}$ Generic point of Ξ.

$\boldsymbol{\xi}_{\omega}^{k}$ k-th extreme point of Ξ_{ω}.

$\boldsymbol{\xi}_{\omega}^{*}$ Extreme point of Ξ_{ω} associated with the maximum reduced cost of $\underline{H}_{DR}(\mathbf{x}, \omega)$.

$\mathbf{A}$ Line-bus incidence matrix.

$\mathbf{b}_{\omega}$ Vector of right-hand-side parameters of the operative model.

$\mathbf{B}_{\omega}$ Spatial decoupling matrix for $\boldsymbol{\xi}$ under the long-term scenario ω.

$\mathbf{B}_{t,\omega}$ Submatrix of $\mathbf{B}_{\omega}$ for period t.

$\mathbf{C}$ Auxiliary matrix for disjunctive constraints.

$\mathbf{c}_{inv}$ Vector of investment costs.

$\mathbf{c}_{\omega}$ Vector of generation costs for the thermal generators under the long-term scenario ω.

$\overline{c}_{\omega}^{*}$ Maximum reduced cost for the problem related to $\underline{H}_{DR}(\mathbf{x}, \omega)$.

d Dimension of the uncertainty vector.

$\mathbf{e}$ Vector of ones with appropriate dimension.

$\overline{\mathbf{F}}$, $\overline{\mathbf{f}}$ Matrix and vector for transmission constraints.

$\mathbf{G}$ Thermal generator-bus incidence matrix.

$\mathbf{h}_{\omega}$ Vector of objective function coefficients of the compact operative model.

L Maximum number of inner loop iterations.

$LB^{(j)}$	Lower bound of the main loop at iteration j.
M	Maximum number of scenarios added to the master problem per iteration of the algorithm.
$\overline{\mathbf{q}}_\omega$	Vector of generation limits for the thermal units under the long-term scenario ω.
$\mathbf{r}_\omega^{dw}, \mathbf{r}_\omega^{up}$	Vectors of ramp-down and ramp-up limits between two consecutive periods for the thermal units under the long-term scenario ω.
$\mathbf{S}$	Angle-to-flow matrix.
$\Omega_\omega, \mathbf{T}_\omega$	Recourse matrix and technology matrix for the long-term scenario ω.
$UB^{(j)}$	Upper bound of the main loop at iteration j.
z_{DR}^*	Optimal value for the distributionally robust transmission expansion planning problem.

5.2.4 Decision Variables or Vectors

$\alpha_{0\omega}$	Dual variable associated with the sum-one probability constraint.
$\underline{\boldsymbol{\alpha}}_\omega, \overline{\boldsymbol{\alpha}}_\omega$	Dual vectors associated with the lower and upper limits, respectively, for the expected value of $\tilde{\boldsymbol{\xi}}$ under long-term scenario ω.
θ_t	Vector of phase angles in period t.
$\phi_t^{(-)}, \phi_t^{(+)}$	Power imbalance vectors in period t.
$\boldsymbol{\pi}_t$	Vector of dual variables of the compact version of the minimum-cost dispatch model.
$\mathbf{f}_t$	Vector of power flows in period t.
p^k	Probability of the extreme point k.
$\mathbf{q}_t$	Vector of thermal generation in period t.
$\mathbf{x}$	Vector of investment decisions.
$\mathbf{y}$	Vector of variables for the compact version of the minimum-cost operational problem.

5.3 Uncertainty modeling

The proposed approach recognizes the need for a multi-scale representation of the uncertainties affecting the TEP problem. The importance of integrating long- and short-term uncertainties in TEP problems has been discussed recently in the literature [67]. In Section 5.3.1, an illustrative example based on a qualitative description of the proposed uncertainty representation is provided, and in Section 5.3.2 the mathematical formalization of the approach is presented.

5.3.1 Qualitative description of the uncertain parameters

In this chapter, the load and RG uncertainty are decomposed into:

1. A long-term component, which unfolds along many years and represents the uncertainty on the expected demand growth and long-term renewable integration.

2. A short-term component, which is characterized by the conditional variability of the net demand (demand minus RG) on an hourly scale.

In regards to the long-term component, in general TEP applications, governmental institutions or private consulting companies derive a few coherent long-term scenarios[2] with different structural hypotheses for explanatory variables characterizing the economic, political, technological, and environmental factors. Based on such hypotheses, the expected demand growth and renewable integration levels are projected in subsequent studies (see [65] for further details).

For example, experts may shape a plausible long-term scenario based on a future disruption in solar technology and the cost reduction of batteries and/or power electronic equipment. In this case, high penetration of distributed generation is expected, and therefore, a reduced expected system net demand (expected demand growth minus expected RG) is projected. However, the resulting short-term net load probability distribution may change significantly if a high economic development scenario with a lower distributed generation integration occurs. Thus, to allow the decision maker to use typical outcomes of long-term studies, in this chapter, a long-term scenario is characterized by two types of ranges: ranges for the expected value of the conditional probability

[2]Scenario analysis is largely used in several real power systems such as WECC, Chile, ERCOT, CAISO, UK National Grid (see [124] and [65]).

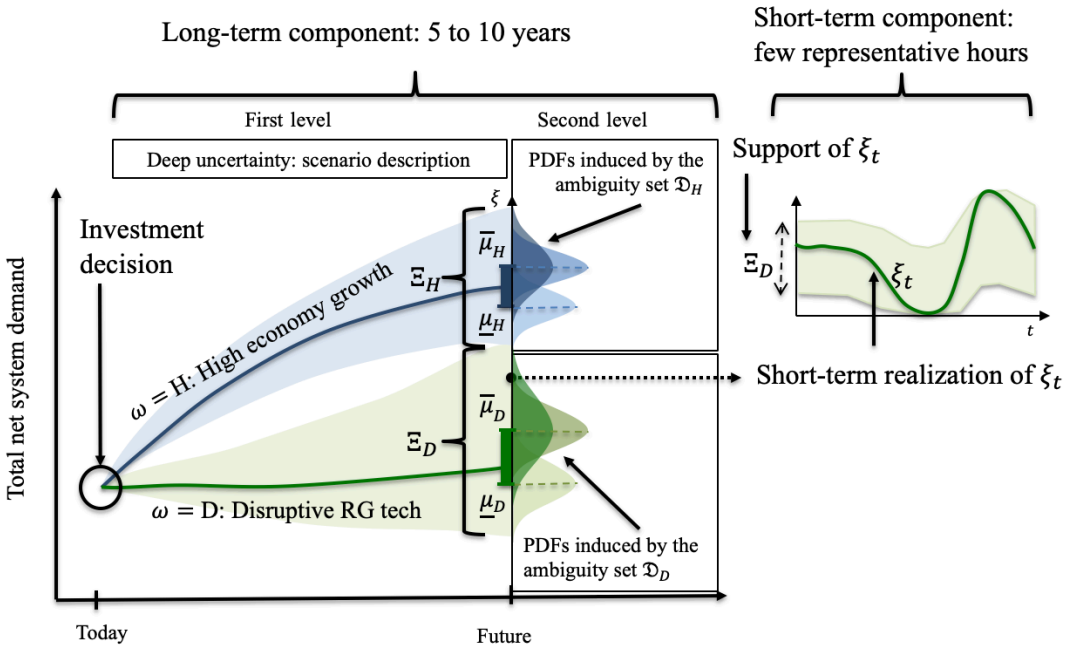

Figure 5.1: Uncertainty components of the net demand (demand minus RG).

distributions, and ranges for the possible outcomes of uncertainty factors (conditional support sets).

The short-term component of the uncertainty model is characterized by multiple conditional ambiguity sets (sets of conditional probability distributions), each of which connects to one corresponding long-term scenario. The information extracted from a long-term scenario to parameterize the related ambiguity set is the range for conditional expected value and range of the conditional support set. This setting allows planners to represent the lack of complete information regarding the underlying processes for the short-term net demand while considering partial information from long-term studies conducted by experts.

For comprehension purposes, a simple example, where the uncertain parameter is the total net demand, is illustrated in Fig. 5.1. Two possible long-term scenarios are depicted, namely, $\omega = H$ and $\omega = D$ representing "**H**igh economic growth" and "**D**isruptive RG technology", respectively. The long-term scenarios determine the support sets (Ξ_H and Ξ_D) and the ranges for the expected value of the net load ($[\underline{\boldsymbol{\mu}}_H, \overline{\boldsymbol{\mu}}_H]$ and $[\underline{\boldsymbol{\mu}}_D, \overline{\boldsymbol{\mu}}_D]$). For each long-term scenario, the set of possible short-term distributions, induced by respective conditional ambiguity set, is abstractly represented in the illustration by different density profiles. In the proposed two-stage DRO framework, the investment decision (first-stage decision) is made under long- and short-term uncertainty components (represented by the circle on the intersection of the axes). The real-time operative dispatch decision (second-stage decision) is

made under perfect information; that is, following the observation of both uncertainty components (signaled by the “short-term realization"legend in the illustration).

5.3.2 Probabilistic description of the uncertain parameters

For the sake of simplicity, the only uncertainty source considered in this chapter is the net demand. It is represented by the vector of random factors $\tilde{\boldsymbol{\xi}} : \mathcal{S} \to \Xi$, with image set, or support set, $\Xi \subset \mathbb{R}^d$ defining all possible net demand extractions profiles. We consider a measurable space $(\mathcal{S}, \mathbb{S})$, where $\mathbb{S}$ is the appropriate sigma-algebra of the sample space $\mathcal{S}$, whose elements represent all possible states of nature. In this setting, $\tilde{\boldsymbol{\xi}}$ is a measurable function on $(\mathcal{S}, \mathbb{S})$ that maps the points from the sample space, $\mathcal{S}$, onto Ξ. The outcomes or realizations of $\tilde{\boldsymbol{\xi}}$ are represented by $\tilde{\boldsymbol{\xi}}(s)$ or, in short, $\boldsymbol{\xi} \in \Xi$, wherever convenient.

In order to represent the concept of long-term scenarios devised by experts, we consider Ω as the set of indices for the long-term scenarios, and we assume the existence of a partition, $\{\mathcal{S}_\omega\}_{\omega\in\Omega}$, of the sample space $\mathcal{S}$, i.e., $\cup_{\omega\in\Omega}\mathcal{S}_\omega = \mathcal{S}$ and $\mathcal{S}_\omega \cap \mathcal{S}_{\omega'} = \emptyset$. In this setting, conditional supports are the images of each part of the sample space, i.e., $\Xi_\omega = \tilde{\boldsymbol{\xi}}(\mathcal{S}_\omega)$, such that the unconditional support set is recovered by their union, i.e., $\cup_{\omega\in\Omega}\Xi_\omega = \Xi$. It is relevant to note that we do not assume that Ξ_ω and $\Xi_{\omega'}$ are disjoint.

The connection between the information provided by experts and the probabilistic framework is given by the following inputs:

1) Conditional expected value ranges, $\{[\underline{\boldsymbol{\mu}}_\omega, \overline{\boldsymbol{\mu}}_\omega]\}_{\omega\in\Omega}$.

2) Conditional support sets, $\{\Xi_\omega\}_{\omega\in\Omega}$.

3) Probabilities $\{\rho_\omega = P(\mathcal{S}_\omega)\}_{\omega\in\Omega}$.

3') Alternatively, $\{\rho_\omega\}_{\omega\in\Omega}$ can also be defined as weights to generate Pareto-optimal solutions, thereby addressing long-term uncertainty under a multi-objective framework.

Based on the conditional support set and expected value ranges for $\tilde{\boldsymbol{\xi}}$, we define the conditional ambiguity sets $\{\mathcal{D}_\omega\}_{\omega\in\Omega}$. Particularly, we assume that for each long-term scenario ω, there exists a restricted (conditional) measurable space $(\mathcal{S}_\omega \subset \mathcal{S}, \mathbb{S}_\omega \subset \mathbb{S})$. The conditional ambiguity set $\mathcal{D}_\omega$ is then defined as the set of all conditional probability measures (restricted to $\mathbb{S}_\omega$) that induce a conditional expected value for $\tilde{\boldsymbol{\xi}}$ within the specified range, i.e.,

$$\mathcal{D}_\omega = \{P \in \mathcal{P}_\omega : \underline{\boldsymbol{\mu}}_\omega \leq \mathbb{E}_P[\tilde{\boldsymbol{\xi}} \,|\, \mathcal{S}_\omega] \leq \overline{\boldsymbol{\mu}}_\omega\}. \tag{5-1}$$

In (5-1), $\mathcal{P}_\omega$ represents the set of all probability measures in the measurable space $(\mathcal{S}_\omega, \mathbb{S}_\omega)$, and $\mathbb{E}_P[\tilde{\boldsymbol{\xi}} \,|\, \mathcal{S}_\omega]$ represents the conditional expected value of $\tilde{\boldsymbol{\xi}}$ under a given probability measure P. For notation purposes, we denote by $\mathbb{E}_P[g(\tilde{\boldsymbol{\xi}}) \,|\, \mathcal{S}_\omega] := \int_{\mathcal{S}_\omega} g(\boldsymbol{\xi}) dP$ the conditional expectation of a given generic function $g(\tilde{\boldsymbol{\xi}})$ with regard to a measure $P \in \mathcal{D}_\omega$ on $(\mathcal{S}_\omega, \mathbb{S}_\omega)$.

For the sake of clarification, for the case depicted in Fig. 5.1; that is, two long-term scenarios $\Omega = \{\omega_1 = H, \omega_2 = D\}$, the inputs of the proposed uncertainty model would be: 1) the conditional expected value ranges, $[\underline{\boldsymbol{\mu}}_H, \overline{\boldsymbol{\mu}}_H]$ and $[\underline{\boldsymbol{\mu}}_D, \overline{\boldsymbol{\mu}}_D]$; 2) the conditional supports for the short-term component of the net load, Ξ_H and Ξ_D; and 3) the probabilities (or weights) associated with each long-term scenario, ρ_H and ρ_D.

5.4 Mathematical TEP model

TEP decisions (investments in candidate lines) are represented by the binary vector $\mathbf{x}$. The set $\mathcal{X}$ defines the feasible investment plans. On the operational side, the cost of operating the system under a given investment plan $\mathbf{x}$, net demand realization $\tilde{\boldsymbol{\xi}}(s)$, and long-term scenario ω is represented by the minimum-cost dispatch function $g(\mathbf{x}, \tilde{\boldsymbol{\xi}}(s), \omega)$. Thus, in cases where the network planner assumes full knowledge regarding the probability measure affecting the uncertain parameter $\tilde{\boldsymbol{\xi}}$, i.e., under the assumption that $P(\cdot|\mathcal{S}_\omega)$ is the true conditional probability measure for each $\omega \in \Omega$, the classical two-stage stochastic TEP approach is generally addressed by variants of the following optimization problem:

$$\min_{\mathbf{x}\in\mathcal{X}} \Big\{ \mathbf{c}_{inv}^\top \mathbf{x} + \sum_{\omega\in\Omega} \rho_\omega \mathbb{E}_P[g(\mathbf{x}, \tilde{\boldsymbol{\xi}}, \omega)|S_\omega] \Big\}. \tag{5-2}$$

Typically, the compact formulation for the operational cost function is given by

$$g(\mathbf{x}, \boldsymbol{\xi}, \omega) = \min_{\mathbf{y}\geq 0} \Big\{ \mathbf{h}_\omega^\top \mathbf{y} \,\Big|\, \mathbf{W}_\omega \mathbf{y} \geq \mathbf{b}_\omega + \mathbf{B}_\omega \boldsymbol{\xi} - \mathbf{T}_\omega \mathbf{x} \Big\}, \tag{5-3}$$

whose right-hand-side is affected by an affine transformation of both investment and uncertainty vectors. Hence, $g(\mathbf{x}, \boldsymbol{\xi}, \omega)$ is a convex function on $\mathbf{x}$ and $\boldsymbol{\xi}$. Note that the decision vector $\mathbf{y}$ stacks all the variables of the operational problem (5-3). The objective function of (5-3) considers operational and imbalance costs through vector $\mathbf{h}_\omega$, while the vectorial inequality comprises all operational constraints through matrices $\Omega_\omega, \mathbf{B}_\omega, \mathbf{T}_\omega$, and vector $\mathbf{b}_\omega$. In the next subsection (Section 5.4.1), the compact formulation

for the short-term operational model (5-3) is detailed. The proposed DRO-TEP model is presented in Section 5.4.2 and a finite reformulation is derived in Section 5.4.3. In Section 5.4.4, benchmark models (ARO-TEP and D-TEP) are presented as particular cases of the DRO-TEP model.

5.4.1 Short-term operation model description

The operational model is used to compute the dispatch cost under a given investment plan $\mathbf{x} \in \mathcal{X}$ and observed net load vector $\boldsymbol{\xi} \in \mathbf{x}i_\omega$, which can accommodate different components (sub-vectors), $\boldsymbol{\xi}_t$, per period. Hence, the compact formulation presented in (5-3) can be expanded as follows:

$$g(\mathbf{x}, \boldsymbol{\xi}, \omega) = \min_{\substack{\mathbf{q},\mathbf{f},\theta \\ \phi_t^{(-)},\phi_t^{(+)} \geq \mathbf{0}}} \sum_{t \in \mathcal{T}} (\mathbf{c}_\omega^\top \mathbf{q}_t + \boldsymbol{\lambda}_\omega^{(-)\top} \phi_t^{(-)} + \boldsymbol{\lambda}_\omega^{(+)\top} \phi_t^{(+)}) \tag{5-4}$$

subject to:

$$\mathbf{G}\mathbf{q}_t + \mathbf{A}\mathbf{f}_t = \mathbf{B}_{t,\omega}\boldsymbol{\xi}_t - \phi_t^{(-)} + \phi_t^{(+)}, \qquad \forall t \in \mathcal{T} \tag{5-5}$$

$$\left|\mathbf{f}_t - \mathbf{S}\theta_t\right| \leq \mathbf{C}(\mathbf{e} - \mathbf{x}), \qquad \forall t \in \mathcal{T} \tag{5-6}$$

$$-\overline{\mathbf{F}}\mathbf{x} - \overline{\mathbf{f}} \leq \mathbf{f}_t \leq \overline{\mathbf{f}} + \overline{\mathbf{F}}\mathbf{x}, \qquad \forall t \in \mathcal{T} \tag{5-7}$$

$$-\mathbf{r}_\omega^{dw} \leq \mathbf{q}_t - \mathbf{q}_{t-1} \leq \mathbf{r}_\omega^{up}, \qquad \forall t \in \mathcal{T} \tag{5-8}$$

$$\mathbf{0} \leq \mathbf{q}_t \leq \overline{\mathbf{q}}_\omega, \qquad \forall t \in \mathcal{T}. \tag{5-9}$$

As is customary in the literature of TEP, the standard optimal dc power flow model is used (see [63] and [143]). The objective function (5-4) accounts for the generation and imbalance costs for all time periods. Constraint (5-5) addresses the nodal power balance for all buses. In this constraint, the matrix $\mathbf{B}_{t,\omega}$ allocates, for each period t and long-term scenario ω, the components of $\boldsymbol{\xi}_t$ (scenario representing uncertainty realization) to the buses of the system. The relation (5-6) addresses the Kirchhoff's Voltage Law (KVL) through disjunctive constraints, where the matrix $\mathbf{C}$ plays an auxiliary role. This matrix has as many rows as the total number of lines (existing and candidates) and as many columns as the number of candidate lines. The rows associated with the existing lines are composed of zeros, enforcing the KVL constraints. Each row representing a candidate line is composed of zeros and one nonzero component. Specifically, a large constant is assigned to the i-th column of the row representing the candidate line i. Thus, the KVL constraints are not enforced for the lines that are not selected. The inequalities in (5-7) account for the transmission capacities of both existing and candidate lines. In these constraints, $\overline{\mathbf{F}}$ is a diagonal matrix with the maximum capacity for the entries

related to the candidate lines and zeros for the existing lines, while $\overline{\mathbf{f}}$ is a vector with the maximum capacity for existing lines and zeros for candidate lines. The expressions (5-8)–(5-9) represent the generation ramping limits and the maximum generation capacity respectively. Due to the imbalance terms in (5-5), problem (5-4)–(5-9) always admits a feasible solution.

5.4.2 Distributionally robust TEP model

In order to address the lack of information regarding the true conditional probability measure $P(\cdot|\mathcal{S}_\omega)$, the recourse function is characterized by an ambiguity-averse preference functional, based on the distributionally robust approach [133]. Thus, the distributionally robust recourse function considers the worst-case conditional expected cost among all expectations induced by the probability measures in $\mathcal{D}_\omega$. Mathematically, we have:

$$H_{DR}(\mathbf{x},\omega) = \sup_{P\in\mathcal{D}_\omega} \mathbb{E}_P[g(\mathbf{x},\tilde{\boldsymbol{\xi}},\omega)|S_\omega]. \tag{5-10}$$

Accordingly, the DRO-TEP problem is defined as an extension of (5-2):

$$z^*_{DR} = \min_{\mathbf{x}\in\mathcal{X}} \Big\{ \mathbf{c}^\top_{inv}\mathbf{x} + \sum_{\omega\in\Omega} \rho_\omega H_{DR}(x,\omega) \Big\}. \tag{5-11}$$

The sup problem in (5-10) is the classical problem of moments [145], which can be expressed as the following semi-infinite (infinitely many variables – columns) linear program:

$$H_{DR}(\mathbf{x},\omega) = \sup_{P\in\mathcal{P}_\omega} \int_{\mathcal{S}_\omega} g(\mathbf{x},\tilde{\boldsymbol{\xi}},\omega)dP \tag{5-12}$$

subject to:

$$\int_{\mathcal{S}_\omega} dP = 1 \qquad : \alpha_{0\omega} \tag{5-13}$$

$$\underline{\boldsymbol{\mu}}_\omega \leq \int_{\mathcal{S}_\omega} \tilde{\boldsymbol{\xi}} dP \leq \overline{\boldsymbol{\mu}}_\omega \qquad : \underline{\boldsymbol{\alpha}}_\omega,\ \overline{\boldsymbol{\alpha}}_\omega. \tag{5-14}$$

5.4.3 Equivalent finite distributionally robust TEP model

By strong duality [146], problem (5-12)–(5-14) admits the following semi-infinite (infinitely many constraints – rows) dual formulation:

$$H_{DR}(\mathbf{x},\omega) = \min_{\alpha_0,\overline{\boldsymbol{\alpha}},\underline{\boldsymbol{\alpha}}} \Big\{ \alpha_{0\omega} + \overline{\boldsymbol{\mu}}^\top_\omega \overline{\boldsymbol{\alpha}}_\omega - \underline{\boldsymbol{\mu}}^\top_\omega \underline{\boldsymbol{\alpha}}_\omega \Big\} \tag{5-15}$$

subject to:

$$\alpha_{0\omega} + \left(\overline{\boldsymbol{\alpha}}_\omega - \underline{\boldsymbol{\alpha}}_\omega\right)^\top \tilde{\boldsymbol{\xi}}(s) \geq g(\mathbf{x}, \tilde{\boldsymbol{\xi}}(s), \omega),\ \forall s \in \mathcal{S}_\omega. \tag{5-16}$$

The infinite set of linear constraints (5-16) can be recast as a single nonlinear worst-case constraint,

$$\alpha_{0\omega} \geq \sup_{s \in \mathcal{S}_\omega} \{g(\mathbf{x}, \tilde{\boldsymbol{\xi}}(s), \omega) - \left(\overline{\boldsymbol{\alpha}}_\omega - \underline{\boldsymbol{\alpha}}_\omega\right)^\top \tilde{\boldsymbol{\xi}}(s)\}. \tag{5-17}$$

This equivalence holds for the following reason: Since (5-17) holds for the supremum in s, it is also valid for all s [147]. Note that the right-hand-side of (5-17) is the supremum of a convex function on $\tilde{\boldsymbol{\xi}}(s)$ over a polyhedral set Ξ_ω. Therefore, the solution s^* for (5-17) is associated with a scenario whose image, $\tilde{\boldsymbol{\xi}}(s^*)$, belongs to the set of extreme points[3] of Ξ_ω, hereinafter referred to as $\mathcal{E}_\omega = \{\boldsymbol{\xi}_\omega^k\}_{k \in K_\omega}$. Consequently, if constraint (5-16) is enforced for $\mathcal{E}_\omega$ only, the same feasible region for $\alpha_0, \overline{\boldsymbol{\alpha}}, \underline{\boldsymbol{\alpha}}$ is found. Thus, problem (5-15)–(5-16) admits the following equivalent finite formulation:

$$H_{DR}(\mathbf{x}, \omega) = \min_{\alpha_0, \overline{\boldsymbol{\alpha}}, \underline{\boldsymbol{\alpha}}} \left\{\alpha_{0\omega} + \overline{\boldsymbol{\mu}}_\omega^\top \overline{\boldsymbol{\alpha}}_\omega - \underline{\boldsymbol{\mu}}_\omega^\top \underline{\boldsymbol{\alpha}}_\omega\right\} \tag{5-18}$$

subject to:

$$\alpha_{0\omega} + \left(\overline{\boldsymbol{\alpha}}_\omega - \underline{\boldsymbol{\alpha}}_\omega\right)^\top \boldsymbol{\xi}_\omega^k \geq g(\mathbf{x}, \boldsymbol{\xi}_\omega^k, \omega),\ \forall k \in K_\omega, \tag{5-19}$$

which constitutes an equivalent finite formulation for the distributionally robust recourse function defined in (5-12)–(5-14).

The equivalent finite primal formulation for the recourse function (5-12)–(5-14) is achieved by computing the dual of problem (5-18)-(5-19); that is,

$$H_{DR}(\mathbf{x}, \omega) = \max_{p^k} \sum_{k \in K_\omega} g(\mathbf{x}, \boldsymbol{\xi}_\omega^k, \omega)\, p^k \tag{5-20}$$

subject to:

$$\sum_{k \in K_\omega} p^k = 1 \tag{5-21}$$

$$\underline{\boldsymbol{\mu}}_\omega \leq \sum_{k \in K_\omega} \boldsymbol{\xi}_\omega^k\, p^k \leq \overline{\boldsymbol{\mu}}_\omega. \tag{5-22}$$

As can be observed, the candidates for worst-case distributions in $\mathcal{D}_\omega$ are discrete. Aiming to achieve an equivalent finite formulation for the DRO-TEP model (5-11), it should be noted that the right-hand-side of (5-19) is the

[3] This is a standard result from convex analysis: The maximum of convex functions within a polyhedral set is achieved at one of the vertices [146].

optimal value of an instance of problem (5-4)–(5-9) for a given $\mathbf{x}$ and a scenario $\boldsymbol{\xi}_\omega^k$ in $\mathcal{E}_\omega$. For notational conciseness, we replace $g(\mathbf{x}, \boldsymbol{\xi}_\omega^k, \omega)$ in (5-19) with the objective function of (5-3), namely $\mathbf{h}_\omega^\top \mathbf{y}_\omega^k$, evaluated on a generic *feasible* operative point, $\mathbf{y}_\omega^k$. In order to obtain an equivalent model, the operative variables $\mathbf{y}_\omega^k$ and feasibility constraints of (5-3) for scenario $\boldsymbol{\xi}_\omega^k$ must be included in the new formulation. This substitution results in the following equivalent extended dual formulation for the recourse function:

$$H_{DR}(\mathbf{x}, \omega) = \min_{\mathbf{y}_\omega^k, \alpha_0, \overline{\boldsymbol{\alpha}}, \underline{\boldsymbol{\alpha}}} \left\{ \alpha_{0\omega} + \overline{\boldsymbol{\mu}}_\omega^\top \overline{\boldsymbol{\alpha}}_\omega - \underline{\boldsymbol{\mu}}_\omega^\top \underline{\boldsymbol{\alpha}}_\omega \right\} \tag{5-23}$$

subject to:

$$\alpha_{0\omega} + \left(\overline{\boldsymbol{\alpha}}_\omega - \underline{\boldsymbol{\alpha}}_\omega\right)^\top \boldsymbol{\xi}_\omega^k \geq \mathbf{h}_\omega^\top \mathbf{y}_\omega^k, \qquad \forall k \in K_\omega \tag{5-24}$$

$$\mathbf{W}_\omega \mathbf{y}_\omega^k \;\geq\; \mathbf{b}_\omega + \mathbf{B}_\omega \boldsymbol{\xi}_\omega^k - \mathbf{T}_\omega \mathbf{x}, \qquad \forall k \in K_\omega. \tag{5-25}$$

The resulting set of constraints in (5-24)–(5-25) is equivalent to (5-19) (in the sense of producing the same optimal value for problem (5-18)–(5-19)), because 1) by optimality, $\mathbf{h}^\top \mathbf{y}_\omega^k$ is bounded from below by $g(\mathbf{x}, \boldsymbol{\xi}_\omega^k, \omega)$; and 2) every point that is feasible for (5-19) is also feasible for the new set of constraints.

Thus, the DRO-TEP problem (5-11) can be recast as the following equivalent finite mixed-integer scenario-based linear program:

$$z_{DR}^* = \min_{\substack{\mathbf{x}, \mathbf{y}_\omega^k, \alpha_{0\omega}, \\ \overline{\boldsymbol{\alpha}}_\omega, \underline{\boldsymbol{\alpha}}_\omega}} \mathbf{c}_{inv}^\top \mathbf{x} + \sum_{\omega \in \Omega} \rho_\omega \left[\alpha_{0\omega} + \overline{\boldsymbol{\mu}}_\omega^\top \overline{\boldsymbol{\alpha}}_\omega - \underline{\boldsymbol{\mu}}_\omega^\top \underline{\boldsymbol{\alpha}}_\omega \right] \tag{5-26}$$

subject to:

$$\mathbf{x} \in \mathcal{X} \tag{5-27}$$

$$\mathbf{h}_\omega^\top \mathbf{y}_\omega^k \leq \alpha_{0\omega} + \left(\overline{\boldsymbol{\alpha}}_\omega - \underline{\boldsymbol{\alpha}}_\omega\right)^\top \boldsymbol{\xi}_\omega^k, \qquad \forall \omega \in \Omega, k \in K_\omega \tag{5-28}$$

$$\mathbf{W}_\omega \mathbf{y}_\omega^k \;\geq\; \mathbf{b}_\omega + \mathbf{B}_\omega \boldsymbol{\xi}_\omega^k - \mathbf{T}_\omega \mathbf{x}, \qquad \forall \omega \in \Omega, k \in K_\omega. \tag{5-29}$$

5.4.4 Particular cases of the distributionally robust TEP model

The DRO-TEP (5-26)–(5-29) can be particularized to the ARO-TEP approach. The ARO-TEP formulation can be achieved by disregarding the moment information; that is, dropping the terms involving $\underline{\boldsymbol{\alpha}}_\omega$ and $\overline{\boldsymbol{\alpha}}_\omega$ of expressions (5-26) and (5-28). Under such an assumption, for each $\omega \in \Omega$, the Cartesian product of (each dimension of) the range for the expected value $[\underline{\boldsymbol{\mu}}_\omega, \overline{\boldsymbol{\mu}}_\omega]$ is equivalent to the whole support set Ξ_ω. Thus, except for degenerate cases, the worst-case probability measure for the ARO-TEP model is such

that all probability mass is assigned to the worst-case short-term scenario.

The D-TEP model is also a particular case of both the DRO-TEP and ARO-TEP models. This particularization is achieved by collapsing the support set and the moment range to a singleton (scenario). Thus, the ARO-TEP model is more conservative than the proposed DRO-TEP model, while D-TEP is less conservative. These benchmarks are used for comparison purposes in the computational experiments.

5.5 Solution methodology

Problem (5-26)–(5-29) can be solved directly, in what we label as the *full-vertex approach* (FVA) [127]. However, this approach is not scalable since the problem size increases exponentially with the dimension (d) of the uncertain parameter. Therefore, decomposition techniques are required.

In Section 5.5.1, we discuss the benchmark CCG algorithm and the issues related to its application to DRO-based problems. An overview of the proposed ECCG algorithm is presented in Section 5.5.2 and the detailed ECCG algorithm is reported in Section 5.5.3. The ECCG algorithm is general enough to be applied to similar problems (e.g. [142]), however, for didactic purposes, the discussions in this section are focused on the proposed DRO-TEP model.

5.5.1 Overview of the traditonal CCG algorithm

The CCG algorithm alternates between a master problem and an oracle subproblem. The master problem is a relaxed version of (5-26)–(5-29) considering a small subset of constraints (5-28)–(5-29). We use $K_\omega^{(j)} \subset K_\omega$ to represent the subset of constraints at iteration j, which are associated with the subset of scenarios $\mathcal{E}_\omega^{(j)} \subset \mathcal{E}_\omega$ (vertices of Ξ_ω). At each iteration j, the master problem determines a lower bound ($LB^{(j)}$) for z_{DR}^* and a trial TEP solution $\mathbf{x}^{(j)}$. The master problem also determines, for each $\omega \in \Omega$, the variables associated with the recourse function ($\alpha_{0\omega}^{(j)}, \overline{\boldsymbol{\alpha}}_\omega^{(j)}, \underline{\boldsymbol{\alpha}}_\omega^{(j)}$) and the operational response ($\mathbf{y}_\omega^{(j)}$). In turn, for each $\omega \in \Omega$, an oracle subproblem identifies the new scenario $\boldsymbol{\xi}_\omega^*$ (not yet included to $\mathcal{E}_\omega^{(j)}$) that most violates constraint (5-28), which is associated with constraint (5-19) in the dual recourse function problem. Equivalently, $\boldsymbol{\xi}_\omega^*$ is the scenario that is related to the new primal variable (new column p), which features the maximum reduced cost, $\overline{c}_\omega^*$, for the constrained primal recourse function problem; that is, (5-20)–(5-22) restricted to the scenarios in $\mathcal{E}_\omega^{(j)}$.

The violated constraints and variables associated with $\boldsymbol{\xi}_{\omega}^{*}$ (for all $\omega \in \Omega$) are added to the master problem at the next iteration. The algorithm terminates when no violated constraints are found by the oracle subproblem or when the upper bound, $UB^{(j)}$, is arbitrarily close to the $LB^{(j)}$.

However, as opposed to the ARO framework, where the value of the worst-case recourse function is given by $g(\mathbf{x}, \boldsymbol{\xi}_{\omega}^{*}, \omega)$, the definition of $H_{DR}(\mathbf{x}^{(j)}, \omega)$ requires more than a single scenario. This implies that approximations that generally involve the reduced cost $\overline{c}_{\omega}^{*}$ are necessary to compute an upper bound. Unfortunately, when the scenarios in $\mathcal{E}_{\omega}^{(j)}$ are insufficient for a reasonable approximation of $H_{DR}(\mathbf{x}, \omega)$, the values of $\overline{c}_{\omega}^{*}$ may be very large, therefore generating loose upper bounds. Moreover, many iterations of the method may be required until all relevant scenarios are determined and included in the master problem.

5.5.2 Overview of the ECCG algorithm

The determination of a tight upper bound $UB^{(j)}$ involves the computation of the true value of the recourse function for all $\omega \in \Omega$; that is, $\{H_{DR}(\mathbf{x}^{(j)}, \omega)\}_{\omega \in \Omega}$. Unfortunately, computing $H_{DR}(\mathbf{x}^{(j)}, \omega)$ might be intractable for high dimensional instances, since it requires the solution of problem (5-20)–(5-22) or its dual, (5-18)–(5-19), considering the entire set of exponentially many extreme points $\mathcal{E}_{\omega}$. Thus, in order to deal with scalability issues while controlling the approximation of the recourse function, we have extended the CCG algorithm by introducing an inner loop. The inner loop is the DWP applied to problem (5-20)–(5-22).

At each main iteration j, the DWP performs up to $n = L$ inner iterations, where a constrained version of the recourse function problem (5-20)–(5-22) (considering only scenarios in $\mathcal{E}_{\omega}^{(j)}$) is alternated with the oracle subproblem. The constrained version of the recourse function problem updates $(\alpha_{0\omega}^{(j)}, \overline{\boldsymbol{\alpha}}_{\omega}^{(j)}, \underline{\boldsymbol{\alpha}}_{\omega}^{(j)})$ and determines a lower (suboptimal) approximation for the true recourse function. The oracle subproblem finds a new short-term scenario $\boldsymbol{\xi}_{\omega}^{*}$ (featuring the maximum reduced cost, $\overline{c}_{\omega}^{*}$) which is then introduced to the constrained recourse problem (5-20)–(5-22). The DWP converges when the maximum reduced cost is below ϵ or the maximum number of (inner) iterations L is reached. As is shown in Section 5.5.4, the upper bound for the ECCG algorithm is controllable and ϵ-tight for large values of L.

The final step of the ECCG algorithm is the selection of the scenarios that are added to the master problem. Because the master problem is the bottleneck of the DRO-TEP problem, it is not advised to include all scenarios determined

by the DWP at each main iteration. Thus, the following selection procedure is adopted. The new scenarios are ranked according to their contribution to the objective value of the constrained recourse problem in the last inner iteration. Then, the $M \leq L$ scenarios with highest ranks are added to the master problem. For comprehension purposes, the proposed algorithm is summarized in Fig.5.2.

5.5.3 Detailed description of the ECCG algorithm

The detailed algorithm is as follows:

1) Initialization: The set of scenarios $\mathcal{E}_{\omega}^{(j)}$ is initialized at $j \leftarrow 0$ with a dummy scenario $\boldsymbol{\xi}_{\omega}^{0} \leftarrow (\overline{\boldsymbol{\mu}}_{\omega} + \underline{\boldsymbol{\mu}}_{\omega})/2$ to ensure the existence of a probability measure capable of producing an expected value within $[\underline{\boldsymbol{\mu}}_{\omega}, \overline{\boldsymbol{\mu}}_{\omega}]$; that is, $\mathcal{E}_{\omega}^{(0)} \leftarrow \{\boldsymbol{\xi}_{\omega}^{0}\}$.

2) ECCG main loop (assessing $LB^{(j)}$ and $\mathbf{x}^{(j)}$): For each iteration j of the main loop, the master problem solution provides a trial solution $\mathbf{x}^{(j)}$ and its corresponding lower bound $LB^{(j)}$. The master problem is expressed as follows:

$$\min_{\substack{\mathbf{x},\mathbf{y}_{\omega}^{k},\alpha_{0\omega},\\ \overline{\boldsymbol{\alpha}}_{\omega},\underline{\boldsymbol{\alpha}}_{\omega}}} \mathbf{c}_{inv}^{\top}\mathbf{x} + \sum_{\omega\in\Omega} \rho_{\omega}\left[\alpha_{0\omega} + \overline{\boldsymbol{\mu}}_{\omega}^{\top}\overline{\boldsymbol{\alpha}}_{\omega} - \underline{\boldsymbol{\mu}}_{\omega}^{\top}\underline{\boldsymbol{\alpha}}_{\omega}\right] \tag{5-30}$$

subject to:

$$\mathbf{x} \in \mathcal{X} \tag{5-31}$$

$$\alpha_{0\omega} + \left(\overline{\boldsymbol{\alpha}}_{\omega} - \underline{\boldsymbol{\alpha}}_{\omega}\right)^{\top}\boldsymbol{\xi}_{\omega}^{k} \geq \mathbf{h}_{\omega}^{\top}\mathbf{y}_{\omega}^{k}, \qquad \forall\omega\in\Omega, k\in K_{\omega}^{(j)} \tag{5-32}$$

$$\mathbf{W}_{\omega}\mathbf{y}_{\omega}^{k} \geq \mathbf{b}_{\omega} + \mathbf{B}_{\omega}\boldsymbol{\xi}_{\omega}^{k} - \mathbf{T}_{\omega}\mathbf{x}, \qquad \forall\omega\in\Omega, k\in K_{\omega}^{(j)}, \tag{5-33}$$

where $K_{\omega}^{(j)} = \{0, 1, ..., |\mathcal{E}_{\omega}^{(j)}|\}$ is the set of indices that enumerates the set of scenarios $\mathcal{E}_{\omega}^{(j)} = \{\boldsymbol{\xi}_{\omega}^{0}, \boldsymbol{\xi}_{\omega}^{1}, ..., \boldsymbol{\xi}_{\omega}^{|\mathcal{E}_{\omega}^{(j)}|}\}$.

3) Dantzig–Wolfe Procedure inner loop (updating $\mathcal{E}_{\omega}^{(j)}$): For each $\omega \in \Omega$, the counter n is initialized with $n \leftarrow 1$, and the DWP is applied to the following constrained version of recourse problem (5-20)–(5-22):

$$\underline{H}_{DR}(\mathbf{x}^{(j)}, \omega) = \max_{p^{k}} \sum_{k\in K_{\omega}^{(j)}} g(\mathbf{x}^{(j)}, \boldsymbol{\xi}_{\omega}^{k}, \omega)\, p^{k} \tag{5-34}$$

subject to:

$$\sum_{k\in K_{\omega}^{(j)}} p^{k} = 1 \qquad : \alpha_{0\omega}^{(j)} \tag{5-35}$$

$$\underline{\boldsymbol{\mu}}_{\omega} \leq \sum_{k\in K_{\omega}^{(j)}} \boldsymbol{\xi}_{\omega}^{k}\, p^{k} \leq \overline{\boldsymbol{\mu}}_{\omega} \qquad : \underline{\boldsymbol{\alpha}}_{\omega}^{(j)}, \overline{\boldsymbol{\alpha}}_{\omega}^{(j)}, \tag{5-36}$$

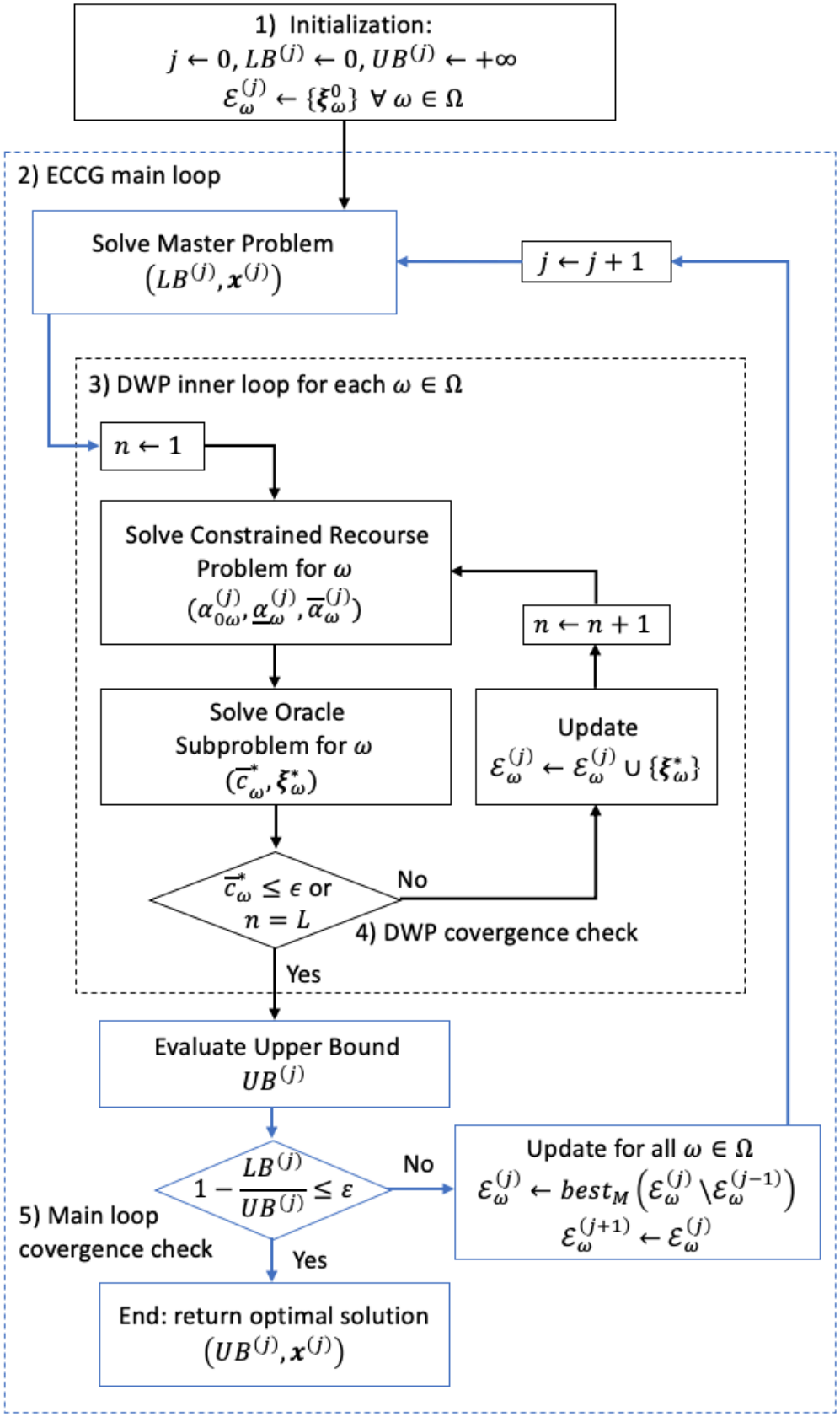

Figure 5.2: Flowchart of the proposed ECCG algorithm.

where $\underline{H}_{DR}(\mathbf{x}^{(j)}, \omega)$ is a lower bound for $H_{DR}(\mathbf{x}^{(j)}, \omega)$. The DWP aims at improving the approximation for $H_{DR}(\mathbf{x}^{(j)}, \omega)$ by determining new columns for (5-34)–(5-36). Thus, we construct an oracle subproblem to identify the scenario $\boldsymbol{\xi}^*_\omega \in \Xi_\omega$ with the highest reduced cost, $\overline{c}^*_\omega$:

$$(\overline{c}^*_\omega, \boldsymbol{\xi}^*_\omega) \leftarrow \max_{\boldsymbol{\xi} \in \Xi_\omega} \Big\{ g(\mathbf{x}^{(j)}, \boldsymbol{\xi}, \omega) - \alpha^{(j)}_{0\omega} - \Big(\overline{\boldsymbol{\alpha}}^{(j)}_\omega - \underline{\boldsymbol{\alpha}}^{(j)}_\omega\Big)^\top \boldsymbol{\xi} \Big\}. \tag{5-37}$$

To solve problem (5-37), we replace function $g(\mathbf{x}^{(j)}, \boldsymbol{\xi}, \omega)$ with the objective function of the dual problem associated with (5-3); that is $\Big(\mathbf{b}_\omega + \mathbf{B}_\omega \boldsymbol{\xi} - \mathbf{T}_\omega \mathbf{x}^{(j)}\Big)^\top \boldsymbol{\pi}$, where $\boldsymbol{\pi}$ represents the dual vector for the constraints in (5-3). This modification to (5-37) results in the following nonlinear problem:

$$\max_{\substack{\boldsymbol{\xi} \in \Xi_\omega \\ \boldsymbol{\pi} \geq 0}} \Big(\mathbf{b}_\omega + \mathbf{B}_\omega \boldsymbol{\xi} - \mathbf{T}_\omega \mathbf{x}^{(j)}\Big)^\top \boldsymbol{\pi} - \alpha^{(j)}_{0\omega} - \Big(\overline{\boldsymbol{\alpha}}^{(j)}_\omega - \underline{\boldsymbol{\alpha}}^{(j)}_\omega\Big)^\top \boldsymbol{\xi} \tag{5-38}$$

subject to:

$$\mathbf{W}^\top_\omega \boldsymbol{\pi} \leq \mathbf{h}_\omega. \tag{5-39}$$

Because $\boldsymbol{\xi}^*_\omega$ belongs to the set of extreme points ($\mathcal{E}_\omega$) of the box-like support set Ξ_ω[4], the value of each component $\xi[i]$ of the decision vector $\boldsymbol{\xi}$, in the optimal solution, is given either the upper ($\overline{\xi}[i]$) or lower ($\underline{\xi}[i]$) limit of the i-th dimension of Ξ_ω. Hence, an auxiliary binary variable $u[i] \in \{0, 1\}$ is used to express each component in the optimal solution as follows: $\xi[i] = u[i]\overline{\xi}[i] + (1 - u[i])\underline{\xi}[i]$. Under this transformation, the bilinear product $\boldsymbol{\xi}^\top \boldsymbol{\pi}$ is linearized by standard integer modeling techniques[5], as done in [63, 65], and [136].

4) Convergence of Dantzig–Wolfe inner loop: At each iteration of the DWP inner loop, the short-term scenario $\boldsymbol{\xi}^*_\omega$ determined by the oracle subproblem updates the set of extreme points, i.e., $\mathcal{E}^{(j)}_\omega \leftarrow \mathcal{E}^{(j)}_\omega \cup \{\boldsymbol{\xi}^*_\omega\}$.

If n equals L or the DWP tolerance level is achieved, i.e., $\overline{c}^*_\omega \leq \epsilon$, the algorithm proceeds **to step 5**. Otherwise, it returns **to step 3** and $n \leftarrow n+1$.

It is relevant to highlight that the DWP is performed separately for each $\omega \in \Omega$. Thus, $\forall \omega \in \Omega$, the DWP identifies up to L scenarios, improving

[4]The optimal scenarios identified by problem (5-37) are extreme points of the polyhedral support set Ξ_ω, as this problem is a maximization of a convex function within a polyhedral set [44]. This fact aligns with the result derived in Section 5.4.3.

[5]The linearization procedure requires the consideration of bounds for the components of the dual vector $\boldsymbol{\pi}$ associated with constraint (5-5). These bounds are set based on an iterative process that scales its initial value whenever one of the bounds are met. The initial value is set to the maximum imbalance cost. In our numerical results, we observed no particular numerical problem.

from below, at each inner iteration, the approximation $\underline{H}_{DR}(\mathbf{x}^{(j)}, \omega)$ for $H_{DR}(\mathbf{x}^{(j)}, \omega)$.

5) Convergence test for the main loop (assessing $UB^{(j)}$): The upper bound for the ECCG algorithm at iteration j is given by $UB^{(j)} = \mathbf{c}_{inv}^{\top}\mathbf{x}^{(j)} + \sum_{\omega\in\Omega}\rho_{\omega}\overline{H}_{DR}(\mathbf{x}^{(j)}, \omega)$, where $\overline{H}_{DR}(\mathbf{x}^{(j)}, \omega) = \underline{H}_{DR}(\mathbf{x}^{(j)}, \omega) + \overline{c}_{\omega}^{*}$. This result is demonstrated in **Theorem 1**, presented in Section 5.5.4.

If $1 - LB^{(j)}/UB^{(j)} \leq \varepsilon$, the algorithm terminates and $\mathbf{x}^{(j)}$ is the ε-optimal solution. Otherwise, for each $\omega \in \Omega$, the scenarios added by the DWP are ranked according to their contribution to $\underline{H}_{DR}$, i.e., the product $g(\mathbf{x}^{(j)}, \boldsymbol{\xi}_{\omega}^{k}, \omega)p^{k}$. The $M \leq L$ scenarios with highest ranks are added to the master problem for the next iteration. This operation is represented in Fig. 5.2 by $\mathcal{E}_{\omega}^{(j)} \leftarrow best_{M}(\mathcal{E}_{\omega}^{(j)} \backslash \mathcal{E}_{\omega}^{(j-1)})$, where $\mathcal{E}_{\omega}^{(-1)} = \emptyset$. Then, $\mathcal{E}_{\omega}^{(j+1)} \leftarrow \mathcal{E}_{\omega}^{(j)}$, update the iteration counter $j \leftarrow j + 1$ and the algorithm returns **to step 2**.

***Remark*:** Note that for a given pair $\{\mathbf{x}^{(j)}, \mathcal{E}_{\omega}^{(j)}\}$, the proposed ECCG algorithm with $M = L$ provides equal or greater lower bound for the iteration $j + 1$ than that obtained by the CCG algorithm. This is because the CCG algorithm is a particular case that adds only $M = L = 1$ of the M scenarios added by the general ECCG algorithm.

5.5.4 Dantzig-Wolfe-like upper bound for the DRO-TEP model

Theorem 1 (ECCG algorithm upper bound)

1. *$UB^{(j)} = \mathbf{c}_{inv}^{\top}\mathbf{x}^{(j)} + \sum_{\omega\in\Omega}\rho_{\omega}\overline{H}_{DR}(\mathbf{x}^{(j)}, \omega)$ is an upper bound for the DRO-TEP problem* (5-11)*, i.e., $z_{DR}^{*} \leq UB^{(j)}$.*

2. *$UB^{(j)}$ is ϵ-tight for $\mathbf{x}^{(j)}$ when $L = +\infty$; that is,*
   $UB^{(j)} \leq \mathbf{c}_{inv}^{\top}\mathbf{x}^{(j)} + H_{DR}(\mathbf{x}^{(j)}, \omega) + |\Omega|\epsilon$.
   Particularly, for $\epsilon = 0$, $UB^{(j)} = \mathbf{c}_{inv}^{\top}\mathbf{x}^{(j)} + H_{DR}(\mathbf{x}^{(j)}, \omega)$.

The proof of **Theorem 1** is better presented using the result of **Proposition 1**.

Proposition 1: *For each $\omega \in \Omega$ and trial solution $\mathbf{x}^{(j)}$, $\overline{H}_{DR}(\mathbf{x}^{(j)}, \omega) = \underline{H}_{DR}(\mathbf{x}^{(j)}, \omega) + \overline{c}_{\omega}^{*}$ is a local upper bound for the recourse function, i.e., $\overline{H}_{DR}(\mathbf{x}^{(j)}, \omega) \geq H_{DR}(\mathbf{x}^{(j)}, \omega)$ for all $\omega \in \Omega$ and $\mathbf{x}^{(j)}$.*

Proof of Proposition 1. Note that, for each ω, owing to optimality of problem (5-37),

$$g(\mathbf{x}^{(j)}, \boldsymbol{\xi}, \omega) - \alpha_{0\omega}^{(j)} - \left(\overline{\boldsymbol{\alpha}}_{\omega}^{(j)} - \underline{\boldsymbol{\alpha}}_{\omega}^{(j)}\right)^{\top}\boldsymbol{\xi} \leq \overline{c}_{\omega}^{*}, \quad \forall \boldsymbol{\xi} \in \Xi_{\omega}. \tag{5-40}$$

As the former inequality holds for each $\boldsymbol{\xi}$, it also holds on average for all probability measures in $\mathcal{D}_\omega$; that is, $\forall P \in \mathcal{D}_\omega$,

$$\int_{\mathcal{S}_\omega} g(\mathbf{x}^{(j)}, \boldsymbol{\xi}, \omega) dP - \alpha_{0\omega}^{(j)} - \left(\overline{\boldsymbol{\alpha}}_\omega^{(j)} - \underline{\boldsymbol{\alpha}}_\omega^{(j)}\right)^\top \int_{\mathcal{S}_\omega} \boldsymbol{\xi} dP \leq \overline{c}_\omega^*. \tag{5-41}$$

Rearranging the terms and using the first-moment constraint in (5-1), the following inequalities also hold for all $\forall P \in \mathcal{D}_\omega$:

$$\begin{aligned} \int_{\mathcal{S}_\omega} g(\mathbf{x}^{(j)}, \boldsymbol{\xi}, \omega) dP &\leq \overline{c}_\omega^* + \alpha_{0\omega}^{(j)} + (\overline{\boldsymbol{\alpha}}_\omega^{(j)} - \underline{\boldsymbol{\alpha}}_\omega^{(j)})^\top \int_{\mathcal{S}_\omega} \boldsymbol{\xi} dP & (5\text{-}42) \\ &\leq \overline{c}_\omega^* + \alpha_{0\omega}^{(j)} + \overline{\boldsymbol{\alpha}}_\omega^{(j)\top} \overline{\boldsymbol{\mu}}_\omega - \underline{\boldsymbol{\alpha}}_\omega^{(j)\top} \underline{\boldsymbol{\mu}}_\omega. & (5\text{-}43) \end{aligned}$$

Particularly, for the worst-case P we have that

$$\int_{\mathcal{S}_\omega} g(\mathbf{x}^{(j)}, \boldsymbol{\xi}, \omega) dP = H_{DR}(\mathbf{x}^{(j)}, \omega). \tag{5-44}$$

Thus, we complete the proof of **Proposition 1** noting that, by strong duality (applied to problem (5-34)–(5-36)), the right-hand-side of (5-43) precisely meets the upper bound. Therefore,

$$\begin{aligned} H_{DR}(\mathbf{x}^{(j)}, \omega) &\leq \overline{c}_\omega^* + \alpha_{0\omega}^{(j)} + \overline{\boldsymbol{\alpha}}_\omega^{(j)\top} \overline{\boldsymbol{\mu}}_\omega - \underline{\boldsymbol{\alpha}}_\omega^{(j)\top} \underline{\boldsymbol{\mu}}_\omega & (5\text{-}45) \\ &= \underline{H}_{DR}(\mathbf{x}^{(j)}, \omega) + \overline{c}_\omega^*. \square & (5\text{-}46) \end{aligned}$$

Proof of Theorem 1. The proof for item 1) is based on the result of **Proposition 1**. We know that

$$\sum_{\omega \in \Omega} \rho_\omega H_{DR}(\mathbf{x}^{(j)}, \omega) \leq \sum_{\omega \in \Omega} \rho_\omega \overline{H}_{DR}(\mathbf{x}^{(j)}, \omega), \tag{5-47}$$

as $\rho_\omega \geq 0$ for all $\omega \in \Omega$. Hence, as $\mathbf{x}^{(j)}$ might not be the optimal solution, $\mathbf{x}^*$,

$$\begin{aligned} z_{DR}^* &= \mathbf{c}_{inv}^\top \mathbf{x}^* + \sum_{\omega \in \Omega} \rho_\omega H_{DR}(\mathbf{x}^*, \omega) & (5\text{-}48) \\ &\leq \mathbf{c}_{inv}^\top \mathbf{x}^{(j)} + \sum_{\omega \in \Omega} \rho_\omega \overline{H}_{DR}(\mathbf{x}^{(j)}, \omega) = UB^{(j)}. & (5\text{-}49) \end{aligned}$$

As for the item 2), by **Proposition 1**, we have $\underline{H}_{DR}(\mathbf{x}^{(j)}, \omega) \leq H_{DR}(\mathbf{x}^{(j)}, \omega) \leq \overline{H}_{DR}(\mathbf{x}^{(j)}, \omega)$. Since the DWP converges for $L = +\infty$, then $\overline{c}_\omega^* \leq \epsilon$ and $\overline{H}_{DR}(\mathbf{x}^{(j)}, \omega) - H_{DR}(\mathbf{x}^{(j)}, \omega) \leq \epsilon$, $\forall \omega \in \Omega$. Thus, $0 \leq UB^{(j)} - \mathbf{c}_{inv}^\top \mathbf{x}^{(j)} - H_{DR}(\mathbf{x}^{(j)}, \omega) \leq |\Omega|\epsilon$. $\square$

5.6

Computational tests

This section reports the results from computational experiments. The first set of experiments is presented in Section 5.6.1, where the solutions of DRO-TEP models are compared, in terms of costs and reliability, with the solutions of benchmark models, namely ARO-TEP and D-TEP. In the second set of experiments, in Section 5.6.2, the computational capability of the proposed ECCG algorithm is compared with the CCG algorithm and the FVA, for different uncertainty vector dimensions.

The computational experiments are based on a modified version of the IEEE 118-bus system, which encompasses 118 buses, 91 loads, 54 generators, 154 existing lines and 32 candidate lines for transmission expansion. Without loss of generality, we assume that the net demand ($\tilde{\boldsymbol{\xi}}$) is the only uncertain parameter. In the experiments, $\tilde{\boldsymbol{\xi}} = [\tilde{\xi}_1, \tilde{\xi}_2, \ldots, \tilde{\xi}_d]$ is modeled as the daily net load, composed of d time periods, within a static TEP study. The uncertain net demand is decoupled into nodal demands by submatrix $\mathbf{B}_t$, as per (5-5). For expository purposes, in all experiments in this section, we used two distinct long-term scenarios, i.e., $\Omega = \{\omega_1, \omega_2\}$, by defining $\{[\underline{\boldsymbol{\mu}}_\omega, \overline{\boldsymbol{\mu}}_\omega]\}_{\omega\in\Omega}$ and $\{\Xi_\omega\}_{\omega\in\Omega}$. In order to create diversity we stressed the system differently in each long-term scenario; that is, buses experiencing uncertain net demand in ω_1 and ω_2 are located in distinct regions of the network and are subjected to different parameters. In summary, ω_1 and ω_2 were constructed using two main principles:

1. ω_1 is much more volatile than ω_2; many more buses in ω_1 are subjected to uncertain net demand than in ω_2.

2. ω_2 produces slightly higher costs than ω_1 for $\boldsymbol{\xi} \in [\underline{\boldsymbol{\mu}}_\omega, \overline{\boldsymbol{\mu}}_\omega]$ for the initial (not expanded) network; that is,

$$g(\mathbf{0}, \boldsymbol{\xi} \in [\underline{\boldsymbol{\mu}}_{\omega_2}, \overline{\boldsymbol{\mu}}_{\omega_2}], \omega_2) \geq g(\mathbf{0}, \boldsymbol{\xi} \in [\underline{\boldsymbol{\mu}}_{\omega_1}, \overline{\boldsymbol{\mu}}_{\omega_1}], \omega_1). \tag{5-50}$$

For the sake of reproducibility, detailed input data used in the experiments of both Sections 5.6.1 and 5.6.2 can be downloaded from [148]. All tests were run using Gurobi 7.0.2 under JuMP (Julia 0.5) on a Xeon E5-2680 processor at 2.5 GHz and 128 GB of RAM.

5.6.1 Assessment of the DRO-TEP model

We assessed instances of the proposed DRO-TEP model against instances of the benchmark models ARO-TEP and D-TEP in terms of cost and reliability. For quick reference, in this subsection, the instances of DRO-TEP,

ARO-TEP and D-TEP models are denoted, respectively, by DRO(ρ_{ω_1},ρ_{ω_2}), ARO(ρ_{ω_1},ρ_{ω_2}), and DET(ρ_{ω_1},ρ_{ω_2}), where ρ_{ω_1} and ρ_{ω_2} refer to the weights of corresponding long-term scenario. The specification of the instances of the benchmark models was performed by adapting the ambiguity set information as described in Section 5.4.4. In this experiment, the daily net demand was divided into six blocks of 4 hours ($d = 6$) and all instances were optimized to optimality.

The experiment was conducted as follows. First, the TEP solution was computed for each instance. Then, the solutions were evaluated in out-of-sample simulations under variants of the Normal and Beta distributions for describing the net demand $\tilde{\boldsymbol{\xi}}$. Each out-of-sample simulation accounted for 10,000 samples of the short-term net demand, representing 5,000 simulated days for each $\omega \in \Omega$. In these simulations, for each individual scenario realization, we used (5-4)–(5-9) to compute the operational dispatch. In total, 4 different distributions were used for each $\omega \in \Omega$, resulting in 8 out-of-sample cases. As low-variance marginal distributions for $\tilde{\xi}_t$, we used: 1) a Normal distribution such that the probability of the event $[\tilde{\xi}_t \in \Xi_{tw} | \, \mathcal{S}_\omega]$ is equal to 95%, where Ξ_{tw} is the projection of Ξ_w for each period t; and 2) a symmetric Beta distribution defined in Ξ_{tw}, with parameter 4.5. As high-variance marginal distributions for $\tilde{\xi}_t$ we used: 1) a Normal distribution such that the probability of the event $[\tilde{\xi}_t \in \Xi_{tw} | \, \mathcal{S}_\omega]$ is equal to 90%; and 2) a symmetric Beta distribution defined in Ξ_{tw}, with parameter 1.5. Even though the net loads typically exhibit temporal correlation, for the sake of simplicity, we assumed independence across different periods.

The main outcomes of the case study are summarized in Table 5.1, where column 1 identifies the instances. Columns 2–4 present TEP solutions, namely, number of invested lines (column 2), investment costs (column 3), and in-sample total costs (column 4) – including the investment, operational, and imbalance costs. Therefore, columns 2 to 4 are classified as in-sample results. Columns 5–20 present out-of-sample results for selected distributions for $\tilde{\boldsymbol{\xi}}$ for both ω_1 and ω_2. The out-of-sample results are divided in 4 blocks, each block corresponding to one different distribution. For each block we present, for both ω_1 and ω_2, the total expected cost and the reliability index (RI). We define RI_ω as the conditional probability (conditioned to long-term scenario ω) of experiencing a load shedding greater than 0.5% of the system nominal demand within a given operative day. Despite the fact that the total cost already incorporates a term related to the dispatch infeasibility (imbalance costs), the RI provides valuable statistical (frequency) information regarding the operative reliability of the solutions.

Instance	TEP solutions			Out-of-sample simulations															
				Low-variance distributions								High-variance distributions							
				Normal distribution				Beta distribution				Normal distribution				Beta distribution			
	New lines	Cost[10^4\$]		Cost[10^4\$]		RI[%]		Cost[10^4\$]		RI[%]		Cost[10^4\$]		RI[%]		Cost[10^4\$]		RI[%]	
		Inv.	Total	ω_1	ω_2	ω_1	ω_2	ω_1	ω_2	ω_1	ω_2	ω_1	ω_2	ω_1	ω_2	ω_1	ω_2	ω_1	ω_2
DRO(100,0)	9	19	90	61	67	4	1	55	61	0	0	69	71	8	4	57	66	1	0
DRO(0,100)	3	7	49	85	48	33	1	59	47	11	0	103	50	43	2	81	47	34	0
DRO(50,50)	8	14	76	57	55	5	1	50	54	0	0	65	57	9	2	52	54	1	0
ARO(50,50)	10	22	100	64	62	4	1	58	61	0	0	71	64	8	2	59	62	1	0
DET(50,50)	-	-	38	81	64	34	23	52	45	12	1	102	76	44	34	76	62	35	21

Table 5.1: TEP problems solutions and out-of-sample assessment

Regarding in-sample outcomes, the solution for DRO(100,0) is more conservative than that for DRO(0,100), determining more invested lines (9 vs. 3) at a higher investment cost ($\$19\text{x}10^4$ vs. $\$7\text{x}10^4$). This result is coherent since ω_1 was designed to be much more volatile than ω_2, which is confirmed by respective total in-sample costs presented in column 4. The solution for DRO(50,50), considering both ω_1 and ω_2, lies between DRO(100,0) and DRO(0,100) in terms of invested lines, investment costs and total cost. As expected, ARO(50,50) is the instance that presents the most conservative solution, encompassing 10 new lines at the cost of $\$22\text{x}10^4$. The solution for the instance DET(50,50), which solely relies on long-term averages (disregarding short-term variability), determined no investments and is the least expensive ($\$38\text{x}10^4$) in terms of total in-sample cost. Nevertheless, in-sample total costs are not comparable across different instances, since, by construction, they assume distinct distributions for $\tilde{\boldsymbol{\xi}}$. As for the out-of-sample assessment, note that DRO(100,0) performs better than DRO(0,100) in terms of cost and RI for ω_1 across all distributions, whereas the opposite holds for ω_2. This result is coherent since the invested lines for these two instances were determined considering solely the corresponding long-term scenario, disregarding the outcomes of the other long-term scenario. In summary, when assessed under ω_2, DRO(100,0) presents reasonable RI, but high relative costs compared to other DRO-based instances. When assessed under ω_1, especially for high-variance distributions, DRO(0,100) presents very high RI and high costs. In contrast, DRO(50,50) performs well under all distributions in terms of costs and reliability. It is particularly interesting to highlight that DRO(50,50) presents 1) similar values for RI as those presented by DRO(0,100) under ω_2, and 2) lower costs than DRO(100,0) for all distributions, even under ω_1. The latter is explained by the fact that, as compared to DRO(50,50), the expensive investments of DRO(100,0), $\$19\text{x}10^4$, which were driven by the worst-case probability for the aggressive ω_1 only, do not pay off in terms of costs in the proposed out-of-sample analysis under more reasonable (unimodal) distributions.

Regarding the benchmark instances, ARO(50,50) consistently presents low RI values under all distributions for both ω_1 and ω_2, as expected. Nevertheless, it is dominated in all cases, in terms of expected cost, by DRO(50,50), which also achieved almost the same values for RI, even under high-variance distributions. As for DET(50,50), it performs well under the low-variance Beta distribution for long-scenario ω_2. However, for all other cases, DET(50,50) is dominated by DRO(50,50) in terms of cost and reliability. It is relevant to highlight that the optimistic solution of DET(50,50) produces high

costs as a consequence of the unacceptable risk levels observed in most cases, which rules out this approach under this experiment parameterization.

As the planner needs to decide the investment strategy under uncertainty of the distribution and long-term scenario, the authors advocate that, within the limitations of this case study, the DRO(50,50) instance produces the best tradeoff in terms of cost and RI among the tested instances. The authors acknowledge however that the extent of the benefits of the proposed approach can be influenced by the system topology, the premises for long-term scenarios, and costs (investments, imbalance, etc.). Notwithstanding, the proposed DRO-TEP approach remains a relevant tool for planners in determining effective investment decisions featuring a consistent balance between expected cost and reliability in a setting where short-term operational uncertainty is ambiguous.

5.6.2 Assessment of the ECCG algorithm

In this subsection, the performance of the proposed ECCG algorithm is assessed against those of the benchmark methods mentioned in Section 5.5, namely, the FVA applied in [127], and the CCG algorithm applied in [136,142]. All 3 methods (FVA, CCG algorithm, and ECCG algorithm) were applied to solve 4 different DRO(50,50) instances comprising 4, 5, 8, and 12 time periods ($d = 4$, 5, 8 or 12).

In order to decide which results to report, we performed a sensitivity analysis on the parameters. As detailed in Section 5.5, the specification of the ECCG algorithm involves 4 parameters / tolerances, namely, the maximum number of inner iterations L, the maximum number of scenarios included to the master problem per main iteration M, the DWP tolerance ϵ, and global tolerance for the problem (main loop) ε. The global tolerance, which was set to $\varepsilon = 1\%$, is the only parameter also applicable to FVA and CCG algorithm. We recall that the CCG algorithm is a particular case of the ECCG algorithm where $M = L = 1$ and the tolerance ϵ is not applicable. As for the 3 other parameters of the ECCG method, our experiments indicated that when L is higher than a certain threshold and ϵ is low, very good approximations for $H_{DR}(\mathbf{x}, \omega)$ are obtained. These approximations can be measured, for example, by the ratio $\overline{c}^*_\omega / \underline{H}_{DR}(\mathbf{x}, \omega)$ (the lower, the better). For the instance sizes ($d = 4$, 5, 8 or 12) that we investigated, increasing L after a certain value almost did not impact the M scenarios selected by the method. Thus, for the sake of brevity and due to space limitations, we decided to report results for fixed $L = 20$ and $\epsilon = 0.10\$$. In this setting, the sensitive parameter for the ECCG algorithm is

Method	Uncertainty Vector Dimension							
	4		5		8		12	
	t. (s)	Iter.	t. (s)	Iter.	t. (s)	Iter.	t. (s)	Iter.
FVA	170	-	1,825	-	T	-	T	-
CCG	289	9	625	10	8,171	15	T	T
ECCG(1)	111	5	195	5	1,262	6	14,510	11
ECCG(2)	75	3	119	3	955	4	12,247	7
ECCG(3)	87	3	158	3	811	3	8,503	5
ECCG(4)	56	2	90	2	1,168	3	6,776	4
ECCG(5)	62	2	98	2	549	2	4,083	3

T - Time limit of 18 hours exceeded without convergence.

Table 5.2: Comparative CPU times (s) and number of iterations

M, which is reported for values ranging from 1 to 5. For quick reference, the instances of ECCG are denoted by ECCG(M). In this experiment, the Gurobi optimality gap was set to 0.5% for the master problem of both decomposition methods (and to $\varepsilon = 1\%$ for the FVA). Table 5.2 displays the computing times and number of iterations

It can be observed in Table 5.2 that the ECCG algorithm dominates the others, particularly, for higher values of d. Superior results were achieved for higher values of M that required fewer iterations of the master problem. The benchmark methods are only practical for low-dimensional uncertainty vectors. The FVA, for instance, failed to converge in 18 hours for $d \geq 8$. The CCG algorithm is also limited to low values of d (failing to converge for $d = 12$), mainly because it produces upper bounds that are not tight, thereby requiring additional iterations to approximate $H_{DR}(\mathbf{x}, \omega)$.

Table 5.3 extends the results presented in Table 5.2 for $d = 8$, detailing each iteration (reported in column 2) of both CCG and ECCG methods. Columns 3-5 provide the computing times for the master problem, the DWP inner loop, and the whole iteration. Columns 5-7 present, respectively, the processing times of a given iteration, the cumulative time, and the gap of the ECCG algorithm. Columns 8-9 display the number of inner loop iterations for ω_1 and ω_2.

Table 5.3 results show that the time to solve the master problem grows across iterations with a much higher rate than the time to solve the subproblems for all cases. Therefore, it is clear that the master problem is the bottleneck for both decomposition methods. The key advantage of the ECCG algorithm over the CCG algorithm is that it requires less iterations of the master problem because of two main factors: 1) tighter upper bounds

Method	Iter.	Time (s)				GAP (%)	Inner iter. (#)	
		Master	DWP	Iter.	Accum.		ω_1	ω_2
CCG	1	13	7	20	20	85.1	1	1
	2	29	9	38	58	57.2	1	1
	3	47	9	56	114	56.1	1	1
	4	99	9	108	222	55.0	1	1
	5	142	11	153	375	45.8	1	1
	6	148	12	160	535	45.3	1	1
	7	244	11	255	790	44.8	1	1
	8	365	13	378	1,168	40.0	1	1
	9	343	12	355	1,523	40.0	1	1
	10	473	11	484	2,007	39.8	1	1
	11	760	13	773	2,780	35.4	1	1
	12	711	14	725	3,505	10.0	1	1
	13	1,319	18	1,337	4,842	7.4	1	1
	14	1,671	17	1,688	6,530	1.4	1	1
	15	1,623	18	1,641	8,171	0.7	1	1
ECCG(1)	1	13	81	94	94	60.8	16	20
	2	23	124	147	241	47.8	19	20
	3	60	128	188	429	41.3	19	20
	4	110	134	244	673	1.6	14	18
	5	147	119	266	939	1.0	13	14
	6	226	97	323	1,262	0.8	12	8
ECCG(2)	1	13	82	95	95	60.8	16	20
	2	48	142	190	285	33.6	20	20
	3	169	134	303	588	10.4	18	17
	4	289	78	367	955	0.6	5	12
ECCG(3)	1	14	83	97	97	60.8	16	20
	2	101	118	219	316	16.2	14	20
	3	386	109	495	811	0.7	10	14
ECCG(4)	1	14	83	97	97	60.8	16	20
	2	151	153	304	401	3.9	14	20
	3	685	82	767	1,168	0.2	9	7
ECCG(5)	1	14	82	96	96	60.8	16	20
	2	321	132	453	549	0.7	14	17

Table 5.3: Detailed iteration data for d=8

due to the DWP, and 2) tighter lower bounds due to the selection of up to M scenarios with high contribution to the recourse function to be added to the master problem at each iteration. The effect of point 1 is observed by comparing the GAP after the first iteration of the CCG, 85.1%, with the GAP for any ECCG method, 60.8%. As the first stage solution is the same for all methods, the difference is solely due to the better approximation of the recourse function. The effect of point 2 is detected by the improved performance with higher values of M.

A convergence plot in Fig. 5.3 further illustrates the results of this subsection.

5.7 Conclusions

In this chapter we have proposed a multi-scale distributionally robust transmission expansion planning model. We have introduced the concept of multiple conditional ambiguity sets to account for the information of long-term studies conducted by experts in current industry practices. Due to intractability issues associated with DRO-TEP models, an enhanced-column-and-constraint-generation algorithm, providing better approximations of the recourse function and tighter bounds, was devised. Results for the IEEE 118-bus system have shown that, in comparison to existing methods, the proposed DRO-TEP model is effective in producing a consistent tradeoff between cost and reliability in out-of-sample tests. As for the computational aspects, the ECCG algorithm has significantly outperformed the CCG algorithm. Notwithstanding, the proposed methodology is not exhaustively developed in this chapter. The foundations of ECCG rely on finding new scenarios for the recourse function, then recomputing the dual variables iteratively. Extending this rationale for different ambiguity sets is an avenue for research. Likewise, devising metrics to select the best M scenarios for the master problem and studying procedures to drop old cuts are interesting research themes.

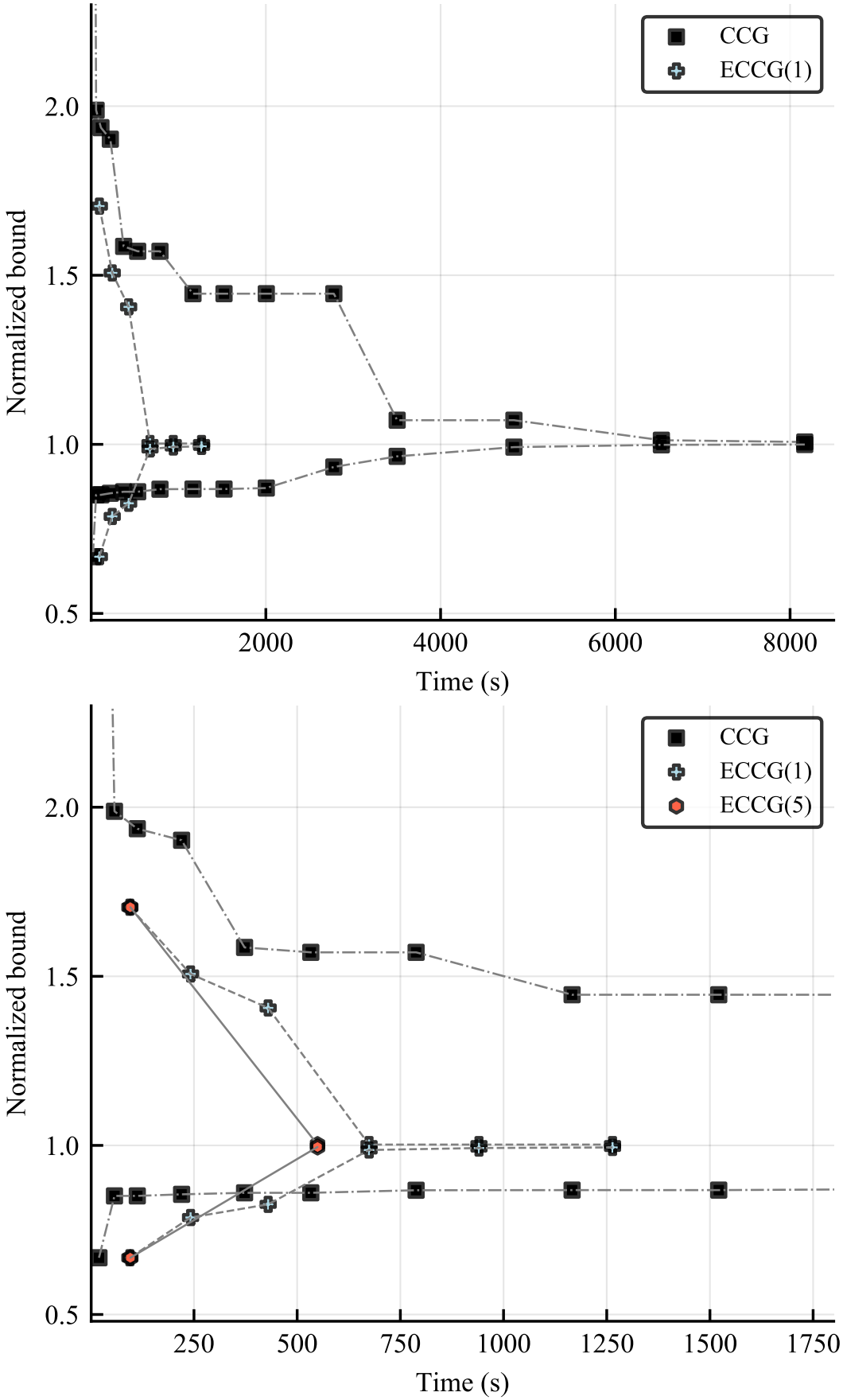

Figure 5.3: Convergence times for selected methods for d=8.

6
Fostering Innovation in Power Systems Models through Inducement Prizes: a Proposition for the Brazilian Power Sector

Electric power systems are large and complex structures. Recent transformations arising due to, among other elements, the high penetration of non-dispatchable renewable generating sources have changed the way power systems are operated, requiring new sophisticated computational models and new problem solving methods. Improvements in these models are subjects of extensive research in academia and industry since they can represent savings of billions of dollars a year. The Brazilian electric power system particularly faces complexities arising from an intricate composition of reservoirs and hydroelectric units arranged in cascade. This paper analyzes challenges and technological gaps of current approaches to power system models in Brazil, as well as how innovations in these models are financed and implemented. The adequacy of innovation inducement prizes in the Brazilian case is then discussed. Finally, we recommend a reorientation of the Brazilian government center (CEPEL), which currently has the role of exclusive developer of the computational models that impact the entire Brazilian power sector.

6.1
Introduction

Power systems are large and complex structures that generate, transport, and distribute the electricity required by virtually every economic activity of modern society. Typically, the main desired characteristics for power systems are reliability, accessibility, and cost affordability. In order to achieve these objectives, appropriate regulation and planning are necessary. Although there is considerable diversity in the mechanisms and rules of the different existing energy markets [1, 149–151], virtually all of them rely heavily on the results of computational models to ensure the desired properties.

The use of optimization-based models is strongly disseminated in the industry, including independent system operators (ISOs), planners, regulators and market participants [152–156]. In this sense, there are also many researchers and academic papers [8,22,23,31,157,158], specialized consultancies

and commercial software aimed at computational optimization associated with energy planning. Furthermore, energy policies as well as regulatory measures that ensure long-term coherence to electrical systems are based on future simulations of the systems. Some examples are power and reserve margin to ensure reliability criteria in various electrical systems, studies for transmission expansion planning, and the calculation of the firm energy certificates in Brazil.

Profound transformations in power systems associated with market deregulation processes [1–3], new environmental constraints, and technology disruptions on both demand and supply side have changed the expectations on the systems and the way they are operated, exacerbating the dependence on computational models. For example, due to large penetrations of non-dispatchable renewable energy generation (REG), there is an increasing stochasticity in power systems requiring sophisticated models to be solved repeatedly under various conditions. These sources are expected to penetrate even further as relevant multilateral international organizations have declared that increasing investments in clean energy technologies is one of the most important mechanism in tackling climate change and its undesired effects. High integration of these clean, however, intermittent and variable energy sources brings additional challenges that have been widely discussed [6–17]. In this configuration, it has been progressively more challenging to satisfy the aforementioned high standards that society demands from power systems. The necessity for addressing these challenges has been driving intense research aimed at new models and algorithms both in industry and academia.

The benefits of increasing the efficiency of power systems operational/planning models are not easily measurable and involve multiple dimensions of analysis. Some studies, although in simplified estimations, have tried to attribute economic values to a more efficient modeling. For example, using a simplified representation of the Brazilian electric power system, [159] reported that planning the multi-year operation without the incorporation of the Kirchhoff's second law and the $N-1$ security criterion generates a time-inconsistency gap (defined in [160]) of about 100% for the cost of hydrothermal operation (hundreds of millions of dollars per year). In [154], it is also estimated from simple assumptions that an increase in market efficiency of 5%, resulting from improvements in the optimal power flow problem, could generate savings of billions of dollars per year, only considering the United States. In addition to the aforementioned issues, at a higher level, the very market design and environmental policies are themes that must be modeled and validated on adequate theoretical and computational frameworks. Obviously, these regulatory aspects have equally

important impacts which are even more difficult to measure. In summary, the challenges of modern power systems deserve very special attention.

In Brazil, which has the largest power system in Latin America, the operation is carried out by a single ISO, the National System Operator (ONS). A single public-owned research center, the Electrical Energy Research Center (CEPEL), is the exclusive developer of the official models used for operation and for large-scale studies, including system expansion. CEPEL focuses on research and development in electric systems and equipment. It has infrastructure of dozens of laboratories and staff featuring excellent technical skills and recognized academic activity. Currently, the promotion of innovation in power systems models in Brazil is done mainly through the funding of CEPEL and some obligatory private R&D projects from companies in the power sector. Despite recent valuable efforts from CEPEL, important challenges and even technological gaps exist for current models used in Brazil. It is relevant, therefore, to propose alternative/complementary ways to foster innovation in computational and theoretical aspects of power system models.

By taking a different and more open approach; that is, by acknowledging the existence of considerable intellectual and computational resources (universities, research centers, private companies, individual researchers and NGOs) capable of contributing innovative ideas, techniques and methodologies, various governmental and private institutions (USBR, USDA, NASA [161], Netflix [162], Google [163], Shell [164], among many others) have adopted open innovation ([165]) schemes to solve some of their technological challenges. These schemes include power system-related initiatives [75, 122, 123]. In this context, several strategies such as innovation inducement prizes, contests, and crowdsourcing schemes have been employed.

Inducement prizes are important mechanisms for fostering innovation featuring relevant advantages over traditional methods such as low cost for implementation (with payment only for success); a multiplier effect, that is, they can stimulate spending on innovative activities greater than the resources offered; interaction between groups of researchers, generating synergies and better results; less bureaucracy than other mechanisms; absence of pre-established biases regarding the technological route, enabling unconventional solutions; etc [76, 166–168]. In [167], there is an extensive literature review on innovation contests, defined as *"IT-based and time-limited competitions arranged by an organization or individual calling on the general public or a specific target group to make use of their expertise, skills or creativity in order to submit a solution for a particular task previously defined by the organizer who strives for an innovative solution"*.

Notwithstanding, according to the literature, the use of innovation inducement prizes should be accompanied by a diagnosis of the suitability of this instrument for the technological challenge to be overcome. In this sense, there are works [76, 169] that pose questions to be answered to determine whether the innovation inducement prize is an adequate instrument to respond to the proposed challenge.

6.1.1 Chapter Objectives

Two main research questions are proposed in this chapter:

1. *"Are inducement prizes adequate instruments for fostering innovation in power power systems models?"*

2. *"Would inducement prizes be applicable and justifiable for the Brazilian power sector case, where there is a single ISO and a government-owned institution which is the single provider of models?"*

In order to address these two questions, first, we outline typical problems/challenges of modern power systems in Section 6.2. Then, the Brazilian power system case is contextualized and discussed in Section 6.3. Innovation inducement prizes and associated requirements are summarized next, in Section 6.4. The suitability of inducement prizes for fostering innovation in theoretical and practical aspects of the power system's problems, particularly, for the Brazilian case is discussed in Section 6.5. Finally, Section 6.6 concludes the paper.

6.2 Power Systems Challenges

On the scale of milliseconds or a few seconds ahead, the ISO monitors the system that is governed by automatic control. This control system aims at maintaining the system's frequency stable by balancing generation and net load. When the net load is increased, a gap between demand and total generation is created and, instantaneously, the speed of rotation, or frequency, of the engines starts to drop. This frequency drop activates the control system of the generators, present in synchronized generators, which in turn increases the power of the machines to restore the frequency to acceptable bounds and thus ensure the stability of the system [98]. It is possible to draw a parallel with a cyclist, that, when facing a more inclined climb feels the pedal heavier and

instantly experiences a drop in speed and therefore a reduction in the rotating angular speed of the pedal. The cyclist' instantaneous reaction would be to increase the force on the pedal to return to the same speed, or frequency of rotation, and thus remain balanced (equivalent to stability). The fundamental problem of power systems is to program, at reasonable cost, the availability of generating resources to act on the automatic response mechanism continuously, while acknowledging engineering constraints. The optimization models are part of the main technologies used to accomplish this planning task.

From a few minutes after automatic response up to years and decades ahead, what is desired is to determine the generation capacity and/or its expansion in such a way that the system is capable to balance future net load and generation at low losses/costs, while recognizing that failures or forecast deviations might occur. In some systems this problem of optimal resource allocation is based on the agents' bids, expressing their cost of opportunity and their risk aversion levels [170, 171]. In other systems, the optimal resource allocation model receives generators' availability and audited costs as inputs [171]. Regardless of which market design is adopted - audited costs or bids -, in both cases, optimization models are widely used to carry out the programming and planning of energy resources.

In summary, the activity of energy operation/planning, from the operation of a few minutes or hours ahead [172, 173], through daily horizons [23], to the planning for the expansion of generation and transmission assets [157], is based on the results provided by computational models. These models are usually arranged in time-horizon layers for which there are different degrees of description of the physical reality and different representations of the relevant uncertainties. However, it is not trivial to define which simplifications should be used at each level. In fact, any criterion for selecting the uncertain factors that should be considered in a given time horizon is debatable. For each scale, there is a vast literature on the impacts of including new modeling elements. Studies show, for example [159], that simplifications in modeling may spark large inconsistencies between reality and what was planned, resulting in an unrealistic assessment of the future, oftentimes leading to risky situations under adverse scenarios. Some authors [63] also point out that it is relevant, in certain cases, to detail short-term uncertainties in planning models for the expansion of generation and transmission, in order to capture the need for investments in lines and plants which would bring flexibility to the operation and enable compliance with the reliability and environmental criteria required by society.

Long-term uncertainties can have equally important impacts. For

generation and transmission expansion planning [63, 157, 158], uncertainties related to environmental, climatic, social and political issues are faced, as well as the possibility of the emergence of disruptive technologies that will substantially alter the load profile [174]. Other aspects that appear as major global challenges to energy markets, which affect all of the aforementioned issues, involve the high penetration of REG and the forecasting of time series (winds, inflows, and solar radiation, for example) related to short- and long-term weather-like events.

Although it is very difficult to detail and categorize the many challenges in electric power systems, some of the most relevant and studied problems are outlined below. Note that these problems/challenges are all influenced by the high penetration of REG.

- **Short-term scheduling problems**: The goal of short-term scheduling problems such as the economic dispatch problem and the optimal power flow problem is to determine setpoints for the generators at minimal cost to meet forecasted load demand. The security-constrained version of the optimal power flow problem requires that the dispatch allows for steady-state points of operations for prescribed security criterion such as the failures of main lines and/or generators. The security-constrained optimal power flow is a nonlinear and nonconvex problem based on the ac optimal power flow constraints ([20] and [21]). Short-term scheduling problems are fundamental building blocks for power systems and are solved many times a day by system operators under various circumstances, either in real-time or in large-scale studies. These needs have been intensified by increasing unpredictability of non-dispatchable renewable generation.
- **Unit commitment problem**: The main purpose of the unit commitment problem [8, 22, 23] is to manage generating resources by scheduling the on/off statuses of generators and determining their dispatch levels in order to meet demand at minimum cost. The programming horizon is usually of many hours or a few days ahead, divided into a few smaller time periods (for example hours). The unit commitment problem normally considers a series of combinatorial engineering constraints, such as minimum uptime and downtime for generators, ramping limitations for generators to increase or decrease the power output, and the network constraints. Computational complexities of this problem potentially arise from a large number of binary variables related to on/off generators' statuses, a large number of nodes or buses, and tight restrictions on the transmission network. Adding to

the complexity, unit commitment models frequently co-optimize energy and reserves to limit risks associated with non-dispatchable renewable generation uncertainties and/or component failures.

– **Network topology optimization**: The aim of this problem is to reduce operational cost or guarantee feasibility by modifying the network topology. Under this category, transmission switching represents the deliberate switching of the on/off status of a transmission line by the operator [24]. Even though counterintuitive, significant operating cost reductions and system reliability enhancements may be achieved by not allowing flow through certain lines [25, 26]. This is explained by Braess' Paradox [27]. Broadly, due to Kirchhoff's voltage law, every network cycle adds constraints to the power flow problem. By removing lines and breaking loops, it is possible to reduce network congestion and approach the desired merit-order dispatch; that is, cheapest generators are dispatched first [27, 28].

  At the distribution level, auxiliary systems perform periodic operations on tap changers and capacitors bank in order to guarantee that the point of operation remains at appropriate levels [29]. This problem is usually called a volt/var control. However, the high insertion of distributed photovoltaic generation (a form of clean and renewable energy) can cause, due to its uncertain and intermittent nature, operational problems [19, 29]. Therefore, as per [19] and [29], new models and strategies for operating distribution systems with a high penetration of distributed photovoltaic generation might be needed.

– **Long-term hydrothermal scheduling problem**: Planning the operation for systems with high penetration of hydro generation, as is the case for Brazil, Norway, and Colombia, among others, is a complex task [30, 31]. The operator needs to coordinate power generation with operational restrictions that involve multiple uses of water such as irrigation, navigability, consumption, etc [32, 33]. In addition, generating plants are sometimes arranged in cascades on the same river [34–36], with inflows subject to significant uncertainty [30, 31, 37, 38]. The long-term hydrothermal scheduling problem normally takes into account multi annual periods (for example in the Brazilian case) and is usually formulated as a multistage (several decision instances) stochastic problem [31, 39, 40]. In a simplified way, hydrothermal scheduling models program the generation from water sources, featuring low operational cost, along with other more expansive sources, aiming at minimal long-term cost, while ensuring the availability of natural resources for

future energy consumption [31]. Because the complexity increases with the number of states (such as reservoir storage levels) and stages (decision instances), relevant simplifications are necessary to apply state-of-the-art techniques for solving this problem [39–42].

– **Transmission expansion problem**: Unlike generation investment, which is generally market-driven and hence decentralized, network infrastructure is generally centrally planned. The transmission expansion planning problem consists in determining which transmission lines will be built aiming at minimizing the combined costs for investment and future operational cost. However, it is relevant to highlight that this problem is generally related to strategic policies, as the outcome of a transmission plan extends far beyond providing a simple least-cost connection between the generation and loads. For example, it may directly or indirectly shape the economic development for covered regions [43], or even facilitate policies for fostering innovation in various generation technologies. As for electrical aspects, the system reliability, operational flexibility, reserves deliverability, and long-run adaptability [43] are key concepts that are significantly affected by the selected transmission capacity updates. On the uncertainty side, planners have been dealing with several deep uncertainties arising from social and economic transformations, political and environmental issues, and technology disruptions, among others [43].

6.3 Brazilian Case

Brazil has the largest electric power system in Latin America. The country's energy consumption in 2017 was 463,900 TWh (52,957 average MWh), according to the state-owned agency Empresa de Pesquisa Energética (Energy Research Company). The system is almost entirely interconnected, with peak power loads of approximately 85,700 MW, according to the ONS. The installed capacity, in 2018, was 157.8 GW. Electricity generation is hydrothermal, however, predominantly hydroelectric (approximately 60.4% of installed capacity and about 70% of actual generation, in 2017). The hydro power is generated from approximately 200 hydro plants of various sizes cascaded in 12 main hydrographic basins. The main reservoirs have multi-year storage capacity. Thermal generation is carried out by gas, nuclear and coal plants (corresponding to 20% of generation in 2017). Completing the portfolio, wind generation has shown significant growth since the 2000s and, in 2017, corresponded to 12.5 GW of installed capacity, featuring a generation share of 7.4%.

The energy transmission assets comprised, in 2017, 129.4 thousand km of grid network with voltages ranging from 230 kV to 765 kV ac, in addition to two 600 kV dc lines. Power interconnections are mainly with Argentina. Currently, there are important ultra-high voltage connection projects between new hydroelectric projects in the Amazon (north) and the region with the highest consumption (south-southeast).

6.3.1 Contextualization

The Brazilian electric power sector has undergone profound changes since the reforms of the 1990s that continued until the 2010s. Before the reforms, the distribution utilities were public and a single state-owned company, Eletrobras, was the owner of the main generation and transmission assets. This state-owned company was responsible for planning the sector's operation and expansion. In this context, CEPEL was created as a government entity belonging to Eletrobras. One of CEPEL's missions was the development of models and algorithms for power systems problems. Between 1990 and the 2010s, the distribution utilities were privatized, as well as a large part of the generation and transmission assets. Currently, the sector has a new institutional organization, which includes a regulatory agency (ANEEL), a single independent operator (ONS), a free contract market (for large consumers, traders and distribution utilities) and an agency linked to ministerial bodies which performs dedicated studies (EPE).

As a legacy of the regulatory and institutional frameworks adopted in the electricity sector before the reforms, CEPEL remains the exclusive official provider of energy planning models used by ONS and other government agencies. The operation remains centralized by ONS and the energy dispatch is based on costs, determined by CEPEL's computational models. These costs, which are calculated as functions of the storage levels in reservoirs, are used as proxies for setting the short-term energy prices. All energy contracts in Brazil are valued based on the cost scenarios produced by CEPEL's models. The same applies to the projects that are candidates for the expansion of the system.

6.3.2 Innovation in Power Sector Models and Obligatory Research and Development

The innovations in the official models for Brazilian power system occur basically through CEPEL, given its unique position as the provider of

computational models for the operation and expansion of the Brazilian power system. The innovations in the last decades had an incremental character, being supported mainly by CEPEL's internal R&D, as well as by research from small power system groups in Brazilian universities, and by the absorption of research (literature) carried out outside Brazil. The financing for this innovation system is predominantly public, mainly composed of the portion of the CEPEL's annual budget destined to the research structure and to the staff. Another source of funding is indirectly associated with energy companies (generation companies, transmission companies, and distribution utilities), which are required by law to dedicate 1% of their revenue to R&D in the electricity sector, 40% of which is discretionarily applied by the company. The R&D values are considerable. According to data from the Brazilian regulatory agency (ANEEL), R$7 Billion[1] were spent between 2011 and 2017, scattered in about 1,800 projects, conducted mostly by research groups in Brazilian universities. Part of this mandatory R&D, R$ 620 million[2], refer to projects classified by the executors themselves as *"planning"*. Another R$ 355 million[3] were classified as projects for *"operating electricity systems"*. However, from the available data, it is difficult to discern how many of these projects were, in fact, related to algorithms or mathematical models for power systems operation. Considering the Brazilian regulatory framework (centralized dispatch based on government models), and from the personal experiences of the authors in participating in projects of this nature, the focus of private agents, with regard to obligatory R&D, is to devise models for energy trading or for proprietary risk management. In other words, mitigation of risks related to prices generated by CEPEL's models and/or maximizing a single producer's profit, in view of expected prices.

There were also at least two R&D project initiatives by ANEEL aiming at exclusive research in mathematical models for energy planning. These were also conducted by groups in Brazilian universities, consuming according to the agency R$ 26 million between 2008 and 2016.

6.3.3 Recent Efforts from CEPEL

In order to deal with the complex Brazilian electric power system, CEPEL has developed several valuable computational models throughout

[1]Conversion rate for US Dollar to Brazilian Real was at 5.16 as of June 30, 2020, but this figure has been much lower, denoting that the amount dedicated to R&D in Dollars is actually larger than dividing R$7 Billion by 5.16.

[2]This amount was calculated from the public spreadsheet provided by ANEEL.

[3]This amount was calculated from the public spreadsheet provided by ANEEL.

its decades of history. These models are organized in layers and address issues such as hydrological inflow forecasting, hydrological risk aversion, REG forecasting, coupling plants/reservoirs in equivalent units, as well as energy planning based on long-, medium- and short-term models. Models are connected by curves/functions, which translate the expected future cost of the operation given the reservoirs' storage level. The main models for planning the operation are called NEWAVE (long- to medium-term model), DECOMP and DESSEM (short-term model). The representation of engineering/technical constraints increases for the short-term planning horizon (DESSEM), while the representation of uncertainty inherent to hydrological inflows increases for long-term planning (NEWAVE).

Recent efforts from CEPEL include:

- **Parallel processing in NEWAVE and DECOMP** based on [175–177]
- **Selective sampling** in the generation of scenarios for the NEWAVE and DECOMP models based on [178].
- **Introduction of non-anticipative constraints** in the dispatch of thermal plants, based on [179].
- **Incorporation of transmission losses** in the DESSEM model [180].
- **River-Level and Routing Constraints** for DESSEM model [181].
- **Increase in the number of equivalent reservoirs** from 4 to 9, based on [182, 183].
- **Aspects related to the use of water in the NEWAVE model**: NEWAVE takes into account the influence of the net water head, due to effects in hydro turbines' productivity. The values for evaporation, storage loss due to water withdrawal, minimum flow energy, and stored water/energy are corrected using second degree polynomials, whose derivative is taken into consideration in the calculation of the expected future cost for the operation. However, depending on the curvature of the polynomial, the problem becomes nonconvex, and this derivative would lead to an inaccurate calculation of the future cost function. In order to correct this, around 2012/2013, the NEWAVE model was improved by approximating/linearizing the polynomials for the nonconvex cases.
- **Risk-averse mechanisms for NEWAVE were implemented**: i) ad hoc risk-averse curves [184, 185], and ii) CVaR consideration, based on [186–188].

– **Processes for "selection" or "elimination" of cuts**: Hydrothermal planning models typically use iterative decomposition methods for determining a solution. These methods divide the planning horizon in many time frames and compute information about the operational cost for each time frame. This information, at each iteration, is propagated to earlier time frames through Benders' cuts[4], which are based on first-order dual approximations (derivatives). The processes for "selection" or "elimination" of cuts enhanced the computational performance of the NEWAVE model. These implemented procedures for managing the cuts are based on [189–191].
– **Implementation of Resampling Methods**: Resampling methods for the simulated scenarios were implemented on NEWAVE, based on the ideas of [54].

6.3.4 Current Challenges

Despite CEPEL's valuable efforts to improve its models, there is currently an important agenda of challenges to be covered. Among the main challenges there are elements corresponding to each of the topics mentioned in Section 6.2. For example, among technological gaps, it can be mentioned that until 2019, the Brazilian market had only 4 submarkets, each of which featuring 3 price ranges (for high, medium, and low demand) that were updated on a weekly basis. As of 2020, indicative hourly prices are released, which will begin to take effect in 2021, also calculated by CEPEL's models. This change is due to the need to signal the scarcity of resources in the hourly time frame, which does not yet happen in Brazil. Currently, the marginal cost of operation is almost uniform across the hours, only showing considerable variability on a monthly scale. The increasing penetration of intermittent renewable generation in northeastern Brazil, requiring reserves with rapid response capacity, was one of the determining factors in the decision to signal hourly marginal costs.

Another aspect about current prices/costs is that they are not determined taking into account relevant elements of the short-term operation, such as cost to turn the units on or off, minimum unit operating time and generators' ramp restrictions. The unit commitment models as well as the medium-term energy planning models disregard these costs, which are allocated to all consumers in the system as general or specific charges. Due to flexibility and controllability, water generators are used to compensate for these short-term operations. In addition, as noted by [159], failure to incorporate aspects of the operation into

[4] A complete review on Benders's cuts is available in [91] and the references therein.

medium-term planning can represent inefficiencies of hundreds of millions of dollars a year.

As mentioned, short-term prices are defined by official models. These models do not consider an individualized representation of the generating units and reservoirs for hydroelectric generation. Until 2020, Newave considered 9 reservoirs, while private models are able to describe more than 100 reservoirs in the Brazilian electrical system and present many other features that do not exist in CEPEL models, such as an integrated unit commitment model, a more precise representation of the transmission lines, and some thermal plant contract restrictions. Even though it is possible to question convergence and optimality issues for individual private models, it is a fact that the new multi-stage integer and/or multi-stage mixed-integer linear techniques that have been devised recently could allow for important upgrades on official models.

There are relevant issues regarding the methodology for expanding the Brazilian electric power system. Currently, there are two types of energy consumers in Brazil. Consumers of the first type are classified as free agents, typically large consumers representing around 30% of demand (2018), who can choose the utility or generator from whom they purchase. The second are captive consumers who are supplied by fixed local distribution utilities. In order to require distribution utilities to contract energy efficiently, the process that defines the new generating entrants to meet the demand expectation for captive customers is centralized through auctions. The redefinition of the energy contracting process carried out in 2004 as part of the reforms in the Brazilian electricity sector represented a considerable advance. A characterization of the expansion of the Brazilian market can be seen in [151]. However, the methodologies for comparing candidates as new generating units overlook relevant information (or attributes), such as ramp capacity, capacity to provide reservoir regularization, capacity to make synchronous compensation, dispatchability, location of the unit and level of uncertainty for REG. Another aspect that deserves consideration is that the price scenarios used to evaluate the developments are generated from an expansion model that has a speculative configuration of assets, which are listed by government agencies, based on methodologies that are not transparent, and/or arbitrary (potentially optimistic).

In addition to presenting technological gaps, these issues expose that perhaps the current approach to foster innovation in models of the Brazilian power system needs to be revised. Therefore, given the current conjuncture of identified challenges, whose potential impacts are in the order of hundreds

of millions of dollars per year, and the challenging agenda for the Brazilian electricity sector, it is necessary to analyze alternative forms of financing innovation.

6.4 Innovation Inducement Prizes

Innovation inducement prizes, whose origins date back to the 18th Century, have been used to redirect the existing energy and workforce that are inert (or underutilized) to solve technological problems. Interesting bibliographic and historical reviews on innovation prizes can be seen in [76, 166, 167]. The prizes, which may or may not be financial resources, are destined to winners of competitions to develop innovative solutions to a previously established technological challenge. Generally, technology platforms such as [192, 193] are used for hosting competitions of such a nature.

6.4.1 Benefits of Innovation Inducement Prizes

Advantages[5] of the innovation inducement prizes according to [166, 168] include:

1. Greater efficiency compared to traditional funding when technological objectives are clear, but means are speculative.

2. The possibility that an objective can be defined without specifying a technological route, enabling unconventional solutions.

3. The use of financial resources only if the solution or minimal standards are achieved.

4. A multiplier effect; that is, contests can stimulate the expenditure in innovative activities greater than the resources offered by the sponsor of the prize.

5. Competitions can be motivating forces to attract participants not directly related to the traditional area of the challenge, or who would never seek public resources or participate in government procurement selection processes because of the excess of bureaucracy related to traditional instruments.

6. Contests can contribute, through awareness and education, to problems that affect society.

[5] We refer the reader to [166, 168] for a complete discussion.

Note that even if a contest does not produce immediately acceptable solutions, there is still a positive externality: Many people are mobilized and gain knowledge about the problem, so that, in the future, they can also develop solutions. Some academic papers analyze results of application of contests to solve technological issues in various fields [194–196].

6.4.2 Innovation Inducement Prize Adequacy

However, as mentioned above, inducement prizes should be accompanied by a preliminary analysis to identify whether innovation inducement prizes are an adequate instrument for addressing a specific challenge/problem (see [76, 169] for a thorough discussion).

In [169] it is suggested that affirmative answers to the following questions are important evidences that prizes can be an effective financing tool.

1. *"Is there a clear, achievable goal?"* or *"Is it of an 'engineering' nature, rather than basic research?"*

2. *"Are there many or few solvers?"*

3. *"Are the solvers willing to accept outcome risk?"*

In [76], another set of questions are suggested:

4. *"Can you define a clear goal (in response to your problem, need or opportunity) and see a way to measure and judge whether the goal has been met?"*

5. *"Do you think that you could generate the best solutions by opening up the problem to a wider pool of innovators?"*

6. *"Do you think you could motivate innovators to participate?"*

7. *"Do you think you could accelerate progress through a prize?"*

8. *"Do you think that the solutions will be adopted or taken to market?"*

6.5 Fostering Innovating through Innovation Inducement Prizes in Brazil

This section argues for the use of innovation inducement prizes to foster innovation for power systems challenges in Brazil.

6.5.1 Arguments for Using Innovation Inducement Prizes in Brazil

During the development of the methodologies used in Brazil for energy planning, especially in the early 1970s to early 1990s, when the available computational capacity and technical literature were far more restrictive, the structuring of a dedicated research center was decisive for the advances in energy planning techniques, many of them constituting the state-of-art models for that period [31]. Today, however, there is a completely different scenario in terms of resources and a much more connected world. There is considerable intellectual and computational capacity (universities, research centers, private companies, individual researchers, and NGOs) capable of contributing innovative ideas, techniques and methodologies. This capacity, with respect to energy planning, is due to the i) increasing number of researchers and academic works in the in related fields, ii) greater computational processing, including extremely cheap cloud processing, and iii) new mathematical modeling and optimization software (some of them open source). Also worthy of note is the non-negligible potential of contributions from ideas and researchers from other fields of study [197].

The idea of an open innovation approach to energy planning is not new. Open energy planning models [156] are already available. A thorough discussions about effectiveness of open modeling in energy planing and open data is presented in [198, 199]. Moreover, notable efforts involving contests and inducement prizes for energy challenges occurred in the past few years. In [122, 123] contests were successfully proposed for developing new methods for forecasting REG outputs. In [75], a contest platform called *Grid Optimization* was proposed by the Advanced Research Projects Agency-Energy (ARPA-E) seeking to increase flexibility, safety and the integration of non-dispatchable renewable generation.

The fact that the main institutions involved in Brazil are government-owned should not be perceived as an obstacle to the introduction of innovation contests. For example, motivated by benefits and possibilities of innovation contests, in 2010, the United States Government developed its own platform, called *challenge.gov* [200], to publicize its contests. Statistics of this platform are presented in [168]: Since 2010, the U.S. government has run

nearly 1,000 challenges in more than 100 federal agencies. It is important to note that this recent increase in the number of contests promoted by United States public agencies came after the publication of measures such as the *Energy Policy Act (2005)*, the *NASA Authorization Act (2005)*, the *American Medical Innovation Fund Prize Act Strategy for Innovation (2009)* and the presidential memorandum *"Guidance on the Use of Challenges and Prizes to Promote Open Government"(2010)*. These elements of legislation encouraged and allowed greater autonomy for agencies to organize and implement contests and prizes (see [166, 168] for a more in-depth discussion on the subject). An interesting analysis of the direct and indirect impacts of the aforementioned challenge.gov platform can be seen in [168].

6.5.2 Adequacy of Innovation Inducement Prizes for Power Systems Challenges

In view of the questions posed in Section 6.4.2, in this subsection, we discuss some aspects of power systems challenges.

Energy planning, in a simplified way, is a multilevel and/or multistage optimization problem that minimizes a cost function (operational, investment, etc), restricted to network and risk constraints associated with equipment failure, uncertainty for future inflows and REG. In this sense, the mathematical problems of energy planning have measurable objectives. However, the definition of the objective function is not trivial and depends, among other aspects, on the planning horizon. In the authors' opinion, a necessary step for prizes to be successfully used in power systems challenges is the construction of a simulator[6] to precisely represent the physical reality of the system. In this way, the solutions presented by the competitors could be evaluated in this simulator, which must be agnostic to the methodology used to obtain the solution. The definition of the characteristics of such a simulator or its construction are not trivial elements. Thus, addressing the first part of question 1 and question 4, we understand that the power system's challenges are related to an objective measurement (although the definition of the metric and an underlying simulator that provides inputs for this metric are complex issues). As for the second part of question 1, energy planning is an applied problem, typically an engineering problem, where the algorithms and underlying applied mathematical theory that are developed come in response to existing problems.

Regarding the capacity for external collaboration with CEPEL (addressing questions 2 and 5), it is important to note that the many international associations and communities focused on issues in power systems

[6] Certainly, different simulators would be necessary for different planning horizons.

involve enormous potential resources (problem solvers). For example, these resources include many researchers in academia, industry professionals (from generation, transmission and distribution utilities), consultancy firms, 17 national laboratories in the United States alone and many others worldwide, etc. There are also many technical/scientific journals dedicated to these themes. Within this context, power systems challenges or, in a broader sense, energy challenges, are studied from the most diverse angles. Researchers belong to different realms of knowledge such as electrical engineering, computer sciences, applied mathematics, physics, etc. Therefore, there is a great deal of knowledge available that can be channeled towards solving issues in the electricity sector. Hence, as indicated by [76], the use of a prize in these cases can arouse the interest of several participants, increasing the probability of presenting a solution to the problem or increasing the quality of the winning solution.

As for question 3, the necessary resources of the participants are basically time and computational resources (modeling and/or optimization software and computational processing). As such, there are no other equipment restrictions or necessary financial investments. Therefore, a wide range of professionals and groups of academics and students from related fields remain potential participants. Incentives to motivate participants, in this case, may involve several elements that range from financial prizes, through recognition and publicity to the winners, and even the feeling of providing solution to a socially significant problem. Recognition from the solution of a problem of this relevance can open important doors for the winners. Thus, addressing question 6, in addition to financial motivation, the authors believe that solving challenges for the Brazilian electricity sector, the largest in Latin America, with one of the most complex hydrothermal systems in the world, would have great appeal.

For [76], the use of innovation contests is recommended for cases in which: i) There are people working on the problem from different angles, but without sufficient coordination or progress has not taken place at the necessary speed; and ii) The knowledge to solve the problem exists, but there are no incentives to mobilize people to invest in its solution. These are evident characteristics for power systems challenges for Brazil. For example, it is worth mentioning the application of Stochastic Dual Dynamic Programming (SDDP) [31], the basis of multi-stage planning methodology for medium- and long-term operation in Brazil. Its use, a few years ago, was restricted to some researchers and rare members of the industry. Currently, however, this technology can be obtained in ready-to-use open-source packages [201, 202]

with very good computational performance. Recently, many other relevant advances for this method and other multi-stage methods for the dispatch of hydrothermal units came from non-Brazilian institutions and/or research groups [41, 42, 52, 55, 203–206]. Therefore, according to [76], the creation of a contest that publicizes the problem, clarifies the beneficial impacts of its solution, builds cooperation tools and creates a sense of urgency through the definition of deadlines will accelerate development (question 7) of innovative solutions to the problem in question.

With respect to question 8, it is important to conjecture that one of the possible reasons why a problem has not yet been solved is the lack of attractiveness of the market for its solution. However, as in the Netflix [162] prize, for example, the incorporation of solutions in proposed contests would be carried out by the organizers themselves in the Brazilian case; that is, the government agency that develops and implements energy planning solutions, CEPEL, and the system operator, ONS, thus increasing the chances that the benefits will be effectively incorporated by society.

6.5.3 Recommendation

In light of the previous discussions; that is, considering

- the relevance of the issue addressed, the magnitude of which ranges from millions to billions of dollars per year and with impacts on energy security;
- the current scheme for financing innovations in power systems models in Brazil and its respective results;
- the important agenda of challenges for the Brazilian power system;
- the enormous amount of qualified resources that can be channeled to propose solution to existing challenges;
- the adequacy of inducement prizes to foster innovation in power systems models;
- the previous experiences of innovation inducement prizes, including government initiatives and/or power system-related initiatives;

we propose a new policy/program. This program aims at fostering innovation in theoretical and computational aspects of electric power systems models in Brazil. The main vector of this proposal is the realization of multiple contests as a way to induce innovations.

A central aspect, in the authors' view, is the role of the Brazilian government, which currently, through its own agency (CEPEL), researches, develops, and implements algorithms and computational innovations. We recommend a review of the current method to encourage innovations in the mathematical-computational models in Brazilian electric power system. Currently, practically all developments are carried out internally and with limited search for external solutions. Recognizing that the community (researchers, associations, students, companies, etc.) can provide innovative solutions to problems, the role of CEPEL would gradually shift from being an exclusive developer and implementer to coordinating knowledge capture efforts to solving technological challenges. Also to focus on developing the best parameters and simulators to evaluate the proposed solutions from participants, for each proposed challenge.

In this new proposed form, CEPEL would seek to capture the high innovative potential and various specialties of the knowledge spread across the world. Basically, CEPEL would be the manager of the knowledge and innovations by reporting relevant issues, organizing contests and platforms for interfacing with participants, in addition to managing other funding mechanisms. It is important to note that this proposed new role does not depend on the market model adopted, whether audited costs (current) or based on the price offers from agents. In both cases, power systems models are paramount to the regulator.

However, it is recognized that structuring a series of contests of this nature is not a trivial task, requiring coordination and organization. There are several and important elements that must be considered in the design of each innovation prize in order to achieve the desired objectives. Note, for example, that the main challenges of Section 6.2 have different time scales requiring distinct representations of the physical constraints and power flow constraints. It is also necessary to structure ways of connecting the different models with different time scales and objectives. Other issues involve organizing data (the tasks are data-intensive), defining the scope of the contests and the definitions and implementations of the proposed simulators, among others. Therefore, even though facing a challenging agenda, given its privileged role, CEPEL is believed to have the ideal expertise to lead a paradigm shift in the search for better models. We believe that a series of pilot challenges, as was the case for the Grid Optimization competition [75], would be an ideal starting approach. Moreover, that particular contest can provide important practical experiences and insights.

For a deeper analysis on the topic of organization of inducement prizes,

which is not the scope of this work, we suggest to the reader the discussions in [76, 168]. In [76], there is a comprehensive guide on designing and structuring prizes. Based on a recent bibliographic review, [168] summarizes the design elements, and also presents guidelines for making the contests.

6.6 Conclusion and Future Steps

Innovation contests have been used successfully by governments and private institutions. In this work, the adequacy of innovation inducement prizes was analyzed to promote solutions for power systems models, which involve complex problems that have important impacts on society. The characteristics of these challenges were discussed and shown to be suitable for inducement prizes since they are engineering problems, whose objectives are measurable. In addition, there is no need for a large research infrastructure or investment to participate in contests of this nature. Another reason is that there is vast related knowledge spread across the world for the main tools needed to generate contributions (operations research, mathematical modeling in power systems, etc).

Therefore, it was proposed in this work the adoption of a policy based on contests to stimulate solutions in power system models for Brazil. In this context, the role of the government agency, which today is the sole researcher, developer and provider of models, would gradually change or, at least, incorporate the management of an open innovation model.

7
Conclusion

This thesis provided mathematical frameworks based on two-stage robust optimization models and on modified versions of the column-and-constraint-generation algorithm (CCGA) for three different electric power system problems, namely: the $N-1$ security-constrained optimal power flow with automatic primary response, the unit commitment with uncertain non-dispatchable renewable generation, and the transmission expansion planning with long- and short-term uncertainties. It also addressed the use of inducement prizes or contests to foster innovation in electric power system's models.

Summaries, main contributions, and conclusion for addressed topics of this thesis are outlined below :

7.1
Regarding the $N-1$ security-constrained optimal power flow problem with automatic primary response

In Chapters 2 and 3, the $N-1$ security-constrained optimal power flow problem was addressed. The formulation for the problem included the $N-1$ security criterion for generators and a specific model for the automatic primary response of synchronized generators which resulted in a complex mixed-integer linear program since the primary response model introduced disjunctions to the scheduling problem. Thus, decomposition strategies with a master problem and subproblems resulted in non-convex subproblems.

In Chapter 2, a dedicated CCGA was devised, where the only optimization problem solved was the master problem; that is, subproblems were not involved. This was possible since the method used i) preprocessed structures based on the power transfer distribution factors (PTDF) that were useful both as feasibility checkers and as dedicated cuts in the post-contingency states, and ii) a numerical procedure to determine the post-contingency variables based solely on the nominal generation. These structures were transformed into primal constraints that were added to the master problem for most violated constraints (lines). Likewise, the disjunctions (binary variables) representing the primary response model for a few contingent states were added

to the master problem for selected states. A method to find high-quality primal solutions and a procedure that monitors the upper and lower bounds for the method were also proposed.

In Chapter 3, it was assumed that data from previous solves were available. An approach combining a deep neural network and the CCGA from Chapter 2 was used. The deep neural network mapped the vector of nodal net loads onto the nominal dispatch, disregarding power flow constraints and the automatic primary response. The feasibility was enforced by robust-based approaches. First, a Lagrangian dual scheme was adopted to penalize physical constraints included in the learning model. Then, an outer procedure that resembles a CCGA was applied directly to the learning model to add new constraints, for a few critical contingent states. The final step involved a modified version of the CCGA from Chapter 2 to restore feasibility.

In summary, the main contributions for the $N-1$ security-constrained optimal power flow problem are as follows.

1. A decomposition approach that combines a CCGA with numerical methods to determine exact solutions to the problem in such a way that the non-convex subproblems do not need to be solved directly.

2. An approach that produces high-quality primal heuristics for the problem.

3. A novel scheme that combines a deep neural network and robust methods to produce near-optimal feasible solutions.

From a computational perspective, the combination of methods proposed in Chapters 2 and 3 significantly outperformed the prior state-of-the-art approach. Additionally, the computational effort required to attain high-quality near-optimal solutions was within industry standards for the tested benchmark systems.

7.2 Regarding the unit commitment under uncertainty for co-optimized electricity markets

In Chapter 4 an alternative to the use of budget-constrained uncertainty sets in two-stage robust unit commitment was proposed. A co-optimized electricity market was considered; that is, the centralized robust joint scheduling of energy and reserves targeting total cost minimization. The uncertainty characterization was directly connected to data. To that end, we proposed modeling the uncertainty in day-ahead unit commitment by an

alternative scenario-based polyhedral uncertainty set built through a novel data-driven approach. Based on the general scenario-based uncertainty set description provided in [112], we defined a new polyhedral uncertainty set as the convex hull of a set of exogenously generated multivariate points, or scenarios, capturing relevant information regarding the uncertainty process over a given time window. The resulting robust counterpart for generation scheduling were efficiently solved by the CCGA until ϵ-global optimality. This relevant practical aspect stems from the reduced complexity of the oracle subproblem, which is solvable in polynomial time.

In the case studies analyzed in the chapter, a relatively small number of past renewable generation profiles were required by the proposed data-driven approach to outperform the budget-constrained uncertainty set.

7.3 Regarding the transmission expansion planning with long- and short-term uncertainties

In Chapter 5, the transmission expansion planning problem with long- and short-term uncertainties was considered. We introduced the concept of multiple conditional ambiguity sets to account for the information of long-term studies conducted by experts. A distributionally robust approach was used to model the short-term uncertainty parameterized by long-term information. Results for the IEEE 118-bus system show that, in comparison to existing methods, the proposed DRO-TEP model is effective in producing a consistent tradeoff between cost and reliability in out-of-sample tests.

In order to solve the resulting problem, an enhanced column-and-constraint-generation algorithm (ECCGA), providing better approximations of the recourse function and tighter bounds than the CCGA, was devised. As for the computational aspects, the ECCG algorithm significantly outperformed the CCG algorithm.

7.4 Regarding Innovation for Power System Models

Chapter 6 discusses, with a focus on Brazil, the importance of an adequate innovation system to drive developments in models in power systems, especially in the context of changing paradigms regarding the penetration of non-dispatchable renewables, smart grids, etc. The paper discusses general challenges of power systems in this current context and the way in which models are managed and improved in Brazil, basically by a single public institution (CEPEL) and by a series of uncoordinated R&D initiatives.

A historical contextualization of the Brazilian case is presented. Recent incremental improvements in CEPEL models are described as well as existing challenges and technological gaps.

The main contribution of the chapter is to argue that innovation inducement prizes are an adequate instruments to foster innovations in power system's models in Brazil. This is due to the fact that the prizes are instruments for channeling knowledge to well-defined engineering problems for which there is a great inert force capable of helping with ideas and solutions and, therefore, promoting innovations. This argument is made based on the prize literature (innovation economics). Finally, the paper argues that the role of CEPEL, which adopts a closed stance regarding innovations in its models (it internally researches, develops, implements and defines the evolution agenda) should be modified.

A
References

[1] W. W. Hogan, "Electricity market restructuring: reforms of reforms," *Journal of Regulatory Economics*, vol. 21, no. 1, pp. 103–132, 2002.

[2] P. L. Joskow, "Lessons learned from electricity market liberalization," *The Energy Journal*, vol. 29, no. Special Issue 2, 2008.

[3] M. Ilic, F. Galiana, and L. Fink, *Power systems restructuring: engineering and economics*. Springer Science & Business Media, 2013.

[4] D. Gielen, F. Boshell, D. Saygin, M. D. Bazilian, N. Wagner, and R. Gorini, "The role of renewable energy in the global energy transformation," *Energy Strategy Reviews*, vol. 24, pp. 38–50, 2019.

[5] United Nations Department of Economic and Social Affairs (UN DESA), "Sustainable Development Goal 7: Ensure access to affordable, reliable, sustainable, and modern energy for all". [Online]. Available: https://sustainabledevelopment.un.org/sdg7

[6] Q. P. Zheng, J. Wang, and A. L. Liu, "Stochastic optimization for unit commitment: A review," *IEEE Trans. Power Syst.*, vol. 30, no. 4, pp. 1913–1924, Jul. 2015.

[7] R. Jiang, J. Wang, and Y. Guan, "Robust unit commitment with wind power and pumped storage hydro," *IEEE Trans. Power Syst.*, vol. 27, no. 2, pp. 800–810, May 2012.

[8] D. Bertsimas, E. Litvinov, X. A. Sun, J. Zhao, and T. Zheng, "Adaptive robust optimization for the security constrained unit commitment problem," *IEEE Trans. Power Syst.*, vol. 28, no. 1, pp. 52–63, Feb. 2013.

[9] R. Jiang, M. Zhang, G. Li, and Y. Guan, "Two-stage network constrained robust unit commitment problem," *Eur. J. Oper. Res.*, vol. 234, no. 3, pp. 751–762, May 2014.

[10] Á. Lorca and X. A. Sun, "Adaptive robust optimization with dynamic uncertainty sets for multi-period economic dispatch under significant wind," *IEEE Trans. Power Syst.*, vol. 30, no. 4, pp. 1702–1713, Jul. 2015.

[11] A. Moreira, A. Street, and J. M. Arroyo, "Energy and reserve scheduling under correlated nodal demand uncertainty: An adjustable robust optimization approach," *Int. J. Electr. Power Energy Syst.*, vol. 72, pp. 91–98, Nov. 2015.

[12] Y. An and B. Zeng, "Exploring the modeling capacity of two-stage robust optimization: Variants of robust unit commitment model," *IEEE Trans. Power Syst.*, vol. 30, no. 1, pp. 109–122, Jan. 2015.

[13] C. Dai, L. Wu, and H. Wu, "A multi-band uncertainty set based robust SCUC with spatial and temporal budget constraints," *IEEE Trans. Power Syst.*, vol. 31, no. 6, pp. 4988–5000, Nov. 2016.

[14] C. Wang, F. Liu, J. Wang, F. Qiu, W. Wei, S. Mei, and S. Lei, "Robust risk-constrained unit commitment with large-scale wind generation: An adjustable uncertainty set approach," *IEEE Trans. Power Syst.*, vol. 32, no. 1, pp. 723–733, Jan. 2017.

[15] C. Shao, X. Wang, M. Shahidehpour, X. Wang, and B. Wang, "Security-constrained unit commitment with flexible uncertainty set for variable wind power," *IEEE Trans. Sustain. Energy*, vol. 8, no. 3, pp. 1237–1246, Jul. 2017.

[16] N. G. Cobos, J. M. Arroyo, and A. Street, "Least-cost reserve offer deliverability in day-ahead generation scheduling under wind uncertainty and generation and network outages," *IEEE Trans. Smart Grid*, vol. 9, no. 4, pp. 3430–3442, Jul. 2018.

[17] N. G. Cobos, J. M. Arroyo, N. Alguacil, and A. Street, "Network-constrained unit commitment under significant wind penetration: A multistage robust approach with non-fixed recourse," *Appl. Energy*, vol. 232, pp. 489–503, Dec. 2018.

[18] G. Giebel, R. Brownsword, G. Kariniotakis, M. Denhard, and C. Draxl, *The State-of-the-Art in Short-Term Prediction of Wind Power: A Literature Overview, 2nd ed.* DTU, Denmark, 2011.

[19] R. Moreno, A. Street, J. M. Arroyo, and P. Mancarella, "Planning low-carbon electricity systems under uncertainty considering operational flexibility and smart grid technologies," *Philosophical Transactions of the Royal Society A: Mathematical, Physical and Engineering Sciences*, vol. 375, no. 2100, p. 20160305, 2017.

[20] L. Platbrood, F. Capitanescu, C. Merckx, H. Crisciu, and L. Wehenkel, "A generic approach for solving nonlinear-discrete security-constrained optimal power flow problems in large-scale systems," *IEEE Transactions on Power Systems*, vol. 29, no. 3, pp. 1194–1203, 2013.

[21] F. Capitanescu, "Critical review of recent advances and further developments needed in ac optimal power flow," *Electric Power Systems Research*, vol. 136, pp. 57–68, 2016.

[22] M. Carrión and J. M. Arroyo, "A computationally efficient mixed-integer linear formulation for the thermal unit commitment problem," *IEEE Trans. Power Syst.*, vol. 21, no. 3, pp. 1371–1378, Aug. 2006.

[23] J. Wang, M. Shahidehpour, and Z. Li, "Security-constrained unit commitment with volatile wind power generation," *IEEE Trans. Power Syst.*, vol. 23, no. 3, pp. 1319–1327, Aug. 2008.

[24] R. Saavedra, A. Street, and J. M. Arroyo, "Day-ahead contingency-constrained unit commitment with co-optimized post-contingency transmission switching," *IEEE Transactions on Power Systems*, In press, 2020.

[25] E. B. Fisher, R. P. O'Neill, and M. C. Ferris, "Optimal transmission switching," *IEEE Transactions on Power Systems*, vol. 23, no. 3, pp. 1346–1355, Aug. 2008.

[26] A. Khodaei and M. Shahidehpour, "Transmission switching in security-constrained unit commitment," *IEEE Transactions on Power Systems*, vol. 25, no. 4, pp. 1937–1945, Nov. 2010.

[27] S. Blumsack, L. B. Lave, and M. Ilic, "A quantitative analysis of the relationship between congestion and reliability in electric power networks," *The Energy Journal*, vol. 28, no. 4, Aug. 2007.

[28] E. S. Johnson, S. Ahmed, S. S. Dey, and J.-P. Watson, "A k-nearest neighbor heuristic for real-time dc optimal transmission switching," *arXiv preprint arXiv:2003.10565*, 2020.

[29] F. Mancilla-David, A. Angulo, and A. Street, "Power management in active distribution systems penetrated by photovoltaic inverters: A data-driven robust approach," *IEEE Transactions on Smart Grid*, vol. 11, no. 3, pp. 2271–2280, 2019.

[30] M. Pereira and L. Pinto, "Stochastic optimization of a multireservoir hydroelectric system: a decomposition approach," *Water resources research*, vol. 21, no. 6, pp. 779–792, 1985.

[31] M. V. Pereira and L. M. Pinto, "Multi-stage stochastic optimization applied to energy planning," *Mathematical programming*, vol. 52, no. 1-3, pp. 359–375, 1991.

[32] T. Archibald, K. McKinnon, and L. Thomas, "An aggregate stochastic dynamic programming model of multireservoir systems," *Water Resources Research*, vol. 33, no. 2, pp. 333–340, 1997.

[33] A. Tilmant and R. Kelman, "A stochastic approach to analyze trade-offs and risks associated with large-scale water resources systems," *Water resources research*, vol. 43, no. 6, 2007.

[34] E. Xi, X. Guan, and R. Li, "Scheduling hydrothermal power systems with cascaded and head-dependent reservoirs," *IEEE Transactions on power systems*, vol. 14, no. 3, pp. 1127–1132, 1999.

[35] J. P. d. S. Catalão, H. M. I. Pousinho, and V. Mendes, "Scheduling of head-dependent cascaded reservoirs considering discharge ramping constraints and start/stop of units," *International Journal of Electrical Power & Energy Systems*, vol. 32, no. 8, pp. 904–910, 2010.

[36] H. Zhang, J. Chang, C. Gao, H. Wu, Y. Wang, K. Lei, R. Long, and L. Zhang, "Cascade hydropower plants operation considering comprehensive ecological water demands," *Energy Conversion and Management*, vol. 180, pp. 119–133, 2019.

[37] S.-E. Fleten and T. K. Kristoffersen, "Short-term hydropower production planning by stochastic programming," *Computers & Operations Research*, vol. 35, no. 8, pp. 2656–2671, 2008.

[38] S. Cerisola, J. M. Latorre, and A. Ramos, "Stochastic dual dynamic programming applied to nonconvex hydrothermal models," *European Journal of Operational Research*, vol. 218, no. 3, pp. 687–697, 2012.

[39] A. Brigatto, A. Street, and D. Valladao, "Assessing the cost of time-inconsistent operation policies in hydrothermal power systems," *IEEE Trans. Power Syst*, vol. PP, no. 99, pp. 1 – 9, Accepted for publication in 2017.

[40] A. Street, A. Brigatto, and D. M. Valladão, "Co-optimization of energy and ancillary services for hydrothermal operation planning under a general security criterion," *IEEE Trans. Power Syst.*, vol. 32, no. 6, pp. 4914–4923, Nov. 2017.

[41] J. Zou, S. Ahmed, and X. A. Sun, "Stochastic dual dynamic integer programming," *Mathematical Programming*, vol. 175, no. 1-2, pp. 461–502, 2019.

[42] M. N. Hjelmeland, J. Zou, A. Helseth, and S. Ahmed, "Nonconvex medium-term hydropower scheduling by stochastic dual dynamic integer programming," *IEEE Transactions on Sustainable Energy*, vol. 10, no. 1, pp. 481–490, 2018.

[43] B. F. Hobbs, Q. Xu, J. Ho, P. Donohoo, S. Kasina, J. Ouyang, S. W. Park, J. Eto, and V. Satyal, "Adaptive transmission planning: Implementing a new paradigm for managing economic risks in grid expansion," *IEEE Power Energy Mag*, vol. 14, no. 4, pp. 30–40, Jun. 2016.

[44] D. Bertsimas and J. N. Tsitsiklis, *Introduction to Linear Optimization*. Belmont, MA, USA: Athena Scientific, 1997.

[45] C. Coffrin and P. Van Hentenryck, "A linear-programming approximation of ac power flows," *INFORMS Journal on Computing*, vol. 26, no. 4, pp. 718–734, 2014.

[46] M. R. Hestenes, "Multiplier and gradient methods," *Journal of optimization theory and applications*, vol. 4, no. 5, pp. 303–320, 1969.

[47] A. Papavasiliou, S. S. Oren, and B. Rountree, "Applying high performance computing to transmission-constrained stochastic unit commitment for renewable energy integration," *IEEE Transactions on Power Systems*, vol. 30, no. 3, pp. 1109–1120, May 2015.

[48] F. Fioretto, T. W. Mak, and P. Van Hentenryck, "Predicting ac optimal power flows: Combining deep learning and lagrangian dual methods," *arXiv preprint arXiv:1909.10461*, 2019.

[49] C. A. Floudas, *Nonlinear and mixed-integer optimization: fundamentals and applications*. Oxford University Press, 1995.

[50] A. Ben-Tal and A. Nemirovski, "Robust convex optimization," *Mathematics of Operations Research*, vol. 23, no. 4, pp. 769–805, 1998.

[51] C. Coffrin, H. L. Hijazi, and P. Van Hentenryck, "The qc relaxation: A theoretical and computational study on optimal power flow," *IEEE Transactions on Power Systems*, vol. 31, no. 4, pp. 3008–3018, 2015.

[52] S. Zhang and X. A. Sun, "Stochastic dual dynamic programming for multistage stochastic mixed-integer nonlinear optimization," *arXiv preprint arXiv:1912.13278*, 2019.

[53] J. R. Birge and F. Louveaux, *Introduction to stochastic programming*. Springer Science & Business Media, 2011.

[54] A. Philpott and Z. Guan, "On the convergence of stochastic dual dynamic programming and related methods," *Operations Research Letters*, vol. 36, no. 4, pp. 450–455, 2008.

[55] A. Shapiro, "Analysis of stochastic dual dynamic programming method," *European Journal of Operational Research*, vol. 209, no. 1, pp. 63–72, 2011.

[56] A. Ben-Tal, A. Goryashko, E. Guslitzer, and A. Nemirovski, "Adjustable robust solutions of uncertain linear programs," *Math. Program.*, vol. 99, no. 2, pp. 351–376, Mar. 2004.

[57] D. Bertsimas and M. Sim, "The price of robustness," *Oper. Res.*, vol. 52, no. 1, pp. 35–53, Jan.–Feb. 2004.

[58] Á. Lorca and X. A. Sun, "Multistage robust unit commitment with dynamic uncertainty sets and energy storage," *IEEE Trans. Power Syst.*, vol. 32, no. 3, pp. 1678–1688, May 2017.

[59] A. J. Wood, B. F. Wollenberg, and G. B. Sheblé, *Power generation, operation, and control*. John Wiley & Sons, 2013.

[60] A. Papavasiliou, S. S. Oren, and B. Rountree, "Applying high performance computing to transmission-constrained stochastic unit commitment for renewable energy integration," *IEEE Transactions on Power Systems*, vol. 30, no. 3, pp. 1109–1120, May 2015.

[61] C. Bandi and D. Bertsimas, "Tractable stochastic analysis in high dimensions via robust optimization," *Math. Program.*, vol. 134, no. 1, pp. 23–70, Aug. 2012.

[62] H. Hoeltgebaum, C. Fernandes, and A. Street, "Generating joint scenarios for renewable generation: The case for non-gaussian models with time-varying parameters," *IEEE Transactions on Power Systems*, vol. 33, no. 6, pp. 7011–7019, Nov. 2018.

[63] A. Moreira, D. Pozo, A. Street, and E. Sauma, "Reliable renewable generation and transmission expansion planning: Co-optimizing system's resources for meeting renewable targets," *IEEE Trans. Power Syst.*, vol. 32, no. 4, pp. 3246–3257, Jul. 2017.

[64] C. Ruiz and A. Conejo, "Robust transmission expansion planning," *Eur. J. Oper. Res.*, vol. 242, no. 2, pp. 390 – 401, 2015.

[65] A. Moreira, G. Strbac, R. Moreno, A. Street, and I. Konstantelos, "A five-level milp model for flexible transmission network planning under uncertainty: A min–max regret approach," *IEEE Trans. Power Syst.*, vol. 33, no. 1, pp. 486–501, Jan. 2018.

[66] C. Liu, C. Lee, H. Chen, and S. Mehrotra, "Stochastic robust mathematical programming model for power system optimization," *IEEE Trans. Power Syst.*, vol. 31, no. 1, pp. 821–822, 2016.

[67] X. Zhang and A. J. Conejo, "Robust transmission expansion planning representing long- and short-term uncertainty," *IEEE Trans. Power Syst.*, vol. 33, no. 2, pp. 1329–1338, Mar. 2018.

[68] B. Zeng and L. Zhao, "Solving two-stage robust optimization problems using a column-and-constraint generation method," *Oper. Res. Lett.*, vol. 41, no. 5, pp. 457–461, Sep. 2013.

[69] A. Velloso, P. Van Hentenryck, and E. S. Johnson, "An exact and scalable problem decomposition for security-constrained optimal power flow," *Electric Power Systems Research*, in press, 2020.

[70] S. Misra, L. Roald, and Y. Ng, "Learning for constrained optimization: Identifying optimal active constraint sets," *arXiv preprint arXiv:1802.09639*, 2018.

[71] A. S. Xavier, F. Qiu, and S. Ahmed, "Learning to solve large-scale security-constrained unit commitment problems," *arXiv preprint arXiv:1902.01697*, 2019.

[72] Z. Yang and S. Oren, "Line selection and algorithm selection for transmission switching by machine learning methods," in *2019 IEEE Milan PowerTech*. IEEE, 2019, pp. 1–6.

[73] A. Velloso, A. Street, D. Pozo, J. M. Arroyo, and N. G. Cobos, "Two-stage robust unit commitment for co-optimized electricity markets: An adaptive

data-driven approach for scenario-based uncertainty sets," *IEEE Trans. Sustain. Energy*, vol. 11, no. 2, pp. 958–969, Apr. 2020.

[74] A. Velloso, D. Pozo, and A. Street, "Distributionally robust transmission expansion planning: a multi-scale uncertainty approach," *IEEE Transactions on Power Systems*, in press, 2020.

[75] "Grid optimization competition," https://gocompetition.energy.gov/, accessed: 2017-10-09.

[76] P. Ballantyne, "Challenge prizes: A practice guide," http://www.nesta.org.uk/publications/challenge-prizes-practice-guide, accessed: 2017-08-31.

[77] O. Alsac and B. Stott, "Optimal load flow with steady-state security," *IEEE Trans. Power App. Syst.*, vol. PAS-93, no. 3, pp. 745–751, May 1974.

[78] F. Bouffard, F. D. Galiana, and J. M. Arroyo, "Umbrella contingencies in security-constrained optimal power flow," in *15th Power Systems Computation Conference, PSCC*, vol. 5, 2005.

[79] Y. Li and J. D. McCalley, "Decomposed SCOPF for improving efficiency," *IEEE Trans. Power Syst.*, vol. 24, no. 1, pp. 494–495, Feb. 2009.

[80] F. Capitanescu, J. M. Ramos, P. Panciatici, D. Kirschen, A. M. Marcolini, L. Platbrood, and L. Wehenkel, "State-of-the-art, challenges, and future trends in security constrained optimal power flow," *Elect. Power Syst. Res.*, vol. 81, no. 8, pp. 1731–1741, Aug. 2011.

[81] Q. Wang, J. D. McCalley, T. Zheng, and E. Litvinov, "Solving corrective risk-based security-constrained optimal power flow with lagrangian relaxation and benders decomposition," *Int. J. Elec. Power*, vol. 75, pp. 255–264, Feb. 2016.

[82] Y. Dvorkin, P. Henneaux, D. S. Kirschen, and H. Pandžić, "Optimizing primary response in preventive security-constrained optimal power flow," *IEEE Syst. Journal*, vol. 12, no. 1, pp. 414–423, Mar. 2016.

[83] M. Velay, M. Vinyals, Y. Besanger, and N. Retiere, "Fully distributed security constrained optimal power flow with primary frequency control," *Int. J. Elec. Power*, vol. 110, pp. 536–547, Sep. 2019.

[84] Z. Zhou, T. Levin, and G. Conzelmann, "Survey of U.S. ancillary services markets," Argonne National Lab.(ANL), Argonne, IL (United States), Tech. Rep., 2016.

[85] F. Li and R. Bo, "Dcopf-based lmp simulation: algorithm, comparison with acopf, and sensitivity," *IEEE Transactions on Power Systems*, vol. 22, no. 4, pp. 1475–1485, 2007.

[86] B. Eldridge, R. P. O'Neill, and A. Castillo, "Marginal loss calculations for the dcopf," *Federal Energy Regulatory Commission, Tech. Rep*, 2017.

[87] A. Marano-Marcolini, F. Capitanescu, J. L. Martinez-Ramos, and L. Wehenkel, "Exploiting the use of dc scopf approximation to improve iterative ac scopf algorithms," *IEEE Transactions on Power Systems*, vol. 27, no. 3, pp. 1459–1466, 2012.

[88] J. F. Restrepo and F. D. Galiana, "Unit commitment with primary frequency regulation constraints," *IEEE Trans. Power Syst.*, vol. 20, no. 4, pp. 1836–1842, Nov. 2005.

[89] K. Karoui, H. Crisciu, and L. Platbrood, "Modeling the primary reserve allocation in preventive and curative security constrained OPF," in *Proc. IEEE PES Trans. Distrb. Conf. Expo*. IEEE, Apr., 2010, pp. 1–6.

[90] J. Wang, M. Shahidehpour, and Z. Li, "Contingency-constrained reserve requirements in joint energy and ancillary services auction," *IEEE Trans. Power Syst.*, vol. 24, no. 3, pp. 1457–1468, Aug. 2009.

[91] R. Rahmaniani, T. G. Crainic, M. Gendreau, and W. Rei, "The Benders decomposition algorithm: A literature review," *Eur. J. Oper. Res.*, vol. 259, no. 3, pp. 801–817, Jun. 2017.

[92] A. J. Ardakani and F. Bouffard, "Identification of umbrella constraints in dc-based security-constrained optimal power flow," *IEEE Trans. Power Syst.*, vol. 28, no. 4, pp. 3924–3934, 2013.

[93] S. Babaeinejadsarookolaee *et al.*, "The power grid library for benchmarking ac optimal power flow algorithms," *arXiv preprint arXiv:1908.02788*, 2019.

[94] A. Street, F. Oliveira, and J. M. Arroyo, "Contingency-constrained unit commitment with $n-k$ security criterion: A robust optimization approach," *IEEE Transactions on Power Systems*, vol. 26, no. 3, pp. 1581–1590, 2010.

[95] A. Khodaei and M. Shahidehpour, "Security-constrained transmission switching with voltage constraints," *International Journal of Electrical Power & Energy Systems*, vol. 35, no. 1, pp. 74–82, 2012.

[96] A. Moreira, A. Street, and J. M. Arroyo, "An adjustable robust optimization approach for contingency-constrained transmission expansion planning," *IEEE Transactions on Power Systems*, vol. 30, no. 4, pp. 2013–2022, 2014.

[97] E. Lannoye, D. Flynn, and M. O'Malley, "Transmission, variable generation, and power system flexibility," *IEEE Trans. Power Syst.*, vol. 30, no. 1, pp. 57–66, 2014.

[98] P. Kundur, N. J. Balu, and M. G. Lauby, *Power system stability and control*. McGraw-hill New York, 1994, vol. 7.

[99] X. A. Sun, "Robust optimization in electric power systems," *in Advances and Trends in Optimization with Engineering Applications*, T. Terlaky, M. F. Anjos, and S. Ahmed, Eds. Philadelphia, PA, USA: SIAM, 2017, pp. 357–365.

[100] H. Sasaki, M. Watanabe, J. Kubokawa, N. Yorino, and R. Yokoyama, "A solution method of unit commitment by artificial neural networks," *IEEE Transactions on Power Systems*, vol. 7, no. 3, pp. 974–981, 1992.

[101] Z. Ouyang and S. Shahidehpour, "A hybrid artificial neural network-dynamic programming approach to unit commitment," *IEEE transactions on power systems*, vol. 7, no. 1, pp. 236–242, 1992.

[102] V. J. Gutierrez-Martinez, C. A. Cañizares, C. R. Fuerte-Esquivel, A. Pizano-Martinez, and X. Gu, "Neural-network security-boundary constrained optimal power flow," *IEEE Transactions on Power Systems*, vol. 26, no. 1, pp. 63–72, 2010.

[103] D. C. Costa, M. V. Nunes, J. P. Vieira, and U. H. Bezerra, "Decision tree-based security dispatch application in integrated electric power and natural-gas networks," *Electric Power Systems Research*, vol. 141, pp. 442–449, 2016.

[104] Y. LeCun, Y. Bengio, and G. Hinton, "Deep learning," *nature*, vol. 521, no. 7553, pp. 436–444, 2015.

[105] J. M. Arroyo and F. D. Galiana, "Energy and reserve pricing in security and network-constrained electricity markets," *IEEE Trans. Power Syst.*, vol. 20, no. 2, pp. 634–643, May 2005.

[106] Y. Chen, P. Gribik, and J. Gardner, "Incorporating post zonal reserve deployment transmission constraints into energy and ancillary service

co-optimization," *IEEE Trans. Power Syst.*, vol. 29, no. 2, pp. 537–549, Mar. 2014.

[107] Federal Energy Regulatory Commission. (2014, Dec.). Operator-initiated commitments in RTO and ISO markets. Price formation in organized wholesale electricity markets. Docket no. AD14-14-000. Washington, DC, USA.

[108] Regulatory Authority for Energy, "The Greek grid and exchange code," 2019, 2019. [Online]. Available: http://www.rae.gr/old/en/codes/main.htm

[109] Y. Guan and J. Wang, "Uncertainty sets for robust unit commitment," *IEEE Trans. Power Syst.*, vol. 29, no. 3, pp. 1439–1440, May 2014.

[110] M. S. Bazaraa, H. D. Sherali, and C. M. Shetty, *Nonlinear Programming: Theory and Algorithms, 3rd ed*. Hoboken, NJ, USA: John Wiley & Sons, 2006.

[111] D. Bertsimas, D. B. Brown, and C. Caramanis, "Theory and applications of robust optimization," *SIAM Rev.*, vol. 53, no. 3, pp. 464–501, 2011.

[112] D. Bertsimas and D. B. Brown, "Constructing uncertainty sets for robust linear optimization," *Oper. Res.*, vol. 57, no. 6, pp. 1483–1495, Nov.–Dec. 2009.

[113] B. Fernandes, A. Street, D. Valladão, and C. Fernandes, "An adaptive robust portfolio optimization model with loss constraints based on data-driven polyhedral uncertainty sets," *Eur. J. Oper. Res.*, vol. 255, no. 3, pp. 961–970, Dec. 2016.

[114] D. Bertsimas, V. Gupta, and N. Kallus, "Data-driven robust optimization," *Math. Program.*, vol. 167, no. 2, pp. 235–292, Feb. 2018.

[115] G. C. Calafiore, "On the expected probability of constraint violation in sampled convex programs," *J. Optim. Theory Appl.*, vol. 143, no. 2, pp. 405–412, Nov. 2009.

[116] C. Liu, C. Lee, H. Chen, and S. Mehrotra, "Stochastic robust mathematical programming model for power system optimization," *IEEE Trans. Power Syst.*, vol. 31, no. 1, pp. 821–822, Jan. 2016.

[117] F. D. Galiana, F. Bouffard, J. M. Arroyo, and J. F. Restrepo, "Scheduling and pricing of coupled energy and primary, secondary, and tertiary reserves," *Proc. IEEE*, vol. 93, no. 11, pp. 1970–1983, Nov. 2005.

[118] I. Blanco and J. M. Morales, "An efficient robust solution to the two-stage stochastic unit commitment problem," *IEEE Trans. Power Syst.*, vol. 32, no. 6, pp. 4477–4488, Nov. 2017.

[119] C. A. Floudas, *Nonlinear and Mixed-Integer Optimization: Fundamentals and Applications*. New York, NY, USA: Oxford Univ. Press, 1995.

[120] J. Riko, "Dynamic planar convex hull," Ph.D. dissertation, *University of Aarhus*, Aarhus, Denmark, 2002.

[121] A. Velloso, A. Street, D. Pozo, J. M. Arroyo, and N. G. Cobos, "Two-stage robust unit commitment for co-optimized electricity markets: An adaptive data-driven approach for scenario-based uncertainty sets – supplementary document – case studies data," 2019. [Online]. Available: http://www.lamps.ind.puc-rio.br/en/publicacao/ddruc2019/

[122] T. Hong, P. Pinson, and S. Fan, "Global energy forecasting competition 2012," *Int. J. Forecast.*, vol. 30, no. 2, pp. 357–363, Apr.–Jun. 2014.

[123] T. Hong, P. Pinson, S. Fan, H. Zareipour, A. Troccoli, and R. J. Hyndman, "Probabilistic energy forecasting: Global energy forecasting competition 2014 and beyond," *Int. J. Forecast.*, vol. 32, no. 3, pp. 896–913, Jul.–Sep. 2016.

[124] L. Börjeson, M. Höjer, K.-H. Dreborg, T. Ekvall, and G. Finnveden, "Scenario types and techniques: towards a user's guide," *Futures*, vol. 38, no. 7, pp. 723–739, Sep. 2006.

[125] F. D. Munoz, B. F. Hobbs, J. L. Ho, and S. Kasina, "An engineering-economic approach to transmission planning under market and regulatory uncertainties: Wecc case study," *IEEE Trans. Power Syst.*, vol. 29, no. 1, pp. 307–317, Jan 2014.

[126] J. Li, Z. Li, F. Liu, H. Ye, X. Zhang, S. Mei, and N. Chang, "Robust coordinated transmission and generation expansion planning considering ramping requirements and construction periods," *IEEE Trans. Power Syst.*, vol. 33, no. 1, pp. 268–280, Jan. 2018.

[127] D. Pozo, A. Street, and A. Velloso, "An ambiguity-averse model for planning the transmission grid under uncertainty on renewable distributed generation," *in Proc. 20th Power Systems Computation Conf. (PSCC'18)*, Dublin, Ireland, Jun. 2018.

[128] Y. Liu, R. Sioshansi, and A. J. Conejo, "Multistage stochastic investment planning with multiscale representation of uncertainties and decisions," *IEEE Trans. Power Syst.*, vol. 33, no. 1, pp. 781–791, Jan 2018.

[129] J. Zhan, W. Liu, and C. Y. Chung, "Stochastic transmission expansion planning considering uncertain dynamic thermal rating of overhead lines," *IEEE Trans. Power Syst.*, vol. 34, no. 1, pp. 432–443, Jan 2019.

[130] H. Scarf, "Robust optimization in electric power systems," *in Studies in the Mathematical Theory of Inventory and Production*, K. S. Arrow, S. Karlin, H. E. Scarf, Eds. Stanford, CA, USA: Stanford University Press, 1958, pp. 201–209.

[131] J. Goh and M. Sim, "Distributionally robust optimization and its tractable approximations," *Oper. Res.*, vol. 58, no. 4-part-1, pp. 902–917, 2010.

[132] E. Delage and Y. Ye, "Distributionally robust optimization under moment uncertainty with application to data-driven problems," *Oper. Res.*, vol. 58, no. 3, pp. 595–612, 2010.

[133] W. Wiesemann, D. Kuhn, and M. Sim, "Distributionally Robust Convex Optimization," *Oper. Res.*, vol. 62, no. 6, pp. 1358–1376, dec 2014.

[134] P. Mohajerin Esfahani and D. Kuhn, "Data-driven distributionally robust optimization using the wasserstein metric: performance guarantees and tractable reformulations," *Math. Program.,*, vol. 171, no. 1, pp. 115–166, Sep. 2018.

[135] F. Qiu and J. Wang, "Distributionally robust congestion management with dynamic line ratings," *IEEE Trans. Power Syst.*, vol. 30, no. 4, pp. 2198–2199, Jul. 2015.

[136] W. Wei, L. Feng, and M. Shengwei, "Distributionally robust co-optimization of energy and reserve dispatch," *IEEE Trans. Sustain. Energy*, vol. 7, no. 1, pp. 289–300, Jan. 2016.

[137] W. Xie and S. Ahmed, "Distributionally robust chance constrained optimal power flow with renewables: A conic reformulation," *IEEE Trans. Power Syst.*, vol. 33, no. 2, pp. 1860–1867, Mar. 2018.

[138] C. Wang, R. Gao, F. Qiu, J. Wang, and L. Xin, "Risk-based distributionally robust optimal power flow with dynamic line rating," *IEEE Trans. on Power Syst.*, vol. 33, no. 6, pp. 6074–6086, Nov. 2018.

[139] F. Alismail, P. Xiong, and C. Singh, "Optimal wind farm allocation in multi-area power systems using distributionally robust optimization approach," *IEEE Trans. Power Syst.*, vol. 33, no. 1, pp. 536–544, Jan. 2018.

[140] A. Gourtani, H. Xu, D. Pozo, and T.-D. Nguyen, "Robust unit commitment with n - 1 security criteria," *Math. Oper. Res.*, vol. 83, no. 3, pp. 373–408, Jun. 2016.

[141] P. Xiong, P. Jirutitijaroen, and C. Singh, "A distributionally robust optimization model for unit commitment considering uncertain wind power generation," *IEEE Trans. Power Syst.*, vol. 32, no. 1, pp. 39–49, 2017.

[142] C. Zhao and R. Jiang, "Distributionally robust contingency-constrained unit commitment," *IEEE Trans. Power Syst.*, vol. 33, no. 1, pp. 94–102, Jan. 2018.

[143] D. Alvarado, A. Moreira, R. Moreno, and G. Strbac, "Transmission network investment with distributed energy resources and distributionally robust security," *IEEE Trans. Power Syst.*, vol. 34, no. 6, pp. 5157–5168, Nov. 2019.

[144] A. Bagheri, J. Wang, and C. Zhao, "Data-driven stochastic transmission expansion planning," *IEEE Trans. Power Syst.*, vol. 32, no. 5, pp. 3461–3470, Sep. 2017.

[145] H. J. Landau, *Moments in mathematics*. American Mathematical Soc., 1987, vol. 37.

[146] S. Boyd and L. Vandenberghe, *Convex Optimization*. Cambridge, UK: Cambridge University Press, 2004.

[147] A. Ben-Tal, L. El Ghaoui, and A. Nemirovski, *Robust optimization*. Princeton Univ Pr, 2009.

[148] A. Velloso, D. Pozo, and A. Street, "Distributionally robust transmission expansion planning: a multi-scale uncertainty approach – Case studies data," 2020. [Online]. Available: https://drive.google.com/file/d/1NoDSa8OwjxtpIT1wTEosGj6n6c8Rxqm3

[149] C. Vazquez, M. Rivier, and I. J. Pérez-Arriaga, "A market approach to long-term security of supply," *IEEE Transactions on power systems*, vol. 17, no. 2, pp. 349–357, 2002.

[150] F. P. Sioshansi, *Competitive electricity markets: design, implementation, performance*. Elsevier, 2011.

[151] L. Maurer and L. A. Barroso, *Electricity auctions: an overview of efficient practices*. World Bank Publications, 2011.

[152] M. E. P. Maceira, V. Duarte, D. Penna, L. Moraes, and A. Melo, "Ten years of application of stochastic dual dynamic programming in official and agent studies in brazil-description of the newave program," *16th PSCC, Glasgow, Scotland*, pp. 14–18, 2008.

[153] R. P. O'Neill, T. Dautel, and E. Krall, "Recent iso software enhancements and future software and modeling plans," *Federal Energy Regulatory Commission, Tech. Rep*, 2011.

[154] M. B. Cain, R. P. O'neill, and A. Castillo, "History of optimal power flow and formulations," *Federal Energy Regulatory Commission*, pp. 1–36, 2012.

[155] M. Howells, H. Rogner, N. Strachan, C. Heaps, H. Huntington, S. Kypreos, A. Hughes, S. Silveira, J. DeCarolis, M. Bazillian *et al.*, "Osemosys: the open source energy modeling system: an introduction to its ethos, structure and development," *Energy Policy*, vol. 39, no. 10, pp. 5850–5870, 2011.

[156] "Open energy modelling initiative," http://www.openmod-initiative.org/, accessed: 2018-02-22.

[157] E. Sauma and S. Oren, "Proactive planning and valuation of transmission investments in restructured electricity markets," *Journal of Regulatory Economics*, vol. 30, no. 3, pp. 261–290, 2006.

[158] A. H. van der Weijde and B. F. Hobbs, "The economics of planning electricity transmission to accommodate renewables: Using two-stage optimisation to evaluate flexibility and the cost of disregarding uncertainty," *Energy Econ.*, vol. 34, no. 6, pp. 2089–2101, Nov. 2012.

[159] A. Brigatto, A. Street, and D. M. Valladao, "Assessing the cost of time-inconsistent operation policies in hydrothermal power systems," *IEEE Transactions on Power Systems*, 2017.

[160] B. Rudloff, A. Street, and D. M. Valladão, "Time consistency and risk averse dynamic decision models: Definition, interpretation and practical consequences," *European Journal of Operational Research*, vol. 234, no. 3, pp. 743–750, 2014.

[161] "Nasa solve," http://www.nasa.gov/solve/, accessed: 2017-10-09.

[162] "Netflix prize," http://www.netflixprize.com/, accessed: 2017-10-09.

[163] "Google lunar xprize," https://lunar.xprize.org/, accessed: 2017-10-09.

[164] "Shell ocean discovery xprize," https://oceandiscovery.xprize.org/, accessed: 2017-10-09.

[165] H. W. Chesbrough, *Open innovation: The new imperative for creating and profiting from technology*. Harvard Business Press, 2006.

[166] T. Kalil, *Prizes for technological innovation*. Brookings Institution, 2006.

[167] S. Adamczyk, A. C. Bullinger, and K. M. Möslein, "Innovation contests: A review, classification and outlook," *Creativity and Innovation Management*, vol. 21, no. 4, pp. 335–360, 2012.

[168] I. Liotard and V. Revest, "Contests as innovation policy instruments: Lessons from the us federal agencies' experience," *Technological Forecasting and Social Change*, 2017. [Online]. Available: http://www.sciencedirect.com/science/article/pii/S0040162517309265

[169] J. Bays, B. Chakravorti, T. G. B. Harris, P. Jansen, D. McGaw, J. Newsum, A. Simon, and L. Taliento, "And the winner is: Capturing the power of philanthropic prizes," 2009.

[170] E. Nicholson, "Operator-initiated commitments in rto and iso markets," FERC, Tech. Rep, Tech. Rep., 2014.

[171] F. D. Munoz, S. Wogrin, S. S. Oren, and B. F. Hobbs, "Economic inefficiencies of cost-based electricity market designs," *The Energy Journal*, vol. 39, no. 3, 2018.

[172] A. Vargas and M. E. Samper, "Real-time monitoring and economic dispatch of smart distribution grids: High performance algorithms for dms applications," *IEEE Transactions on Smart Grid*, vol. 3, no. 2, pp. 866–877, Jun 2012.

[173] R. P. O'Neill, A. Castillo, and M. B. Cain, "The iv formulation and linear approximations of the ac optimal power flow problem," *Published online at http://www. ferc. gov/industries/electric/indus-act/market-planning/opf-papers/acopf-2-iv-linearization. pdf*, 2012.

[174] R. J. Lempert, *Shaping the next one hundred years: new methods for quantitative, long-term policy analysis*. Rand Corporation, 2003.

[175] R. Pinto, A. Sabóia, R. Cabral, F. Costa, A. Diniz, and M. Maceira, "Metodologia para aplicação de processamento paralelo no planejamento de curto-prazo (modelo decomp)," *XX Seminário Nacional de Produção e Transmissão de Energia Elétrica, SNPTEE*, 2009.

[176] R. J. Pinto, C. T. Borges, and M. E. Maceira, "An efficient parallel algorithm for large scale hydrothermal system operation planning," *IEEE Transactions on Power Systems*, vol. 28, no. 4, pp. 4888–4896, 2013.

[177] T. N. Santos, A. L. Diniz, and C. L. T. Borges, "A new nested benders decomposition strategy for parallel processing applied to the hydrothermal scheduling problem," *IEEE Transactions on Smart Grid*, vol. 8, no. 3, pp. 1504–1512, 2016.

[178] D. D. Penna, M. E. P. Maceira, and J. M. Damázio, "Selective sampling applied to long-term hydrothermal generation planning," in *17th PSCC-Power Syst. Comp. Conf.*, 2011.

[179] A. L. Diniz and M. E. Maceira, "Multi-lag benders decomposition for power generation planning with nonanticipativity constraints on the dispatch of lng thermal plants," in *Stochastic Programming: Applications in Finance, Energy, Planning and Logistics*. World Scientific, 2013, pp. 443–464.

[180] T. N. Dos Santos and A. L. Diniz, "A dynamic piecewise linear model for dc transmission losses in optimal scheduling problems," *IEEE Transactions on Power systems*, vol. 26, no. 2, pp. 508–519, 2010.

[181] A. L. Diniz and T. M. Souza, "Short-term hydrothermal dispatch with river-level and routing constraints," *IEEE Transactions on Power Systems*, vol. 29, no. 5, pp. 2427–2435, 2014.

[182] M. d. A. Ennes, M. Maceira, A. Diniz, D. Penna, and C. Vasconcellos, "Representação de subsistemas e submercados de forma diferenciada no planejamento da operação hidrotérmica," *Seminário Nacional de Produção e Transmissão de Energia Elétrica, Brasília*, 2013.

[183] V. L. de Matos, E. C. Finardi, and E. L. da Silva, "Comparison between the energy equivalent reservoir per subsystem and per cascade in the long-term operation planning in brazil," *EngOpt*, 2008.

[184] C. VASCONCELLOS, "Aprimoramentos na metodologia de superfície de aversão ao risco (sar) para o problema de planejamento de médio/longo prazo da operação de sistemas hidrotérmicos," Ph.D. dissertation, Tese de

Mestrado, Engenhria Elétrica Universidade Federal do Rio de Janeiro . . . , 2016.

[185] A. L. Diniz, M. E. P. Maceira, C. L. V. Vasconcellos, and D. D. J. Penna, "A combined sddp/benders decomposition approach with a risk-averse surface concept for reservoir operation in long term power generation planning," *Annals of Operations Research*, pp. 1–33, 2019.

[186] A. B. Philpott and V. L. De Matos, "Dynamic sampling algorithms for multi-stage stochastic programs with risk aversion," *European Journal of operational research*, vol. 218, no. 2, pp. 470–483, 2012.

[187] A. Diniz, M. Tcheou, M. Maceira, and D. Penna, "Uma abordagem direta para consideração do cvar no problema de planejamento da operação hidrotérmica," *XII SEPOPE–Simpósio de Especialistas em Planejamento da Operação e Expansão Elétrica, Rio de Janeiro-RJ*, 2012.

[188] A. Shapiro, W. Tekaya, J. P. da Costa, and M. P. Soares, "Risk neutral and risk averse stochastic dual dynamic programming method," *European journal of operational research*, vol. 224, no. 2, pp. 375–391, 2013.

[189] A. Shapiro, W. Tekaya, M. P. Soares, and J. P. da Costa, "Worst-case-expectation approach to optimization under uncertainty," *Operations Research*, vol. 61, no. 6, pp. 1435–1449, 2013.

[190] V. L. De Matos, A. B. Philpott, and E. C. Finardi, "Improving the performance of stochastic dual dynamic programming," *Journal of Computational and Applied Mathematics*, vol. 290, pp. 196–208, 2015.

[191] R. B. S. Brandi, T. P. Ramos, B. H. Dias, A. L. M. Marcato, and I. C. da Silva Junior, "Improving stochastic dynamic programming on hydrothermal systems through an iterative process," *Electric Power Systems Research*, vol. 123, pp. 147–153, 2015.

[192] "Kaggle competitions," https://www.kaggle.com/competitions, accessed: 2017-10-09.

[193] "Xprize," https://www.xprize.org/, accessed: 2017-10-09.

[194] K. R. Lakhani, K. J. Boudreau, P.-R. Loh, L. Backstrom, C. Baldwin, E. Lonstein, M. Lydon, A. MacCormack, R. A. Arnaout, and E. C. Guinan, "Prize-based contests can provide solutions to computational biology problems," *Nature biotechnology*, vol. 31, no. 2, pp. 108–111, 2013.

[195] L. B. Jeppesen and K. R. Lakhani, "Marginality and problem-solving effectiveness in broadcast search," *Organization science*, vol. 21, no. 5, pp. 1016–1033, 2010.

[196] F. Murray, S. Stern, G. Campbell, and A. MacCormack, "Grand innovation prizes: A theoretical, normative, and empirical evaluation," *Research Policy*, vol. 41, no. 10, pp. 1779 – 1792, 2012, the need for a new generation of policy instruments to respond to the Grand Challenges. [Online]. Available: http://www.sciencedirect.com/science/article/pii/S004873331200217X

[197] K. R. Lakhani and L. B. Jeppesen, "Getting unusual suspects to solve r&d puzzles," *Harvard Business Review*, vol. 85, no. 5, pp. 30–32, 2007.

[198] M. Bazilian, A. Rice, J. Rotich, M. Howells, J. DeCarolis, S. Macmillan, C. Brooks, F. Bauer, and M. Liebreich, "Open source software and crowdsourcing for energy analysis," *Energy Policy*, vol. 49, pp. 149–153, 2012.

[199] S. Pfenninger, J. DeCarolis, L. Hirth, S. Quoilin, and I. Staffell, "The importance of open data and software: Is energy research lagging behind?" *Energy Policy*, vol. 101, pp. 211–215, 2017.

[200] "Government challenges," https://www.challenge.gov/list/, accessed: 2017-10-09.

[201] O. Dowson and L. Kapelevich, "Sddp. jl: a julia package for stochastic dual dynamic programming," *Optimization Online*, 2017.

[202] L. Ding, S. Ahmed, and A. Shapiro, "A python package for multi-stage stochastic programming," *Optimization Online*, pp. 1–41, 2019.

[203] A. Philpott, F. Wahid, and J. Bonnans, "Midas: A mixed integer dynamic approximation scheme," *Mathematical Programming*, pp. 1–32, 2019.

[204] A. Shapiro and L. Ding, "Stationary multistage programs," *Optimization Online*, 2019.

[205] V. Guigues, A. Shapiro, and Y. Cheng, "Duality and sensitivity analysis of multistage linear stochastic programs," *arXiv preprint arXiv:1911.07080*, 2019.

[206] S. Ahmed, F. G. Cabral, and B. F. P. da Costa, "Stochastic lipschitz dynamic programming," *arXiv preprint arXiv:1905.02290*, 2019.